SYNTHESIS OF NANOSTRUCTURED SEMICONDUCTORS VIA PULSED LASER ABLATION IN LIQUIDS AND THEIR CHARACTERIZATION

BY

TALAL FARHAN AHMED QAHTAN

A Thesis Presented to the
DEANSHIP OF GRADUATE STUDIES

KING FAHD UNIVERSITY OF PETROLEUM & MINERALS

DHAHRAN, SAUDI ARABIA

In Partial Fulfillment of the
Requirements for the Degree of

MASTER OF SCIENCE

In

PHYSICS

JANUARY, 2014

KING FAHD UNIVERSITY OF PETROLEUM & MINERALS

DHAHRAN- 31261, SAUDI ARABIA

DEANSHIP OF GRADUATE STUDIES

This thesis, written by **Talal Farhan Ahmed Qahtan** under the direction his thesis advisor and approved by his thesis committee, has been presented and accepted by the Dean of Graduate Studies, in partial fulfillment of the requirements for the degree of

MASTER OF SCIENCE IN PHYSICS.

M. A. Gondal

Prof. M.A. Gondal
(Advisor)

Dr. Abdul-Aziz Al-Jalal
Department Chairman

Dr. Z.H. Yamani
(Member)

Dr. Salam A. Zummo
Dean of Graduate Studies

Dr. M.M. Faiz
(Member)

31/12/13

Date

عمادة الدراسات العليا
DEANSHIP OF GRADUATE STUDIES

DEDICATED

To my mother and deceased father who inspire me to think, dream and plan for a bright future

To my beloved wife and my lovely son who are the secrets of my happiness

ACKNOWLEDGMENTS

After praise and thanks for Almighty Allah (S.W.T.) who gave me the health, ability and patience to accomplish this research, I would like to thank all people who helped and supported me to accomplish this Thesis.

First of all, I am pleased to express my appreciation and deep thanks to my thesis advisor, Prof. Dr. M.A Gondal for his great patience, constant motivation, encouragement and constructive suggestions. I have learned so much from him during this work in so many ways in a short period of time. His skillful scientific guidance during this work makes me as a free thinker and an independent researcher.

I also would like to acknowledge and express my deep thanks for my thesis committee members, Dr. Z.H. Yamani, Director of the Center of Excellence in Nanotechnology (CENT) at King Fahd University of Petroleum and Minerals (KFUPM), for his constant support, assistance, constructive instructions and to Dr. M.M. Faiz for his attention and constructive feedback.

I also would like to acknowledge Taiz University for supporting and financially giving me a chance to join KFUPM, and KFUPM for supporting and providing the facilities to carry out this work.

I would like to extend my thanks to the Physics Department at KFUPM, and the chairman Dr. Abdul-Aziz Al-Jalal in particular for his assistance, support and making things easier which helped me to finish this work.

Thanks go to Dr. Mahioub Al-Buhairii, Dr. Sahar Ahmed Amin and Dr. Leila Abdul Jalil from Physics Department, Taiz University, Yemen for his constant encouragement and support.

I wish to express my thanks to all people who helped me in so many ways: Dr. Dalaver Anjum from King Abdullah University of Science and Technology for TEM images, Dr. Tawfik Saleh for IR analysis, Dr. Abbas Hakeem and Mr. Muhammad Luqman from CENT for FESEM images, Mr. Muhammad Dastageer for Photoluminescence measurements, Mr. Mohammad Said for XRD analysis.

Thanks go to my colleagues, Mr. Drmosh, Mr. Maganda, Mr. Subkhi, Mr. Hasan Abdullah and Mr. Anas Ahmed for their moral support.

May Almighty Allah forgive my deceased father and grant his soul heavenly peace and a higher place in Jannat Al-Firdaus (Aameen) who inspire me to think, dream and plan for a bright future.

The love and affection from my family including mother, brothers, sisters, wife and my lovely son, who supported me in the difficult times and for their prayer to accomplish this work successfully, are greatly appreciated.

TABLE OF CONTENTS

LIST OF FIGURES

LIST OF ABBREVIATIONS

PLA	:	Pulsed Laser Ablation
PLD	:	Pulsed Laser Deposition
PLAL	:	Pulsed Laser Ablation in Liquids
NPs	:	Nanoparticles
CuO	:	Cupric Oxide or Copper (II) Oxide
Cu_2O	:	Cuprous Oxide or Copper (I) Oxide
QDs	:	Quantum Dots
CdSe	:	Cadmium Selenide
DW	:	Deionized Water

ABSTRACT

Full Name : Talal Farhan Ahmed Qahtan

Thesis Title : Synthesis of Nanostructured Semiconductors via Pulsed Laser Ablation in Liquids and their Characterization

Major Field : Physics

Date of Degree : January, 2014

This work is related with the development of a cost effective, novel and one-step process, called pulsed laser ablation in liquids (PLAL) technique, for the synthesis of high purity, stable and less agglomeration nanostructured semiconductors. Nanostructured copper oxides (cupric and cuprous oxides) and CdSe were synthesized using the pulsed laser ablation in liquids technique. In order to synthesize nanostructured copper oxides, a high purity copper target was fixed at the bottom of a glass cell in the presence of deionized water mixed with hydrogen peroxide in different concentrations (0, 1, 3 and 5 %). The effect of the oxidizing media (deionized water and hydrogen peroxide) on the composition, morphology and optical properties of the synthesized nanomaterial produced by PLAL were studied. XRD and TEM studies indicate that in the absence of hydrogen peroxide, the synthesized nanoparticles were in two phases (Cu/Cu_2O) with the spherical nanoparticle structure, whereas in the presence of hydrogen peroxide, the synthesized nanoparticles exhibited two other phases (Cu/CuO) with nanorod-like structure. The optical studies of the material prepared in the presence of hydrogen peroxide revealed considerable red shift (0.8 eV) in the band gap energy compared to the one prepared in the absence of it. Also, the synthesized nanoparticles in the presence of

hydrogen peroxide showed a reduced photoluminescence intensity indicating reduced electron hole recombination rate. The red shift in the band gap energy and the reduced electron hole recombination rate make the synthesized nanoparticles an effecient photocatalyst to harvest solar radiation. The most relevant spectral lines on the FTIR spectrum for the samples were the absorption bands in the region between 450 and 700 cm^{-1} which are the characteristic bands of copper-oxygen bonds. The laser ablation approach for the synthesis of Cu_2O and CuO nanoparticles have unique advantages of being a clean method with controlled optical and morphological properties.

The effect of annealing temperature on synthesized nanostructured copper oxides in deionized water was also studied. In the initial unannealed colloidal suspension, the nanoparticles of Copper (Cu) and Cuprous oxide (Cu_2O) were identified. Further the suspension was dried and annealed at different temperatures and we noticed the product (Cu/Cu_2O) was converted predominantly into CuO at annealing temperature of 300 ºC for 3 hours. As the annealing temperature was raised from 300 to 900 ºC, the grain size of CuO increased from 9 ±1 to 26 ± 1 nm. The structure and the morphology of the prepared samples were investigated using X-ray diffraction and Transmission Electron Microscopy. Photoluminescence and UV absorption spectrometry studies revealed that the band gap and other optical properties of nanostructured Cu/Cu_2O were changed due to post annealing. Fourier transform IR spectrometry also confirmed the transformation of Cu/Cu_2O into CuO which is very encouraging result. To the best of our knowledge, such transformation has not been reported in earlier publications.

Pulsed laser ablation in liquids was also applied to synthesize cadmium selenide quantum dots from the commercially available micron sized cadmium selenide powder in acetone

medium using the pulsed laser radiation with 250 mJ energy. The thermal agglomeration due the nanosecond pulse duration of the laser was successfully eliminated by using unfocussed laser beam and thereby providing a favorable condition for the synthesis of quantum dots. It is worth mentioning that there is no report of synthesis of quantum dots using nanosecond pulsed laser. All previous studies were conducted using very expensive and too sophisticated femtosecond lasers. The morphological and optical characterization by XRD, HRTEM, optical absorption of the synthesized cadmium selenide quantum dots reveal that the material possesses similar characteristics to the one synthesized using femtosecond laser pulse. Relative to the cadmium selenide bulk material, the synthesized cadmium selenide quantum dots of average size 3 nm showed a blue shift in the band gap energy from near infrared spectral region to visible region, making this material capable and beneficial for solar energy harvesting applications like photocatalysis and solar cells.

ملخص الرسالة Abstract (Arabic)

الاسم الكامل: طلال فرحان احمد قحطان

عنوان الرسالة: تحضير وتوصيف اشباه موصلات ذات بنية نانوية بواسطة الإستئصال الليزري في السوائل

التخصص: فيزياء

تاريخ الدرجة العلمية: يناير 2014 م

تهدف هذه الدراسة إلى تحضير وتوصيف اشباه موصلات ذات بنية نانوية من أكاسيد النحاس (أكسيد النحاسيك والنحاسوز) وسيلينايد الكادميوم بواسطة الإستئصال الليزري في السوائل. لهذا الغرض تم استخدام ليزر نادميوم ياج يعمل عند الطول الموجي 532 نانومتر لإرسال نبضات ليزرية الى مادة عالية النقاوة مغمورة في سائل مناسب. لغرض دراسة تأثيرالوسط المؤكسد على خواص أكاسيد النحاس النانوية تم وضع قطعة من معدن النحاس عالي النقاوة داخل خلية زجاجية تحتوي على ماء مقطر ممزوج بمحلول بيروكسيد الهيدروجين بتراكيز مختلفة (صفر، واحد، ثلاثة وخمسة في المائة من الحجم). بعد فحص الجسيمات النانوية المحضرة أشارت التحاليل الناتجة من جهاز حيود الأشعة السينية وتقنية المجهر الألكتروني النافذ عالي الدقة إلى تكون جسيمات كروية الشكل من النحاس/أكسيد النحاسوز في حالة التركيز الصفري وجسيمات ذات شكل عصوي من النحاس/أكسيد النحاسيك في حالة التراكيز الاخرى. كما أظهرت تحاليل الخواص البصرية للعينات المنتجة بان قيمة طاقة الفجوة في حالة التركيزالصفري حوالي 3.3 الكترون فولت بينما تساوي 2.5 في حالة التراكيز الاخرى. كما ان جهاز طيف نفاذ الأشعة الحمراء قد اكد تكون أكسيد النحاسوز في حالة التركيز الصفري وأكسيد النحاسيك في حالة التراكيز الاخرى.

هدفت هذه الدراسة أيضاً الى التعرف على مدى تأثير درجة الحرارة على جسيمات النحاس/أكسيد النحاسوز النانوية المحضرة بواسطة الإستئصال الليزري للنحاس في الماء المقطر. لهذا الغرض تم تحضير اربع عينات ومن ثم تم تجفيفها ووضعها في فرن كهربائي لمدة ثلاث ساعات عند ثلاث درجات حرارية مختلفة (300، 600 و 900 درجة مئوية). لوحظ ان أغلبية الجسيمات النانوية المتكونة من النحاس وأكسيد النحاسوز تبدأ بالتحويل الى أكسيد النحاسيك عند درجة حرارة 300 درجة مئوية ويستمر هذا التحول بزيادة درجة الحرارة من 600 الى 900 درجة مئوية مع زيادة حجم الجسيمات.

تضمنت هذه الدراسة أيضاً إستخدام تقنية الإستئصال الليزري في السوائل لتحضير نقاط كمية لسلينايد الكادميوم من جسيمات ميكرومترية لسلينايد الكادميوم في الأسيتون بإستخدام شعاع ليزر غير مركز طاقتة 250 ميجا جول. باستخدام تقنية حيود الأشعة السينية، تقنية المجهر الألكتروني النافذ و تحليل الخواص البصرية للنقاط الكمية المنتجة وجد انها تمتلك حجم متوسط مقداره 3 نانومتر وطاقة فجوة في المنطقة المرئية (2.4 الكترون فولت) مما يجعل هذه المواد مفيدة في تطبيقات الخلايا الشمسية.

CHAPTER 1

INTRODUCTION

The fabrication of devices at atomic and molecular scale was predicted by physicist Richard Feynman in his famous talk entitled "*There's plenty of room at the bottom*" at an American Physical Society meeting on December 29th, 1959 [1]. The term "Nanotechnology" was coined by Professor Norio Taniguchi at the University of Tokyo and it has been in use as early as 1974 [2]. Nanotechnology is a technology which deals with different structures of matter of the order of 10^{-9} of a meter. In 2006, Nanotechnology was defined by the US National Nanotechnology Initiative as follows: "*Nanotechnology is development at the atomic levels in the length scale of approximately 1-100 nanometer range, to provide a fundamental understanding of phenomena and materials at the nanoscale and to create and use structures, devices and systems that have novel properties and functions*" [3]. The term "*nano*" refers to a billionth (10^{-9}). The term "*Nanomaterials*" refers to a ultrafine parts of the material where at least one of its dimensions is in nanometer scale (from 1nm to 100 nm). The nanomaterials are classified into three categories: One dimension nanomaterials (thin films), two dimension nanomaterials (nano wires, nano tubes and nano rods) and three dimension nanomaterials (nanparticles/NPs). The invention and development of high resolution imaging tools such as the scanning tunneling microscope (STM), atomic force microscope (AFM), transmission electron microscope (TEM) and scanning electron microscope (SEM) play

an important role in the characterization of nanomaterials and advancement of nanoscience.

Nanomaterials show different physical and chemical properties from that of its bulk counterparts. These unique characteristics arise due to the quantum confinement and the increase of surface area to volume ratio which are inversely proportional to particle size [4-6]. Hence, synthesis and application of nanomaterials have attracted great attention from researchers for their applications in different areas such as sensing, energy harvesting and photo-catalysis. Several methods have been applied to synthesize nanomaterials such as wet chemical synthesis, vapor phase condensation, rapid thermal decomposition of precursors in solution, sputtering and plasma reactors [7-8]. Some of these methods, especially the chemical methods, are capable of producing large quantities, but they typically require many steps (pretreatment, mixing, chemical reaction, filtration, drying and heat-treatment) [9-10]. Such treatments may alter the material purity, promote grain growth, and introduce contaminants. Purification of such contamination to obtain nanomaterial with a high degree of purity could add extra cost [11-12].

Pulsed laser ablation (PLA) is a process in which a pulsed laser beam is applied to remove/eject material from a solid surface. There are two kinds of PLA depending on the surrounding medium during the interaction between the laser beam and the material. PLA of materials in the presence of gases or in vacuum has been used to synthesize a wide variety of thin films and this is well known as Pulsed Laser Deposition (PLD) technique. On the other hand, PLA of a powder/solid target which is dispersed /immersed in liquid is now known as Pulsed Laser Ablation in Liquids (PLAL) [11-14].

1.1 Pulsed Laser Ablation in Liquids Mechanisms

In general, there are two main approaches to synthesize the nanostructured materials. Namely, bottom up and top down approach. Synthesis of nanomaterials using PLAL technique falls under top-down approach category. In PLAL technique, the production system does not require costly chambers and high vacuum pumps. Also, the preparation of well crystallized NPs using PLAL could easily be attained in one-step procedure without subsequent heat-treatments. In addition, pure NPs could be produced using this technique without the formation of by-products. Furthermore, the entire product could be collected in solution and the obtained colloidal solution can be easily handled. Moreover, in this technique, the size (micrometer/nanometer), composition (pure metals, semiconductors, metal oxides, metal peroxides, alloys, nitrides, carbides, etc.) and morphology (particles, cubes, rods, sheets, tubes, plates, flowers, etc.) of the synthesized materials depend on incident pulsed laser beam characteristics including pulse duration, wavelength, pulse repetition rate, laser fluence and ablation time, in addition to the confinement of the liquid medium [12-15]. Finally, it makes it possible to use this technique to resize and reshape the synthesized (by PLAL or other methods) colloidal NPs by the secondary ablation which will be revealed later during this study.

Two mechanisms are suggested in PLAL to generate nanostructured materials which are summarized in the following sections:

1.1.1 Thermal Evaporation Mechanism

When a high intense pulsed laser beam strikes a solid target, most of the beam is absorbed by the medium at a localized spot and this absorption of the beam leads to the

creation of a high pressure and temperature plasma (laser-induced plasma) at the solid/liquid interface. There are two suggested models by Yang et al. and Zeng and coworkers for the interaction between the produced plasma and the liquid environment which in turn leads to synthesize the nanomaterials. Yang et al. [11-12] proposed that the laser-induced plasma evaporates and excites the confining liquid, converting it to plasma (plasma-induced plasma). The reaction between these two kinds of plasmas was responsible of the production of the nanostructured materials [16]. On the other hand, Zeng and coworkers [14, 16-19] proposed that the laser-induced plasma expand adiabatically leading to a quick condensing of the plasma which in turn leads to the fabrication of clusters. These clusters interact with the liquid medium, resulting in the fabrication of nanostructred material.

1.1.2 Explosive Ejection Mechanism

In this mechanism, hot nanodroplets are ejected from the target into the surrounding liquid at high speed due to the pulsed laser beam which in turn interacts with the liquid gradually from the surface. The morphology and the chemical composition of the products are governed by the interaction between the ejected nanodroplets and the ambient liquid which in turn depends on the medium reactivity and laser parameters [20-23].

In addition, PLA of a powder material dispersed in a transparent liquid is used to decrease the size of the particles into the nano scale. The synthesized nanoparticles may have the same or different shape, phase and composition depending on the interaction between the ablated particles and the surrounding medium. In this case, two mechanisms are suggested for the ablation of powder targets. The first mechanism is a thermal process

in which a pulsed laser beam melts and evaporates the large particles into small species (atoms and molecules) which in turn rearrange themselves into nanostructured particles that have the same or different morphology and structure depending on the reactivity of surrounding medium and laser parameters [14, 24-29] The second is known as columbic explosion mechanism in which laser beam ejects electrons from the outer surface of the suspended particles via photoelectron or thermal effect [14, 29-32]. The electrostatic repulsion between the induced surface charges (positive charges) on the different parts of the particles leads to the explosion of the primary particle into many smaller parts, a process called fragmentation. This leads to synthesis of ultrafine nanoparticles [14, 29-32].

1.2 Objectives

The main objective of this thesis is to synthesize ultrafine nanostructured semiconductors using pulsed laser ablation in liquid. The specific objectives are the following:

1. To design a homemade set up that could improve and achieve efficient conditions for pulsed laser ablation in liquids.
2. To synthesize Cu_2O, CuO and CdSe nanoparticles using pulsed laser ablation in liquid technique.
3. To characterize the synthesized nanoparticles using different analytical techniques.

CHAPTER 2

LITERATURE REVIEW

The main aim of this chapter is to summarize the recent published literature which have attracted great attention on development of PLAL technique and using it to synthesize the copper oxides and cadmium selenide (CdSe) nanoparticles. PLA was developed soon after the ruby laser was invented in the 1960s [11-12]. Since the early 1980s, PLA of materials in the presence of gases or in vacuum has been used to synthesize a wide variety of thin films. In 1987, Patil et al. [11] revealed for the first time, the possibility of using PLA of a metallic iron as a solid target in deionized water (DW) as a confining liquid to synthesize a layer of metastable iron oxides on iron. The potential of using PLAL technique for surface oxidation, nitriding or carbiding of metals was examined by Ogale [11]. This opened new routes for material processing via PLAL technique. In 1993, the possibility of this technique to synthesize colloidal solutions of metalic target in the presence of organic solvents and water was reported by Neddersen et al. [13]. In the early 2000s, researchers started to generate and control the size of nanostructured noble metals by pulsed laser ablation in the presence of aqueous solutions and surfactants. Since then, PLAL has been applied to synthesize a wide variety of nanostructured materials which gained high popularity as these methods allow one to obtain nanomaterial with a high degree of purity (as laser beams being a completely clean tool) and one can ablate nearly all kinds of materials, as laser beam posses high power density after focusing (10^6~ 10^{14} W/cm^2) [12-15].

2.1 Copper Oxides Nanoparticles

Transition metals show unique characteristics like existence of various oxidation states, formation of paramagnetic compounds, high melting point, high boiling point, effective homogeneous and heterogeneous catalytic activity and all these properties can be ascribed to the partially filled d shells. Transition metal oxides form a series of compounds with a wide range of unique electronic properties and they have important phases such as dielectrics, semiconductors and metals, and could be utilized very well as materials for magnetic, electrochromic, optical and catalytic applications [33]. The advent of the nanostructured material has brought about the improved attributes in terms of magnetic, electronic, catalytic, sensing and optical characteristics compared to their bulk counterparts [34-40]. Copper oxide is one of the most extensively studied transition metal oxides and finds widespread applications as well. The predominant oxides of copper are cupric oxide or Copper (II) oxide (CuO) and cuprous oxide or Copper (I) oxide (Cu_2O), ignoring the presence of other forms of oxides which are quite marginal. From application point of view, CuO is more versatile than Cu_2O, where the former is widely applied in the fields of solar energy conversion, nanofluid and gas sensors, [41-43] and the latter is mostly applied in the areas of bacterial disinfection [44] and solar cells [45]. Both CuO and Cu_2O are p-type semiconductors possessing monoclinic and cubic crystal structures respectively and the band gap energy for CuO is in the range of 1.2 to 2.1 eV while for Cu_2O is in the range of 2.1 to 2.6 eV. These variations are quite evident in the published literature [46-48].

In 1999, Yeh et al. [49] studied the production of Cu NPs by PLA of suspended CuO powder in 2-propanol using Nd: YAG nanosecond laser operating either at 1064 or 532 nm of wavelength.

In 2008, Amikura et al. [50] reported the synthesis of Cu_4O_3 and Cu NPs using PLAL. In this study, Nd: YAG nanosecond laser (532 nm wavelength, 6 ns pulsed duration and operating at 184-210 mj/Pulse of energy) was applied to ablate Cu plate in DW and decane to synthesize Cu_4O_3 and Cu NPs respectively.

In 2009, Lin et al. [51] used PLAL (532 nm wavelength, focused nanosecond laser (10 ns), 5 Hz repetition rate, 100 mj/pulse energy and 60 minutes ablation time) to synthesize CuO nanorod from the ablation of Cu target in DW. By applying electric field during the ablation and without focusing, the authors were able to synthesize spin-like CuO. Lee et al.[52] produced spin-like CuO and cu NPs using 532 nm from Nd: YAG nanosecond laser (4-6 ns pulse duration and 8.9 mj/cm^2 energy density) for the ablation of suspended CuO powder in methanol.

In 2010, Niu et al. [53-54] produced CuS nanowires using 1064 nm from Nd: YAG laser (1 ms pulse duration, 20 Hz pulse repetition, 10^6 W/cm^2 laser fluence and for 5 min ablation time) to ablate Cu target in 1-Dodecanethiol. The authors were able to synthesis hollow CuO NPs from the ablation of Cu plate in water + ethanol using Nd: YAG laser (1064 nm, 0.6 ms pulse duration, 1 Hz pulse repetition, 106 W/cm^2 laser fluence and 5 min ablation time).

In 2011, Nath and Khare[55] used Nd: YAG nanosecond laser (532 nm, 10 ns) to ablate Cu plate in DW. By changing the focusing condition to adjust the energy density, CuO

NPs (≤200 nm), CuO/Cu_2O and Cu/Cu_2O composites were synthesized at 500 J/cm^2, 80 J/cm^2 and 9 J/cm^2 respectively. Kawasaki [56] synthesized Cu NPs (10 nm) using pulsed laser ablation (164 nm) from suspended CuO powder in acetone. The as prepared Cu NPs were converted into Cu_2O NPs by oxidation process in the open air. Muniz-Miranda et al. [57] used PLAL to synthesize from Cu colloidal suspensions. The authors used Nd: YAG laser (1064 or 532 nm, 10 ns pulse duration, 10 Hz pulse repetition, 2.5 mj/cm^2 energy density and 10-30 min ablation time) as ablation source to synthesize Cu colloidal suspensions by the ablation of Cu plate in aqueous solution.

However there is no authentic report or published data regarding the effect of oxidizing medium and annealing temperature on the properties of copper oxide nanoparticles using PLAL technique. Hence, the work in this direction could be considered as a pioneer work.

2.2 CdSe Nanoparticles

Semiconductors at the nanoscale exhibit unique physical and chemical properties, compared to their macroscopic counterparts, and these characteristics are strongly size-dependent, especially as the particle size gets smaller than the exciton Bohr radius (Quantum dots) of the bulk material. Hence, during the last few decades, the semiconductor nanocrystals have seen enormous research interests both in basic and technological applications. The most important materials for the optoelectronic applications, in general, are Zinc Sulfide (ZnS) [58-59], Zinc oxide (ZnO) [60], Cadmium sulfide (CdS) [61] and Cadmium Selenide (CdSe) [62] and in particular, CdSe quantum dots (QDs), due to their interesting size dependent optical and electronic properties. CdSe took over a major role in the vital applications in the field of nano-electronics [63], laser,

and biological applications [64-65]. Several methods for synthesis of CdSe QDs, such as solution-based synthesis with organometallic and nonorganometallic precursors [66-68] and deposition-based synthesis (ionic layer adsorption, chemical bath deposition, atomic layer deposition, pulse laser deposition) [69-75] have been reported.

In 2012, Mahmoud et al. [76] used a chemical method in which 2-mercaptoethanol was used as capping agent to synthesize CdSe quantum dots (QDs). The synthesized CdSe QDs have cubic phase with zinc blende structure and average particle size achieved was 2.3, 3.1, 4.1, 5, and 6 nm and optical band gap energy 2.5, 2.3, 2.2, 2.1 and 1.93 eV corresponding to chemical reaction temperature (65 ºC , 75 ºC, 85 ºC and 95 ºC, respectively).

The work and the literature on the synthesis of colloidal QDs using PLAL is very limited [77-79]. In 2006, Ruth and Young [77] used PLAL with 600 ns pulsed laser for the synthesis of CdSe NPs in different liquids and their product material failed to exhibit any photoluminescence (PL) for the excitation wavelength between 250 and 500 nm. In 2009, Semaltianos et al [78], were able to get the PL of the CdSe QDs prepared by PLA (using laser having 180 fs of pulsed duration) of CdSe target in methanol. However to the best of our knowledge and literature available, there is not any single report on synthesis of CdSe QDs using nanosecond pulsed laser. Hence, this work is the first of its kind to report the synthesis of CdSe QDs using nanosecond laser. The size-dependent photoluminescence and electroluminescence property of II–VI semiconductors family has attracted much attention from researchers to study the members of this family in some details for both fundamental research and technological applications [80-81].

CHAPTER 3

SETUP AND CHARACTERIZATION TECHNIQUES

3.1 Experimental Setup for Synthesis of Nanoparticles (NPs)

An intense pulsed laser beam from a Q-switched Nd-YAG laser (Brilliant B) operating at 532 nm wavelength using second harmonic generator was used as an ablation source. This laser can deliver maximum pulse energy of 450 mJ with a pulse width of 5 ns and operates at a 10 Hz pulse repetition rate. With an appropriate turning prism and lens, the laser beam was routed and focused on the sample target. In order to avoid any crater on the target surface due to the high intense laser beam, the target was rotated using a magnetic rotator whose speed was controlled by a stepping motor. The target was kept in the presence of an appropriate liquid medium. The height of the liquid level in the beaker was maintained approximately 2-4 mm above the surface of the target in order to avoid the laser beam travelling a longer path length through the liquid and hence to minimize the absorption loss. The schematic diagram of the ablation system applied for the synthesis is depicted in Fig. 3-1. In case of powder targets, the defocusing setup (Fig. 3-2) was used to ablate a suspended powder in 40 ml of appropriate liquid for 15 minutes. In order to get homogeneous solution, a speed magnetic stirrer was used during the experiment. Fig. 3-3 shows a photograph of the focusing arrangement of the setup applied in this work.

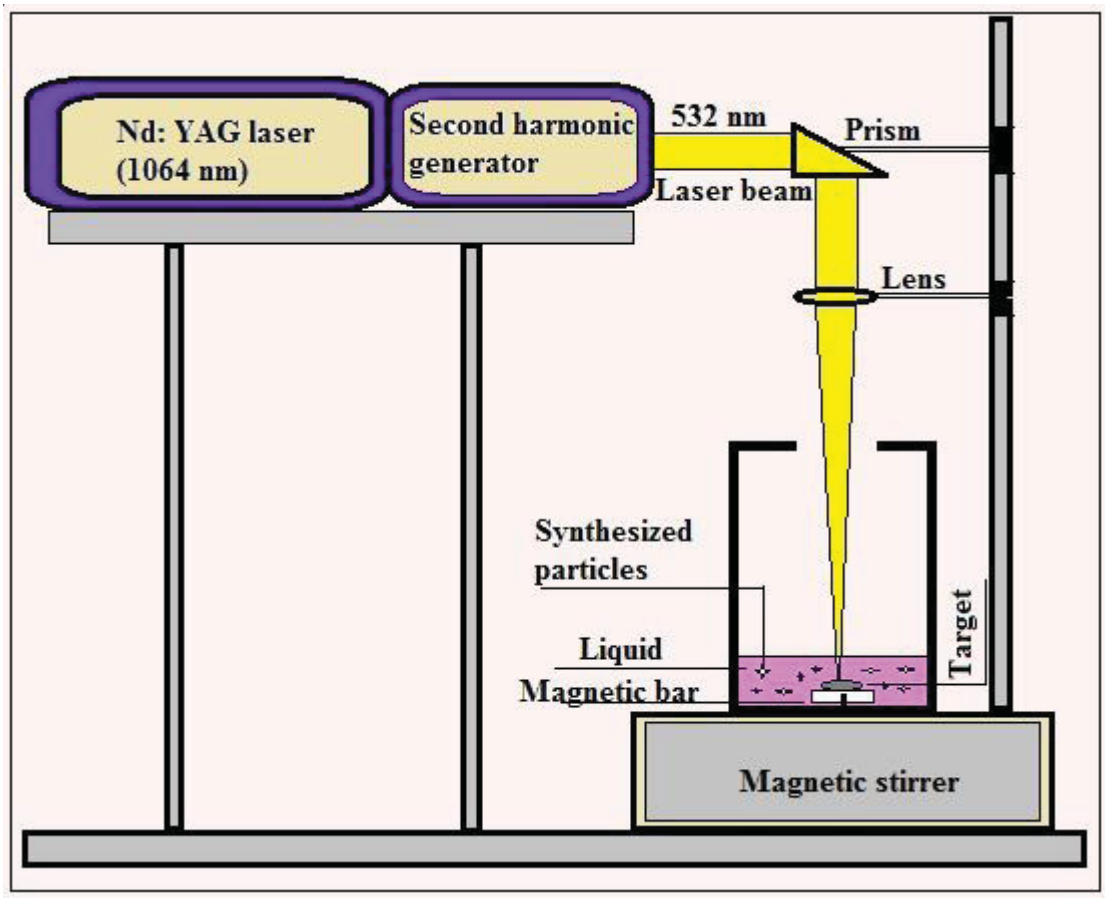

Figure 3-1 Schematic diagram of the focusing arrangement of the setup for synthesis of nanostructured semiconductors from solide target using PLAL technique.

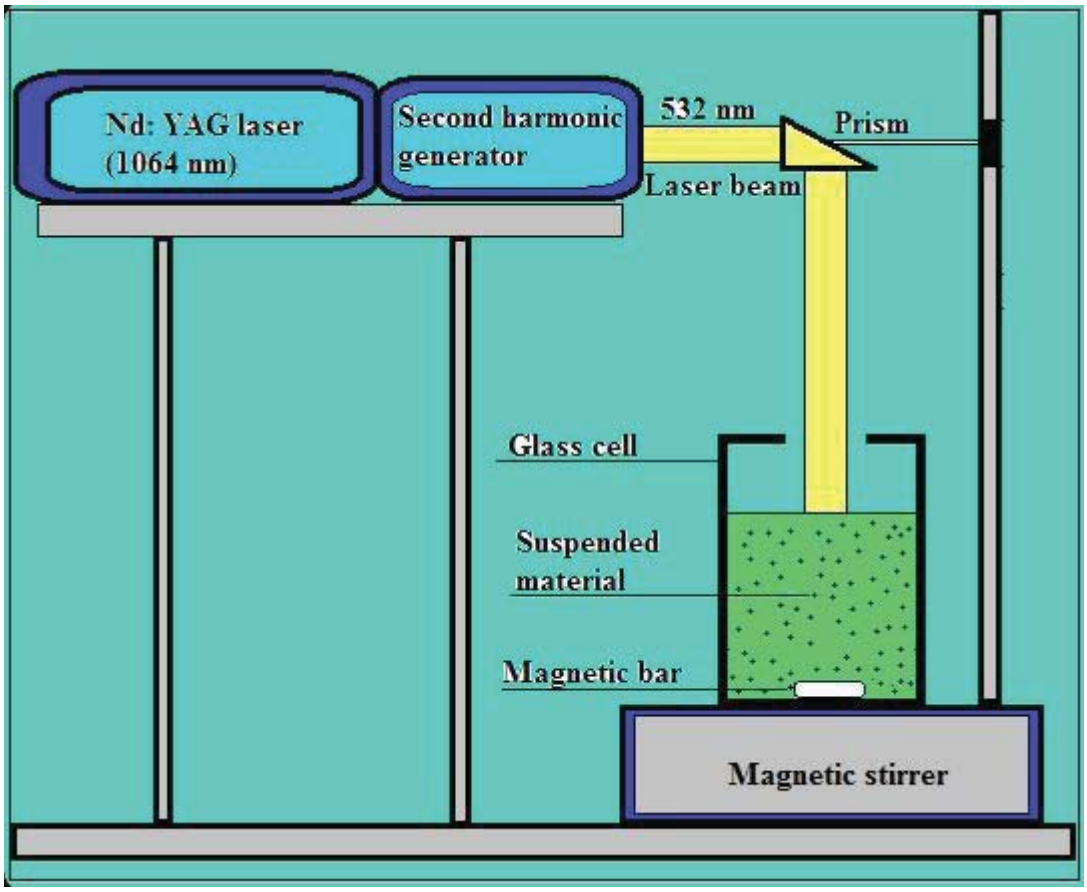

Figure 3-2 Schematic digram of the defocusing arrangement of the setup for synthesis of nanostructured semiconductors from powder target by PLAL technique.

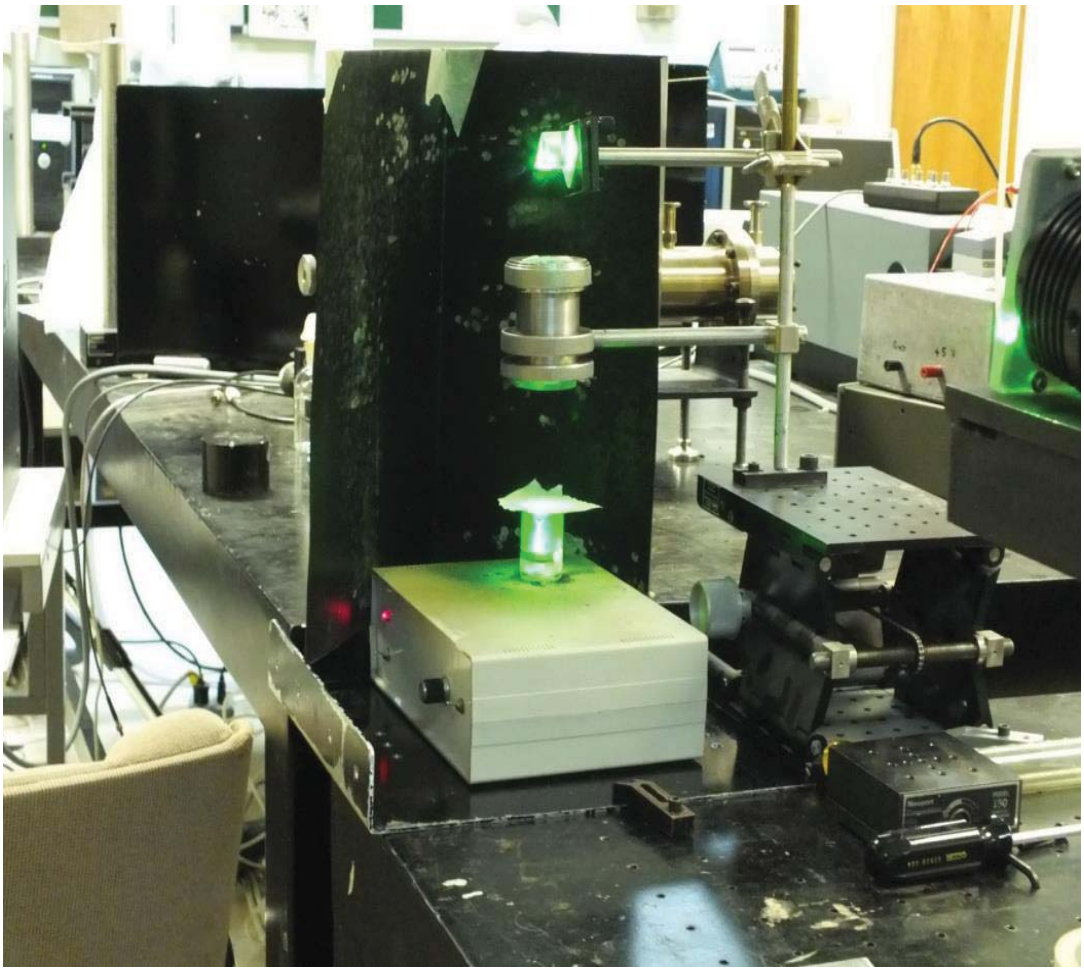

Figure 3-3 Photograph of PLAL setup developed at Laser Laboratory of KFUPM.

It is relevant to mention the problems that we faced at the beginning of this work related with experimental work which could affect the ablation efficiency. These steps are mentioned briefly in the following points:

1. Adjusting the diameter of the magnetic rotator:

   Fig. 3-4 shows (a) a glass cell, (b) a magnetic rotator, (c) a target and (d) the final design (a-c together) that was used in the experiment. The diameter of the magnetic rotator (2.5 cm) should be very close to the diameter of the glass cell (2.8 cm) to minimize the vibrations on the liquid surface which in turn decrease the reflectance of laser beam from the liquid surface and increase the ablation efficiency.

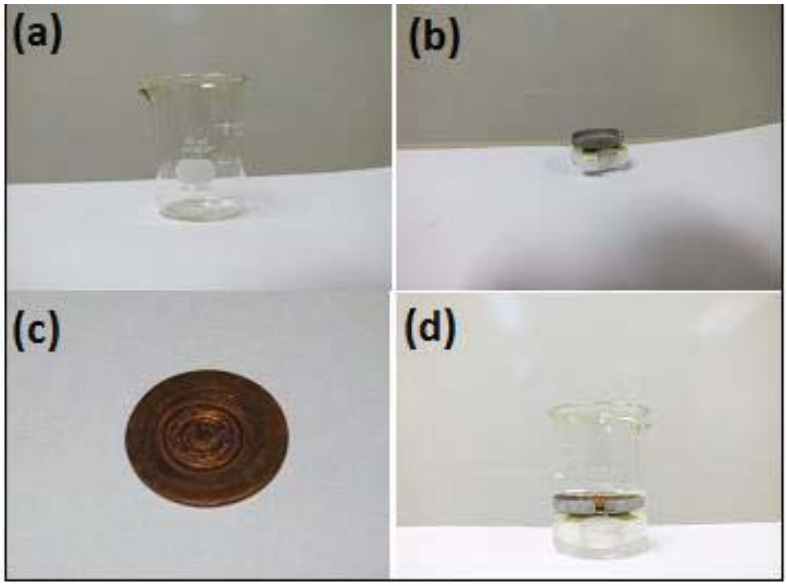

Figure 3-4 Photographs of the essential parts in PLAL: a- glass cell, b- magnetic rotator c- target d- (a-c) all parts together.

2. Adjusting liquid level above the target surface:

   The ablation efficiency could be affected by the liquid level above the target surface. To study this effect, the liquid level was varied from 1 to 10 mm in height from the target surface, and it was found that the typical liquid level should be in the range 2-4 mm as shown in Fig. 3-5. If it is less than this range, the ablated material could fly in air due to the incomplete confinement for the ablated material by the liquid. On the other hand, if it is more than this range, the laser beam could travel a longer path length through the liquid and this means more laser energy absorption by the liquid. In addition, there is a probability that liquid can act as lens and could diverge the laser beam and thus decreasing the ablation efficiency.

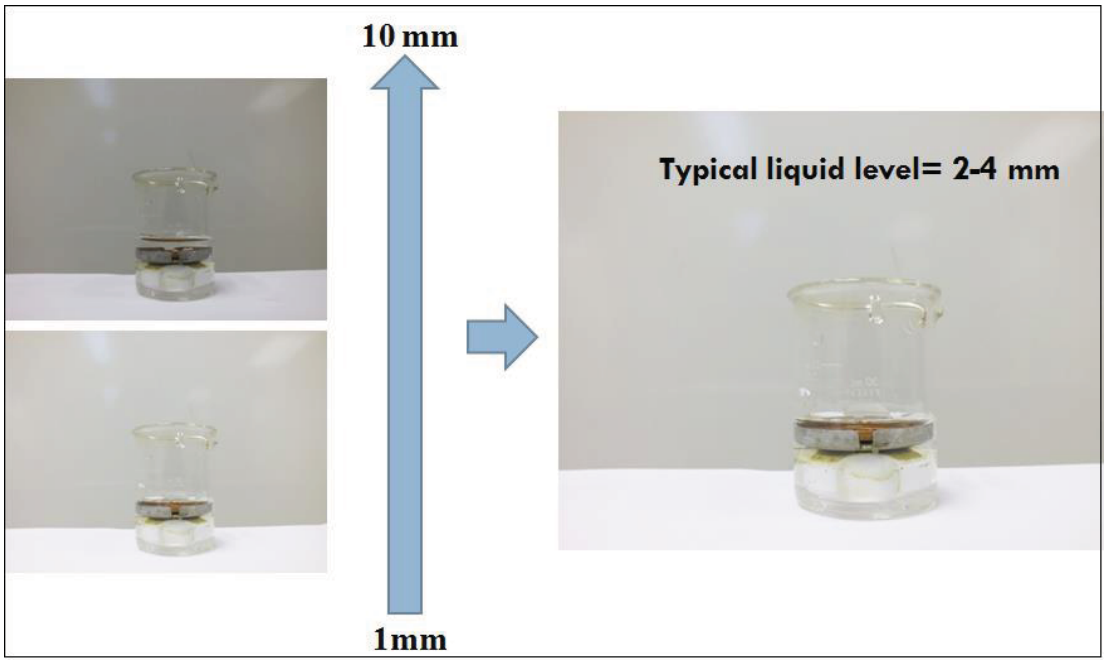

Figure 3-5 Photographs of the glass cell and the magnetic rotator with different volumes of liquid.

3. The height of the magnetic rotator:

   Two different designs of magnetic holders were used in the experiment as shown in Fig. 3-6-a and -b. Design (b) gives better results, because it allows one to use 7 ml of liquid while one can use just 3 ml in design (a) when typical liquid level above target in both of them is 2 mm. The lesser amount of liquid in design (a) means higher concentration of ablated material for the same period of time and this means higher absorption, reflection and lower ablation efficiency.

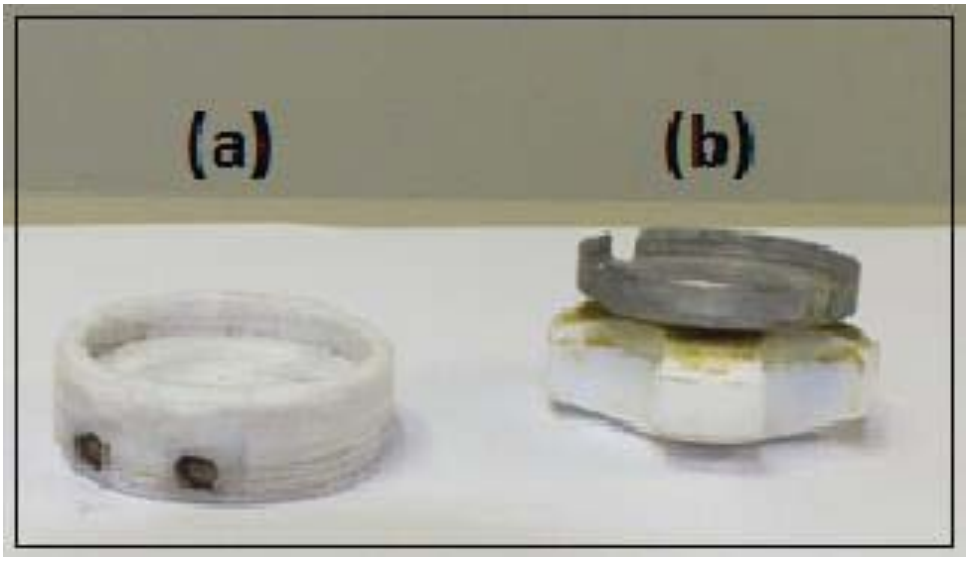

Figure 3-6 Photographs of different designs of magnetic rotator.

3.2 Characterization Techniques for Synthesized Nanoparticles

After 15 minutes of ablation, the produced colored colloidal suspension of nanostructured semiconductors were collected and dried in an oven at low temperature. The structure, composition and the morphology of the product material were investigated using X-ray diffraction spectroscopy (XRD), Energy Dispersive X-ray Spectroscopy (EDS), Field Emission Scanning Electron Microscopy (FE-SEM) and Transmission Electron Microscopy (TEM). The optical properties of nanostructured semiconductors were investigated using spectroflurometer (PL), UV-Vis spectrophotometer and Fourier Transform Infrared Spectroscopy (FTIR).

3.2.1 X-ray Diffraction (XRD)

The XRD was carried out using X-ray diffractometer (Shimadzu XRD Model 6000) using Cu-Kα radiation, operated at 40kV and 30mA. This system is located in the Surface Science Laboratory, Physics Department, King Fahd University of petroleum and minerals (KFUPM) and depicted in Fig. 3-7.

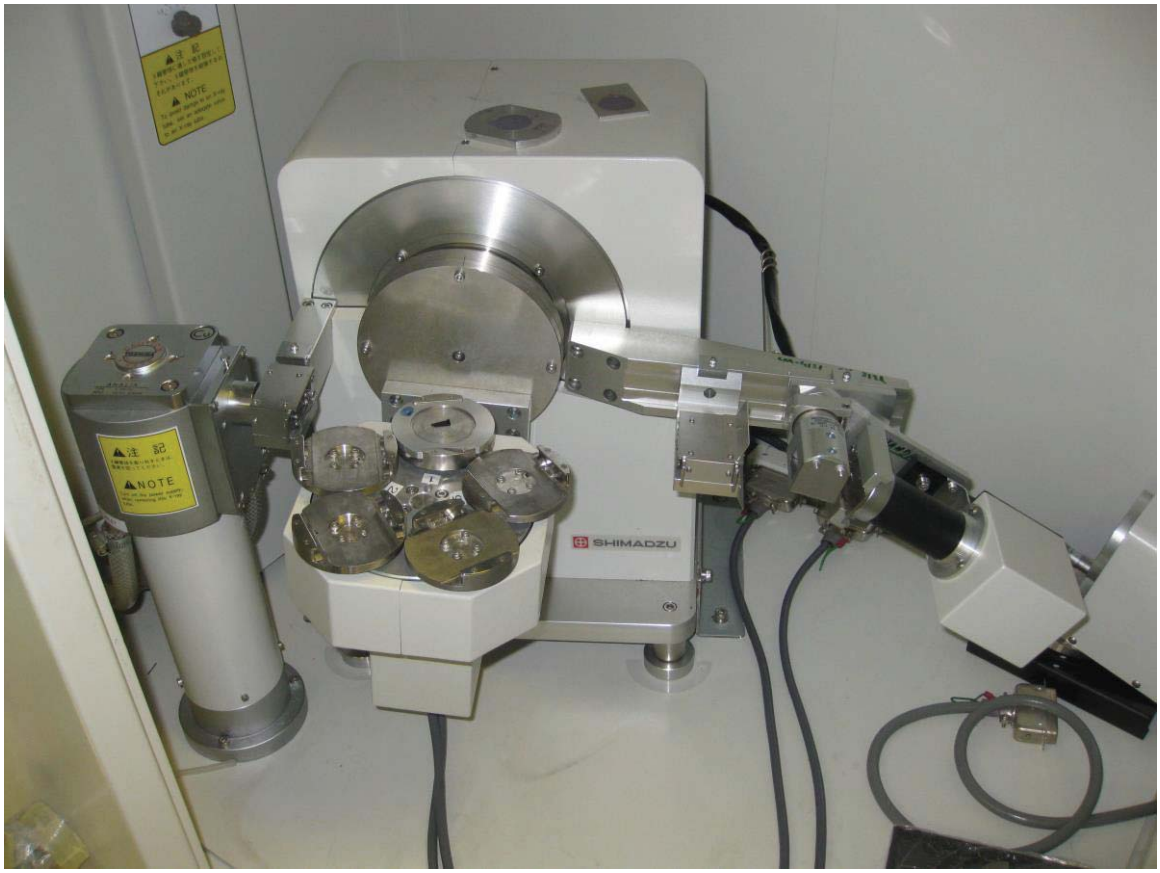

Figure 3-7 Photograph of the X-ray diffractometer used in this study.

3.2.2 Field Emission Scanning Electron Microscopy (FE-SEM)

For surface morphology studies the Field Emission Scanning Electron Microscopy (FESEM, TESCAN Ultra-High Resolution) was used by operating at 20kV with different magnification powers. This Scanning electron microscope is also equipped with an X-ray energy dispersive spectroscope (EDS) detector as shown in Fig. 3-8. This system is located in Center of Excellence in Nanotechnology (CENT), KFUPM.

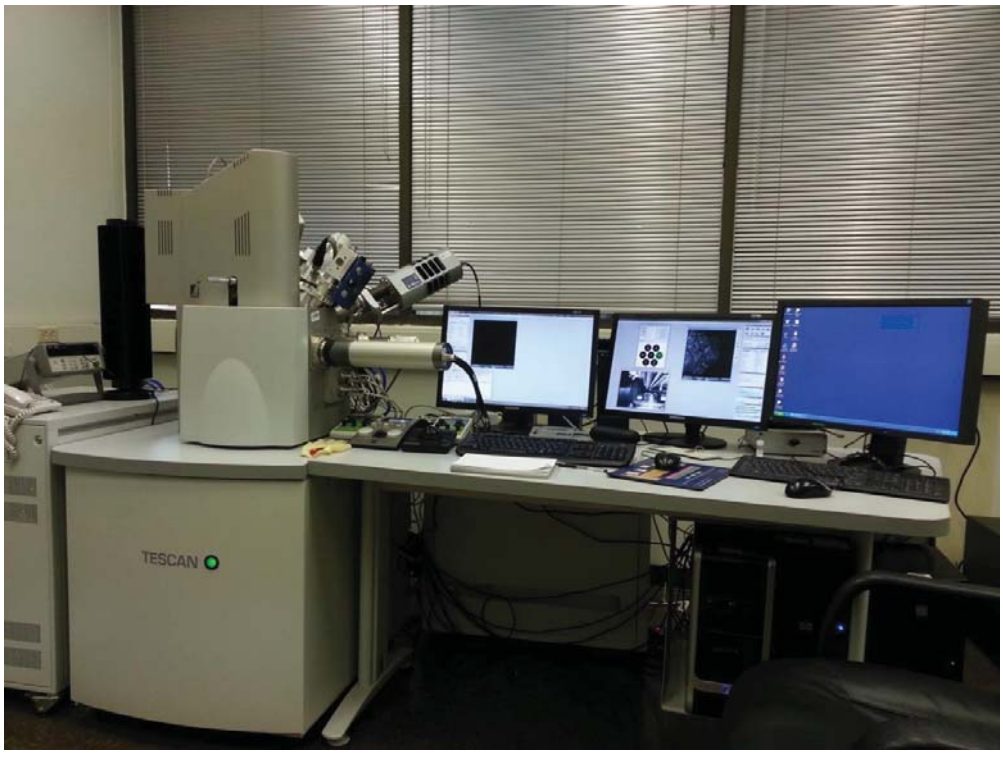

Figure 3-8 Photograph of FE-SEM and EDS systems used in this work.

3.2.3 High Resolution Transmission Electron Microscopy (HRTEM)

FEI Company's Titan 80-300 CT TEM instrument was employed to perform the conventional TEM (CTEM), selected area electron diffraction (SAED), X-ray energy dispersive spectroscopy (EDS), and electron energy loss spectroscopy (EELS) analyses of the nanostructured semiconductors. The microscope was operated by setting the electron beam to 300 keV. All the electron micrographs were recorded on a charged coupled device (CCD) camera of model US 4000 from Gatan, Inc. that is attached below the projection chamber of the microscope. Whereas the EELS spectra were recorded on another CCD camera of model US 1000 attached to end of electron energy filter of model GIF Tridiem from Gatan, Inc. The entire data acquisition and analysis were carried out in Gatan Microscopy Suite v.1.8.3 . This system is located in the Imaging and Characterization Core Lab, King Abdullah University of Science and Technology (KAUST) and depicted in Fig. 3- 9.

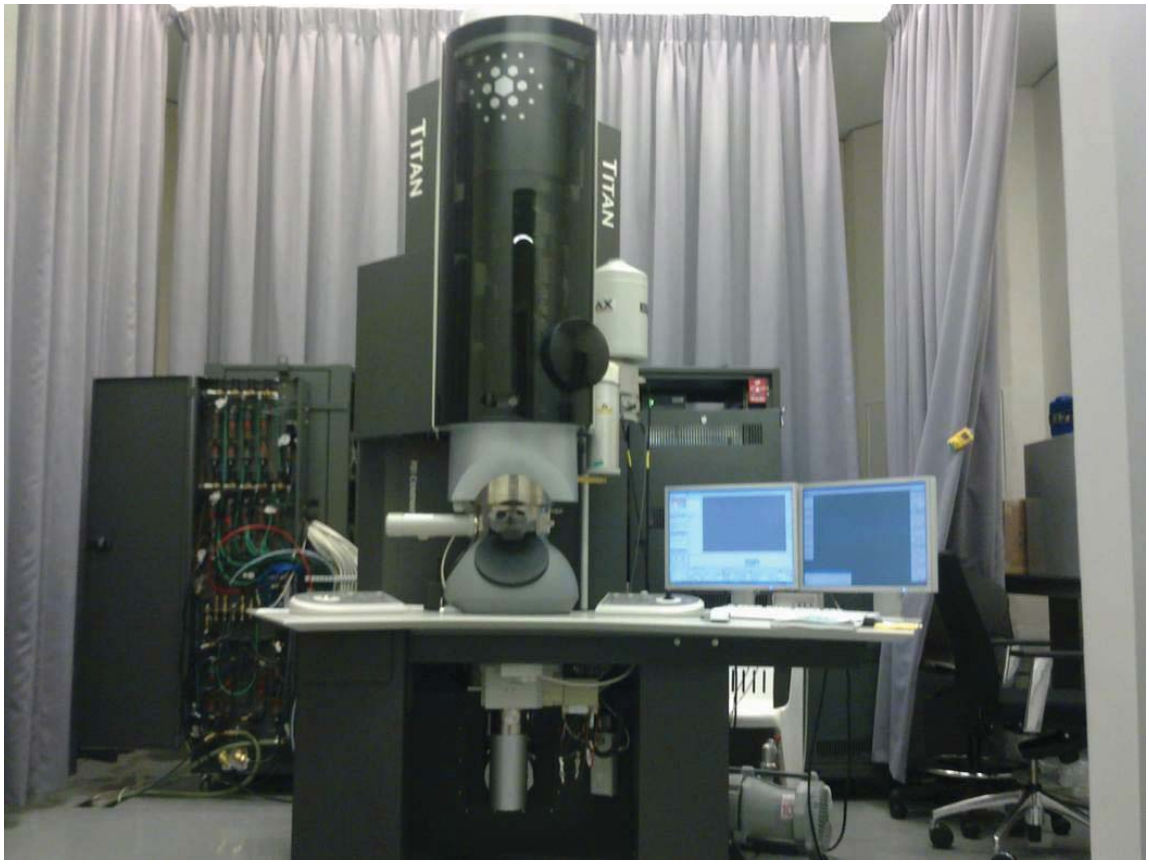

Figure 3-9 Photograph of HRTEM system used in this work.

3.2.4 UV-Vis Spectrophotometer for Band Gap Measurements

The UV-Vis absorption spectrum was obtained with the spectrophotometer (Jasco 670). This system is located in Laser Research group, Physics Department, KFUPM and depicted in Fig. 3-10.

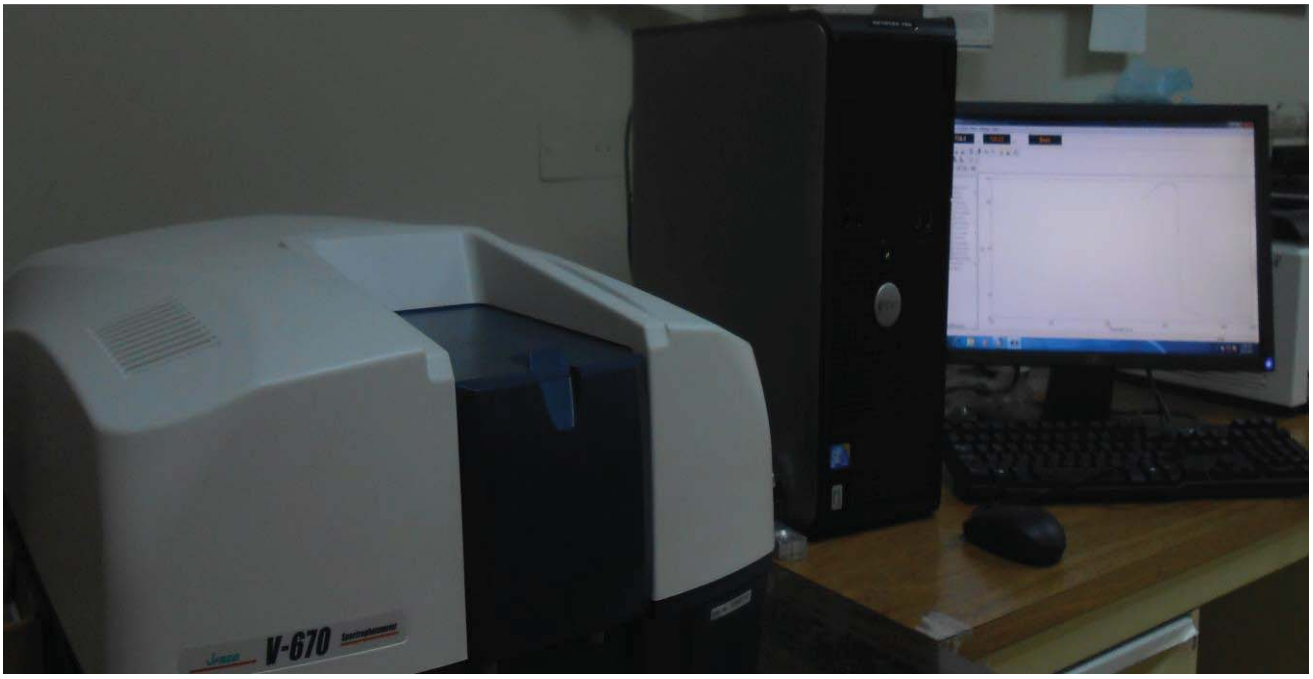

Figure 3-10 Photograph of UV-Vis spectrophotometer used in this work.

3.2.5 Spectroflurometer for Photoluminescence Study

The photoluminescence data were taken using Shimadzu Spectrofluorometer with 1200 grooves/mm, and with a suitable excitation wavelength. This system is located in the Laser Research group, CENT, KFUPM and depicted in Fig. 3-11.

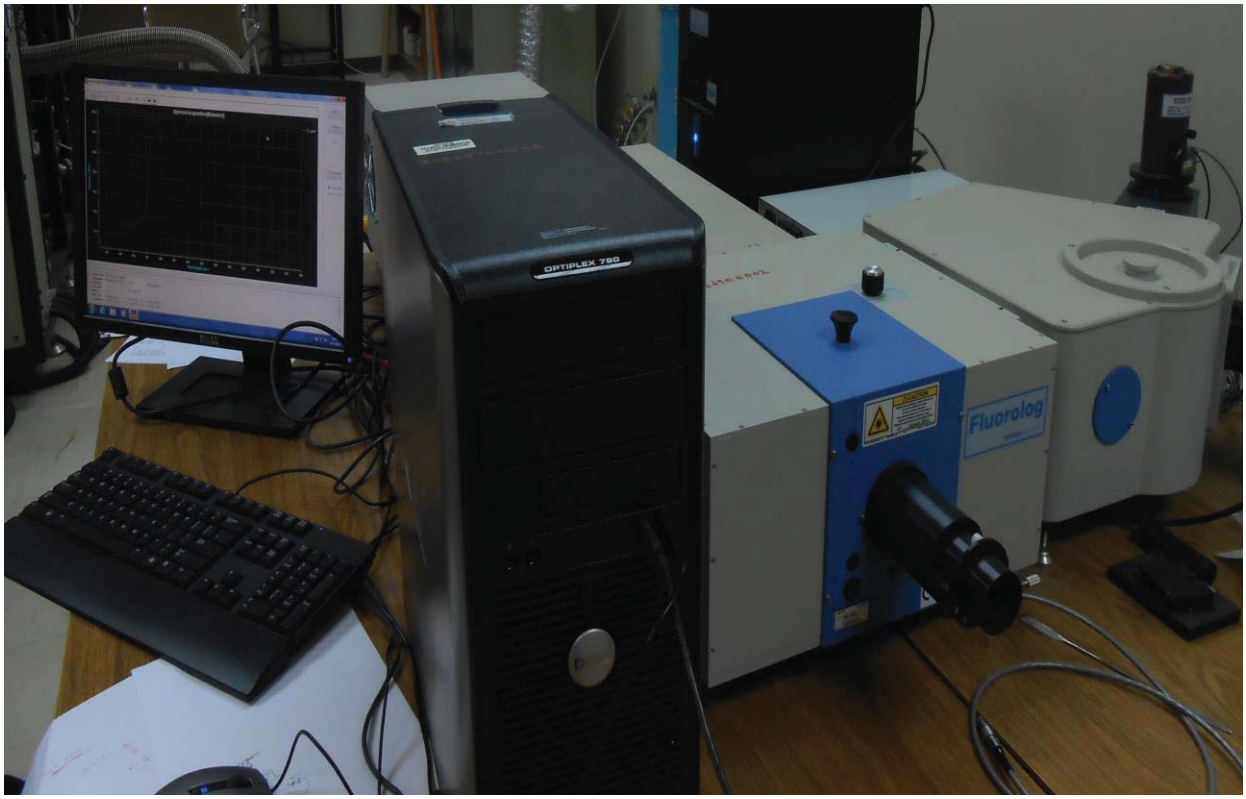

Figure 3-11 Photograph of Spectroflurometer used in this work.

3.2.6 Fourier Transform Infrared Spectroscopy (FTIR)

In order to confirm the type of bonding in the nanostructured semiconductors, the FTIR spectrum was measured and recorded on FTIR spectrophotometer using dry KBr as standard reference in the range of 400–4000 cm^{-1}. This system is located in the Chemistry Department, KFUPM and shown in Fig. 3-12.

Figure 3-12 Photograph of FT-IR spectrophotometer used in this work.

CHAPTER 4

RESULTS AND DISCUSSION

In this chapter, results and discussion regarding the synthesis of nanostructured semiconductors (copper oxides and CdSe NPs) using PLAL technique are presented. The composition, morphology and optical properties of the synthesized nanoparticles are also discussed.

4.1 Synthesis of Copper Oxides NPs

In this section, the synthesis of copper oxides NPs using PLAL technique is discussed. The effects of oxidizing medium and temperature on the composition, morphology and optical properties of the synthesized copper oxide NPs are presented in details in the following two subsections.

4.1.1 Effects of Oxidizing Medium

In this section, the effect of oxidizing media (different concentration of H_2O_2 mixed with DW) on the composition, morphology and optical properties of the synthesized nanoparticles is described. The experimental setup depicted in Fig. 3-1 was employed for this purpose. The target used was 1mm thick metallic copper (purity 99.99% Advent Research Materials Ltd) and it was fixed on the magnetic rotator which was immersed in the liquid medium in the glass cell. Typical energy density and the liquid level above the target surface were 3 J/cm^2 and 2 mm respectively. In this study, we kept all the experimental parameters the same except the concentrations of H_2O_2 in the DW. Different concentrations of hydrogen peroxide (1, 3 and 5% by volume) were added in

the DW during the experiment. After 15 minutes of ablation, the synthesized colored colloidal suspension was collected and dried at a temperature of 40 ^{o}C for 3 hours. The products obtained from PLAL process were characterized with the analytical tools such as, XRD, EDS, TEM, HRTEM, UV-VIS absorption, Photoluminescence and FTIR. The results indicated that the higher concentration of H_2O_2 favors not only the production of Cu/CuO but also reshape the copper oxide nanostructures. As it is evident from Fig. 4-1, the suspension of synthesized nanomaterial in the liquid medium show different colors, the darkest one on the left side is the synthesized nanomaterial made without the presence of H_2O_2 in liquid medium.

This dark color is due to the presence of predominant copper and Cu_2O in the product material and as we use higher concentration of H_2O_2 in liquid medium, the color of the suspension of the synthesized nanomaterial gets lighter, indicating the presence of less copper and more CuO, which will be more evident from the subsequent discussions below. The possible chemical reactions between the removed copper NPs due to the ablation and the liquid medium (H_2O/H_2O_2) are as follows:

$$2Cu + 2H_2O\ (h\nu_{532\ nm}) \rightarrow 2CuOH + H_2$$

$$2CuOH \rightarrow Cu_2O + H_2O$$

$$2Cu_2O + H_2O_2 \rightarrow 4CuO + H_2,$$

With the increased concentration of H_2O_2, there could be a significant increase in the conversion of Cu_2O into CuO as depicted in the following chemical reaction.

$$2Cu + H_2O_2 \rightarrow Cu(OH)_2 \quad \text{and } Cu(OH)_2 \rightarrow CuO + H_2O$$

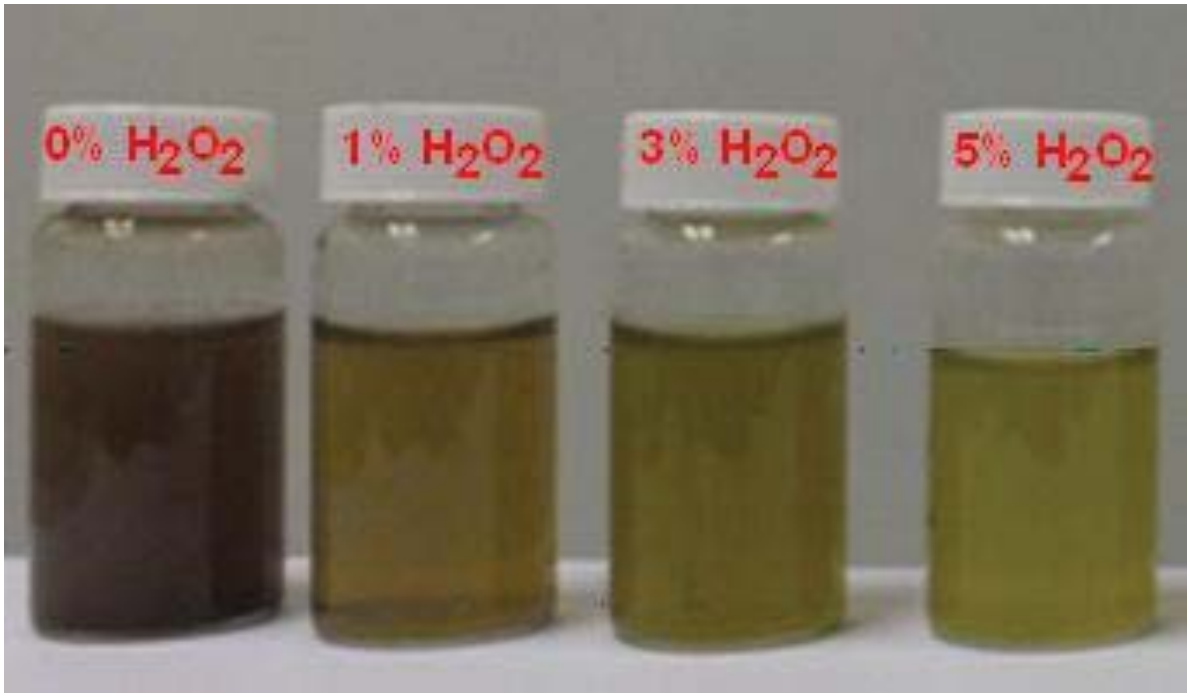

Figure 4-1 The appearance and color of the synthesized nanomaterial samples by varying the concentrations of H_2O_2 in the DW as indicated in the figure.

4.1.1.1 Structure and Morphology of Synthesized Material

EDS spectra for a selected 16 μm^2 on the surface of the prepared samples are presented along with the quantifications annotated in the inset in Fig. 4-2, 4-3, 4-4 and 4-5 respectively.

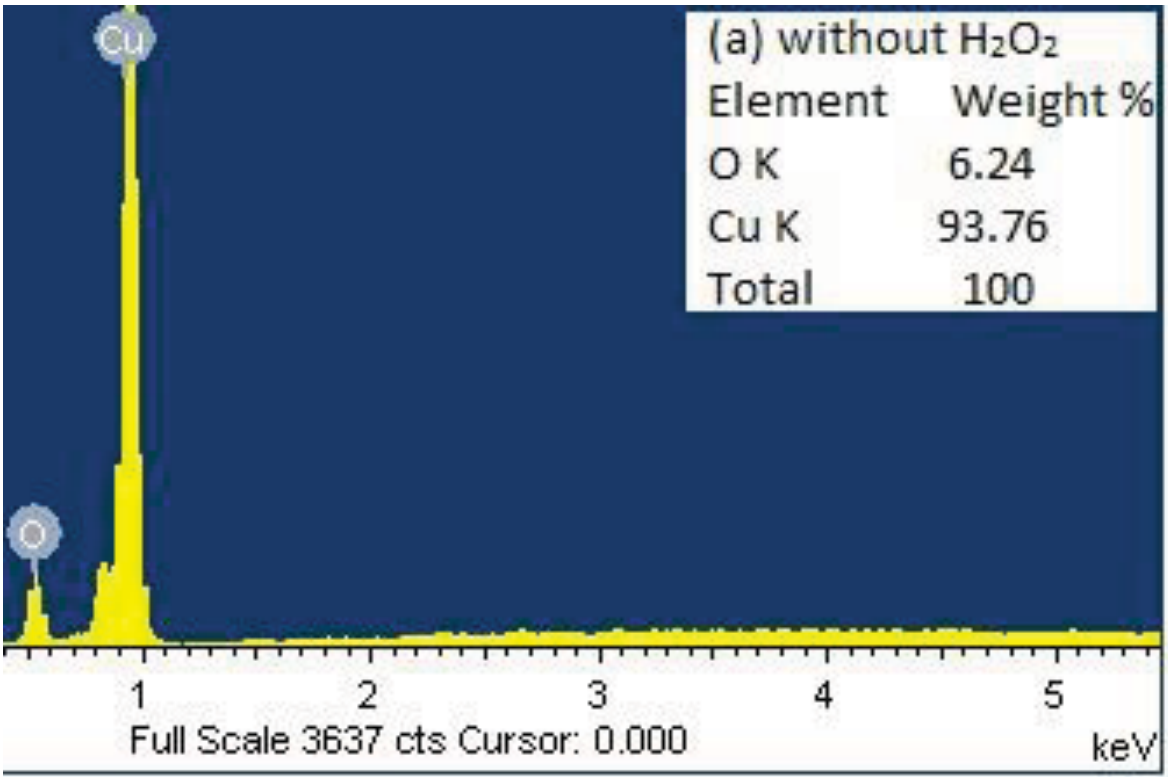

Figure 4-2 EDS spectrum of the synthesized nanomaterial in 0 % of H_2O_2 in the DW as indicated on the figure.

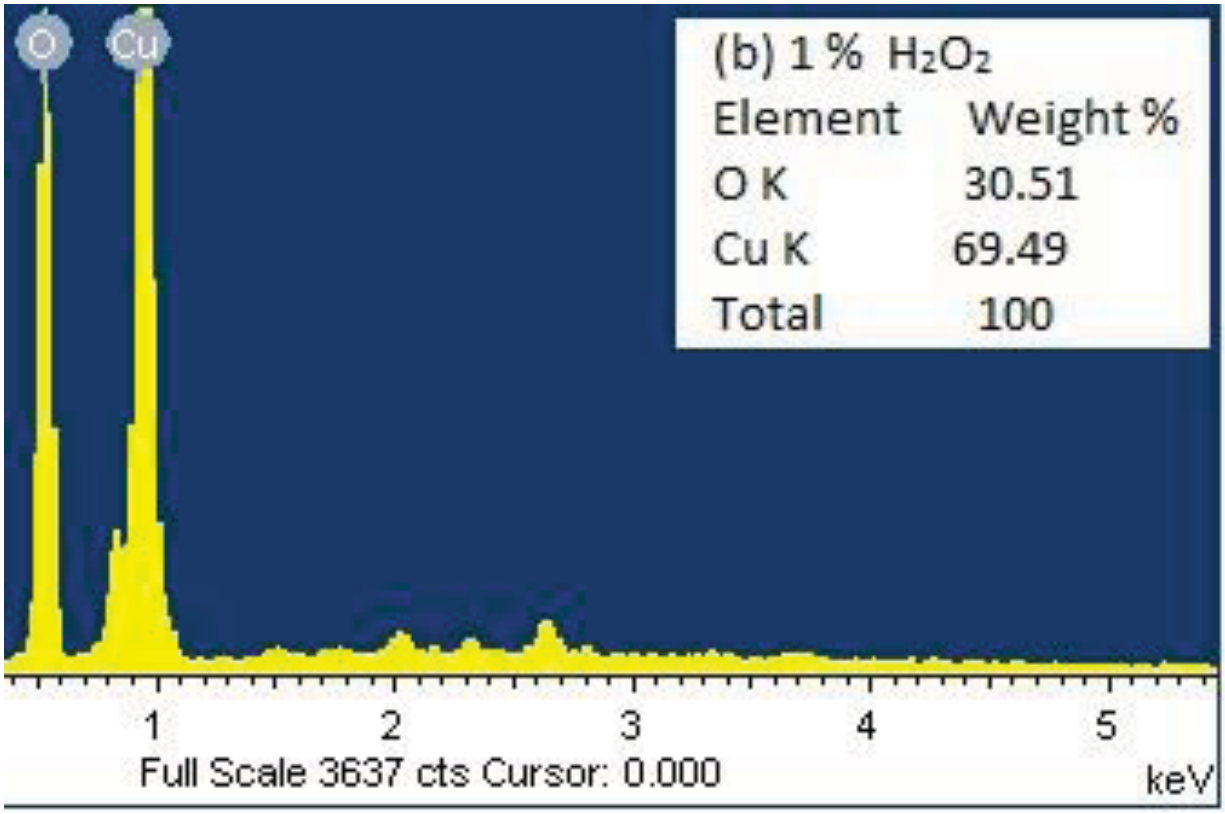

Figure 4-3 EDS spectrum of the synthesized nanomaterial in 1 % of H_2O_2 in the DI water as indicated on the figure.

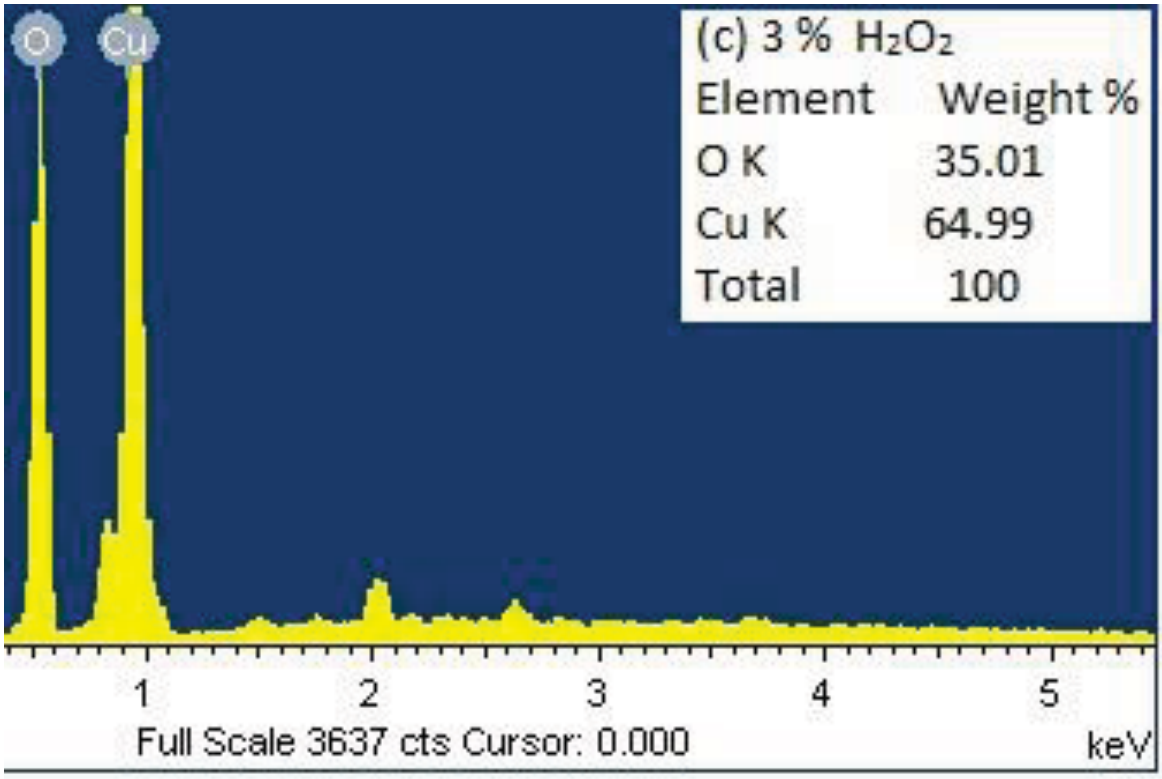

Figure 4-4 EDS spectrum of the synthesized nanomaterial in 3 % of H_2O_2 in the DW as indicated on the figure.

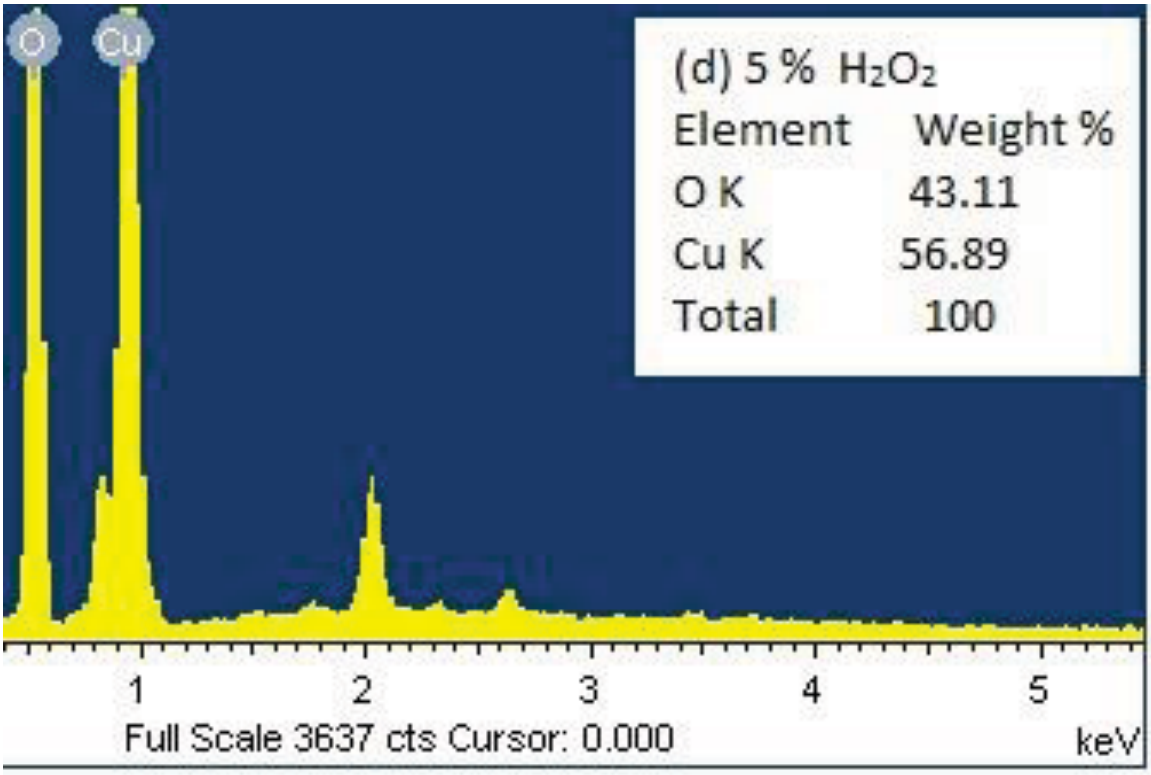

Figure 4-5 EDS spectrum of the synthesized nanomaterial in 5 % of H_2O_2 in the DW as indicated on the figure.

The presence of copper and oxygen in the EDS confirms the presence of copper oxide and also the results showed the increase of the relative mass percentage of oxygen to copper with the increased concentration of H_2O_2 as clear from Fig. 4-2 through 4-5. The additional peak at about 2 keV may be from the coating material. X-ray diffraction patterns of the synthesized nanomaterial are shown in Fig. 4-6, -7, -8 and -9.

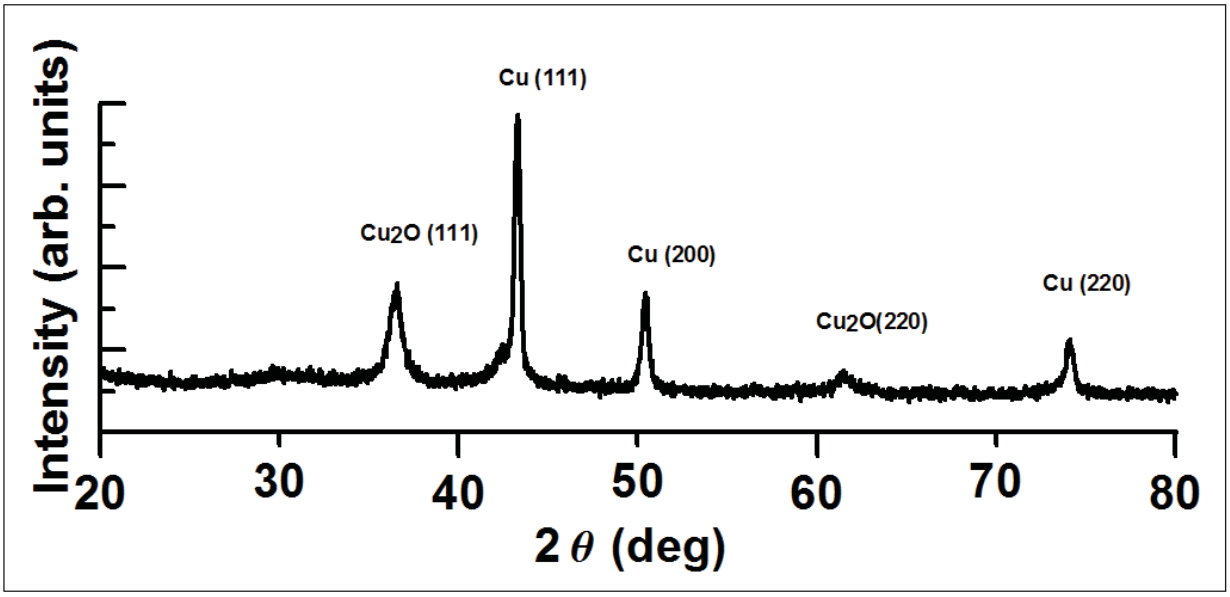

Figure 4-6 X-ray diffraction of the synthesized nanomaterial in 0 % of H_2O_2 in the DW.

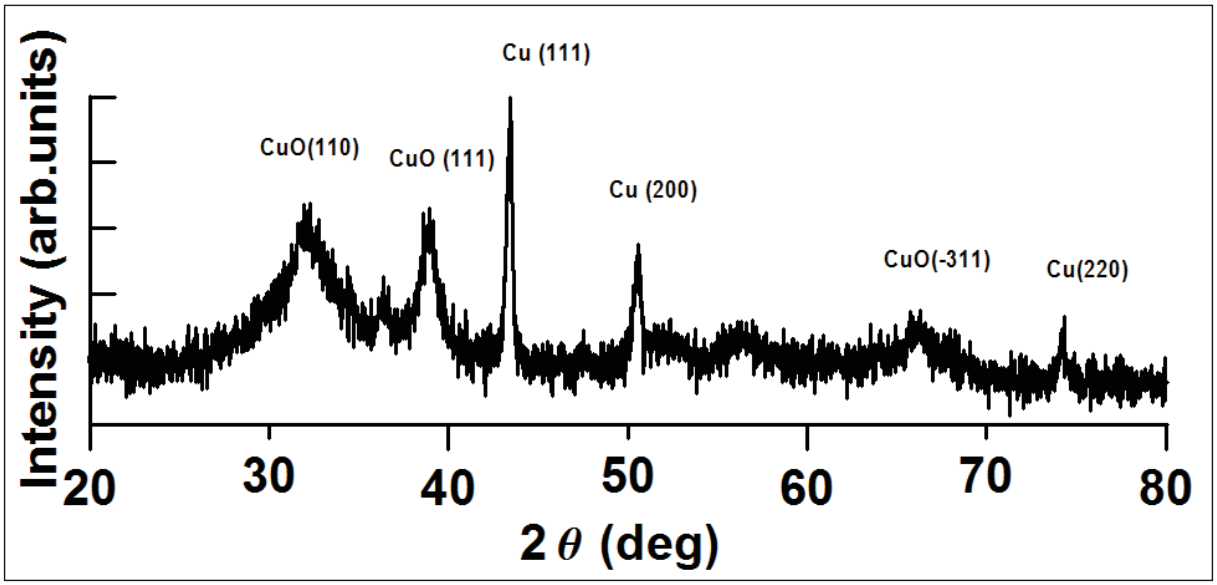

Figure 4-7 X-ray diffraction of the synthesized nanomaterial in 1 % of H_2O_2 in the DW.

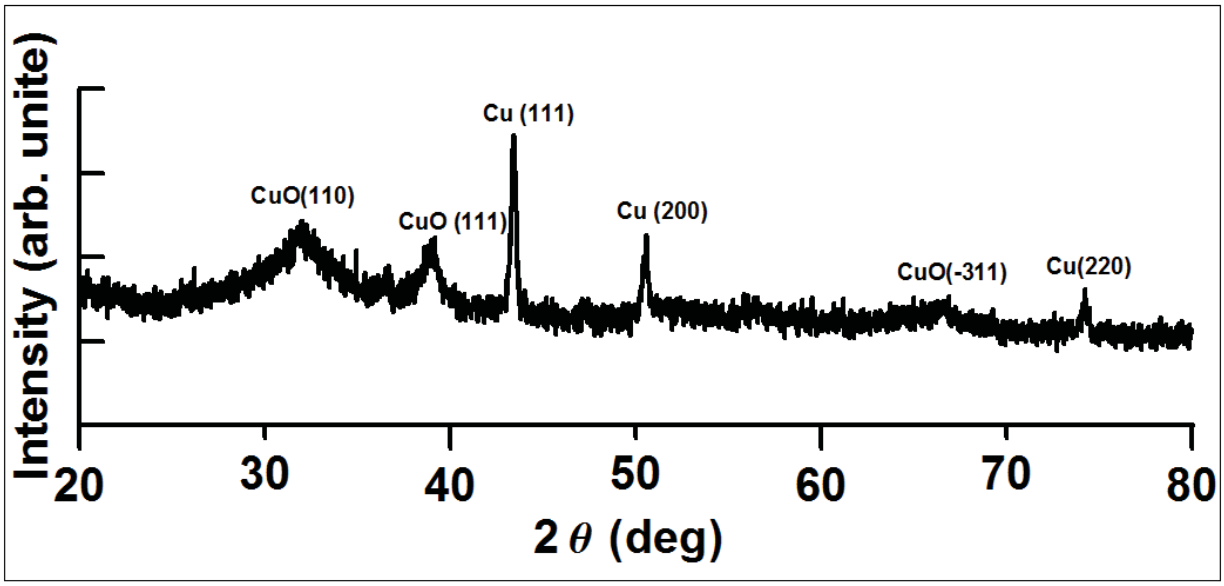

Figure 4-8 X-ray diffraction of the synthesized nanomaterial in 3 % of H_2O_2 in the DW.

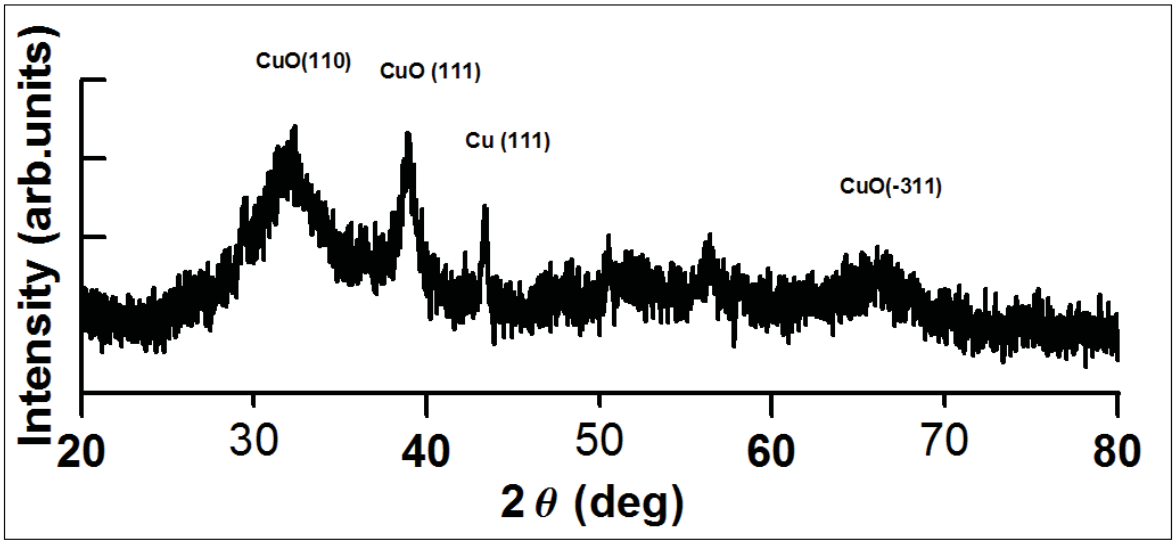

Figure 4-9 X-ray diffraction of the synthesized nanomaterial in 5 % of H_2O_2 in the DW.

In the absence of H_2O_2 in DW, the two phases present in the synthesized material are Cu and Cu_2O as shown in Fig. 4-6 and as 1% of H_2O_2 is added to the liquid medium, the Cu_2O in the product material disappears and CuO appears and its level in the product material increases with the increase of H_2O_2 from 1% to 5% (Fig. 4-7, 4-8 and 4-9) and this result is understandable from the increased oxygen in the liquid medium. The XRD results substantiate the results of EDS. In addition to this, it is quite clear from Fig. 4-7, 4-8 and 4-9 that the FWHM of copper diffraction peaks is smaller than that of cupric oxide ones, indicating that the mean crystal size of the copper grains is higher than that of cupric oxide.

In addition to the change of phase composition of the product material with increased H_2O_2 concentration, there is a change of the shape of the nanostructure observed with the increased H_2O_2 concentration. It is clear from the TEM image in Fig. 4-10 with no H_2O_2 present, the product material show spherical shape with an average size less than 10 nm, whereas the synthesized nanomaterial with 5% H_2O_2 concentration in DW (Fig. 4-12) shows rod-like nanostructure. HRTEM images of product material with 0% and 5% H_2O_2 concentration (Fig. 4-11 and 4-13 respectively) show the random orientations of the small crystals indicating the polycrystalline nature of the synthesized nanomaterials. In addition, the crystallization of the synthesized nanomaterial in 0% of H_2O_2 is much better than that in 5% H_2O_2 which is in a good agreement with XRD patterns.

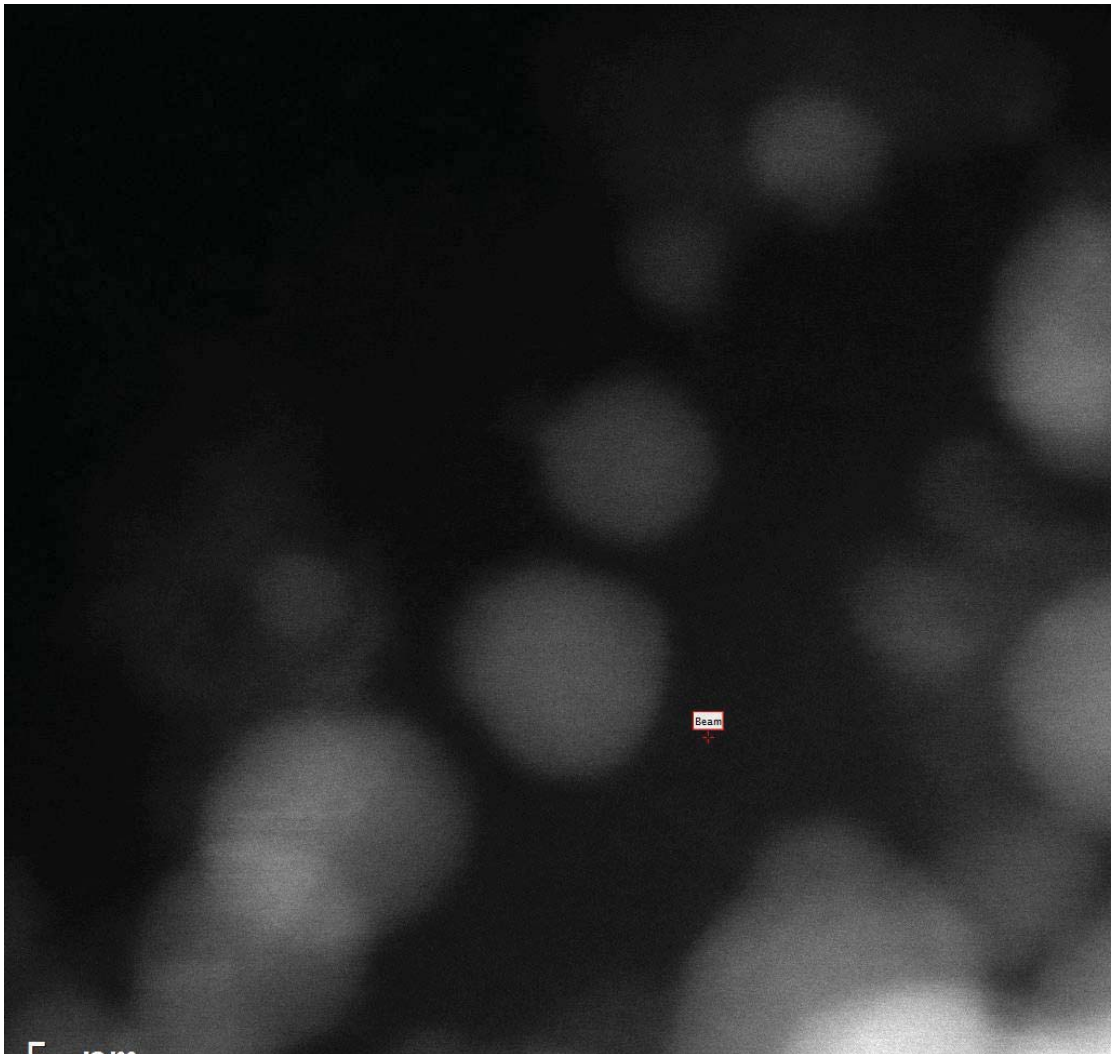

Figure 4-10 TEM image of the synthesized nanomaterial in 0% of H_2O_2 in the DW.

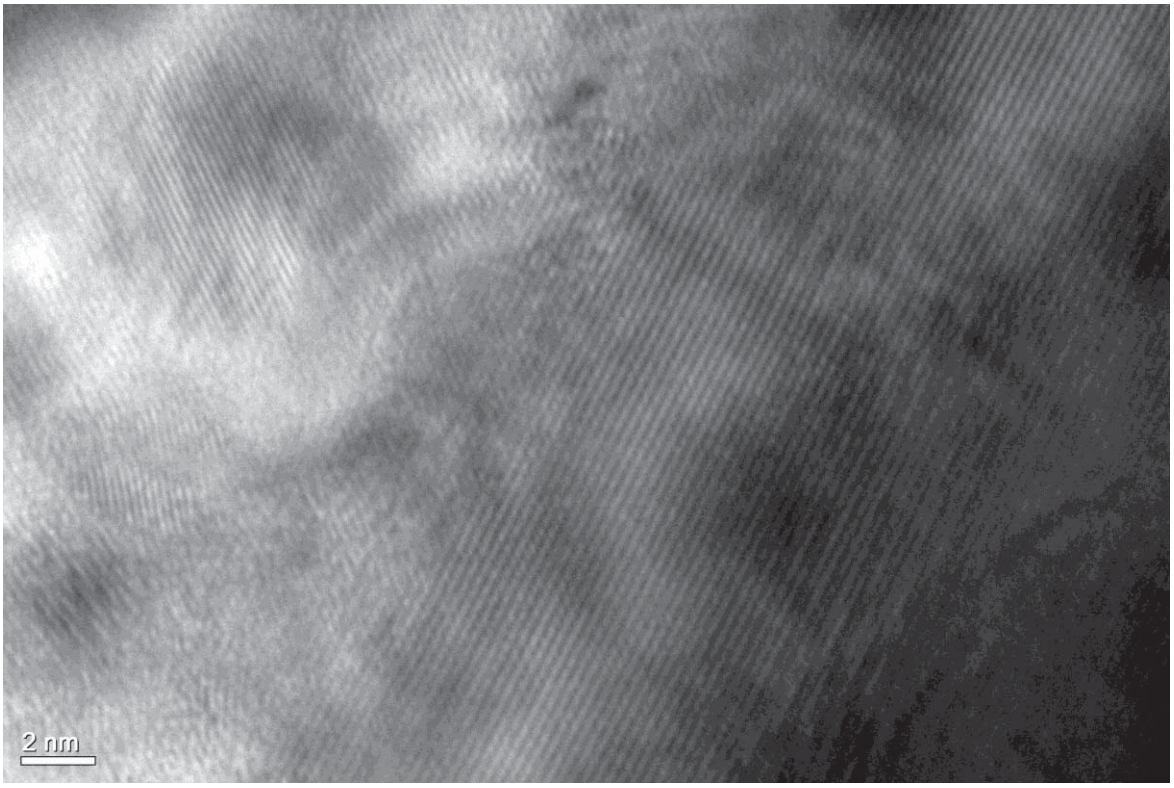

Figure 4-11 HRTEM image of the synthesized nanomaterial in 0% of H_2O_2 in the DW.

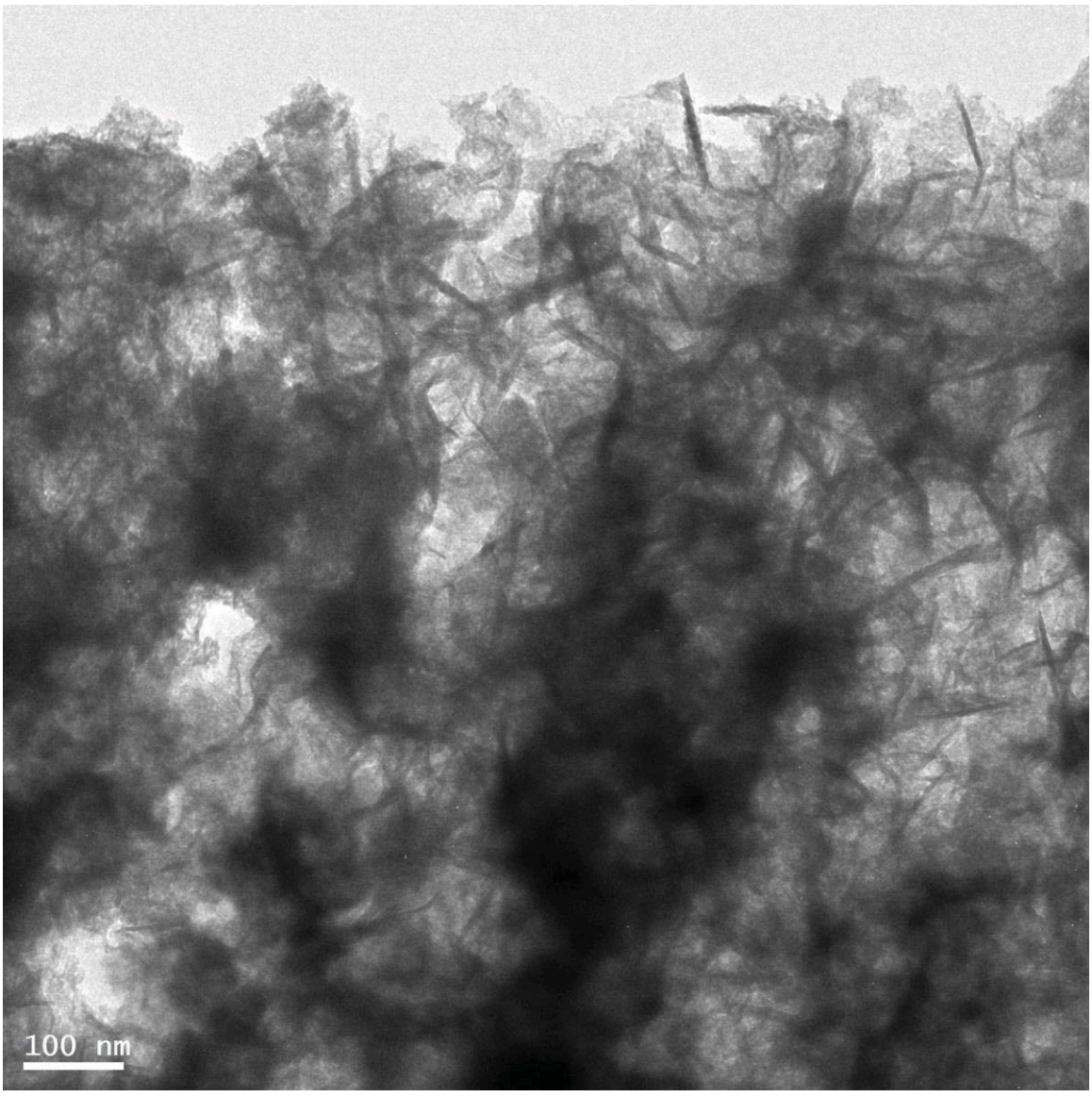

Figure 4-12 TEM image of the synthesized nanomaterial in 5% of H_2O_2 in the DW.

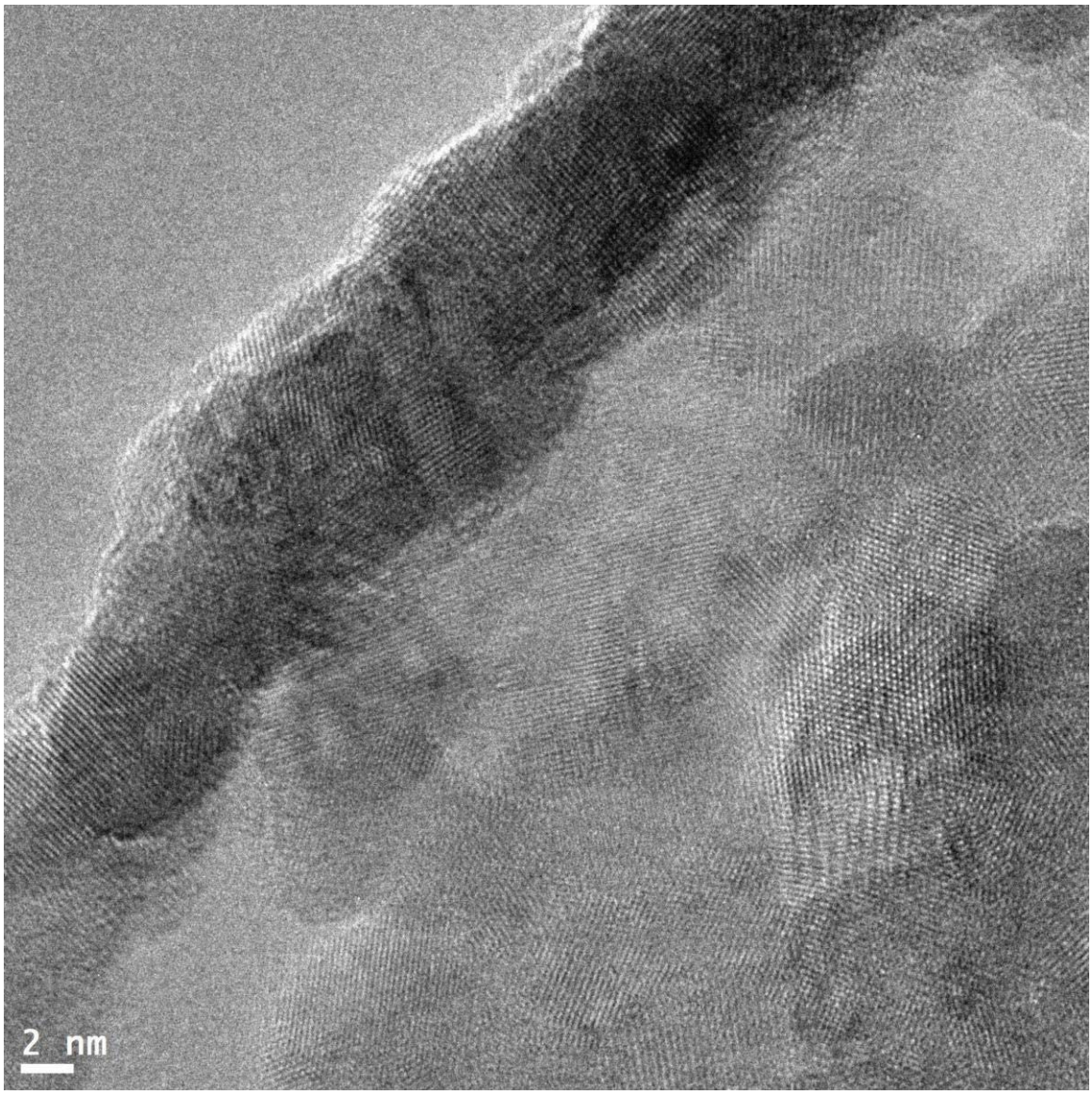

Figure 4-13 HRTEM image of the synthesized nanomaterial in 5% of H_2O_2 in the DW.

4.1.1.2 Optical Characterization of the synthesized Material

Optical characterization such as absorption, photoluminescence, and FTIR was also carried out on the synthesized nanomaterials at room temperature. For all the absorption spectra depicted in Fig. 4-14, 4-15, 4-16 and 4-17, the incident laser beam parameters were kept constant except that the concentration of H_2O_2 present in the liquid medium. Fig. 4-14 for 0% H_2O_2 in DW, Fig. 4-15 for 1% H_2O_2 in DW, Fig. 4-16 for 3% H_2O_2 in DW, Fig. 4-17 for 5% H_2O_2 in DW.

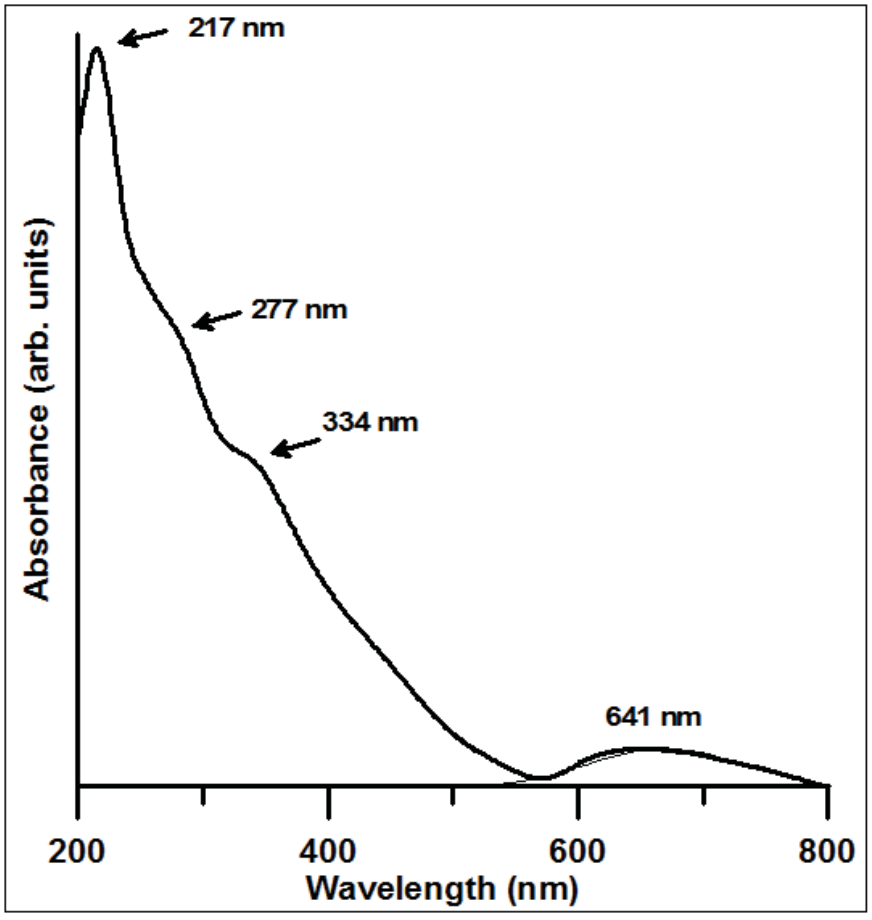

Figure 4-14 Absorption spectrum of synthesized nanomaterial in 0 % of H_2O_2 in the DW.

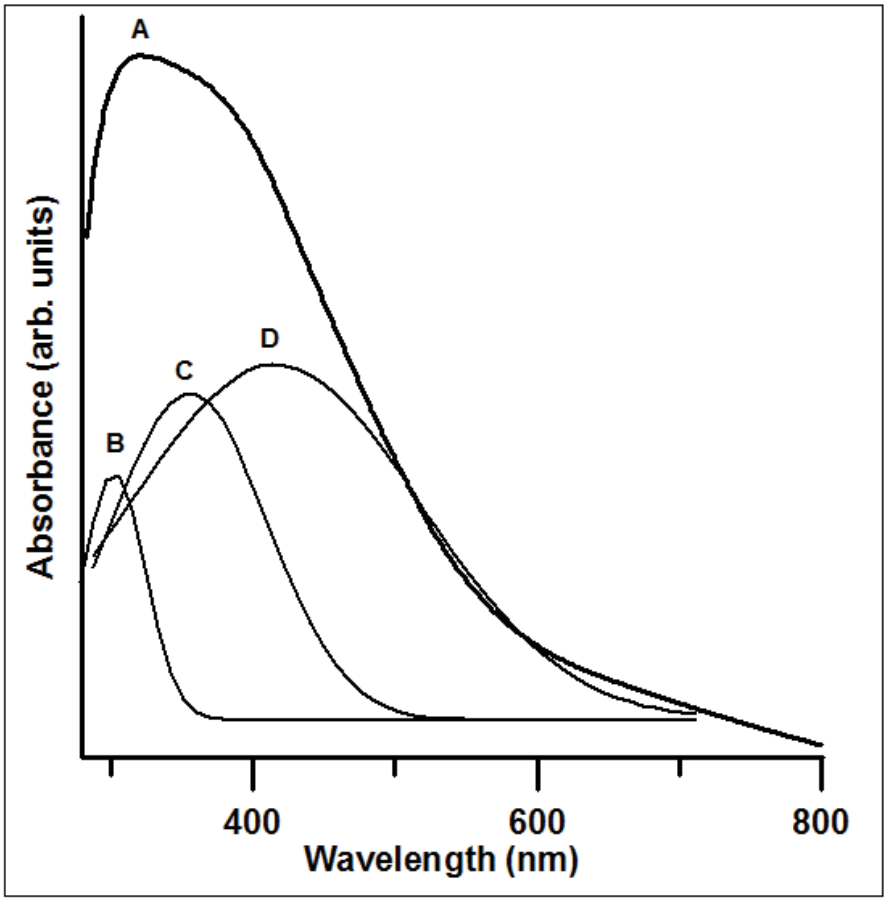

Figure 4-15 Absorption spectrum (A) of synthesized nanomaterial in 1 % of H_2O_2 in the DI water. The Guassian Peak fit is shown in (B), (C) and (D).

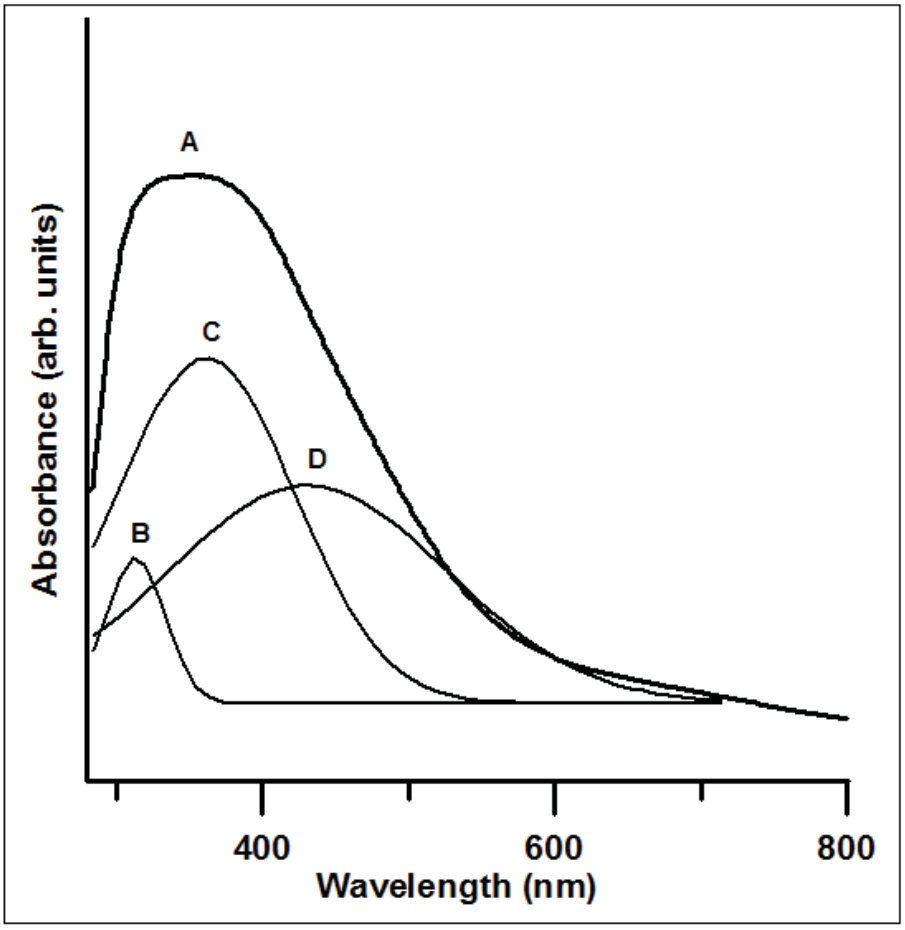

Figure 4-16 Absorption spectrum (A) of synthesized nanomaterial in 3 % of H_2O_2 in the DI water. The Guassian Peak fit is shown in (B), (C) and (D).

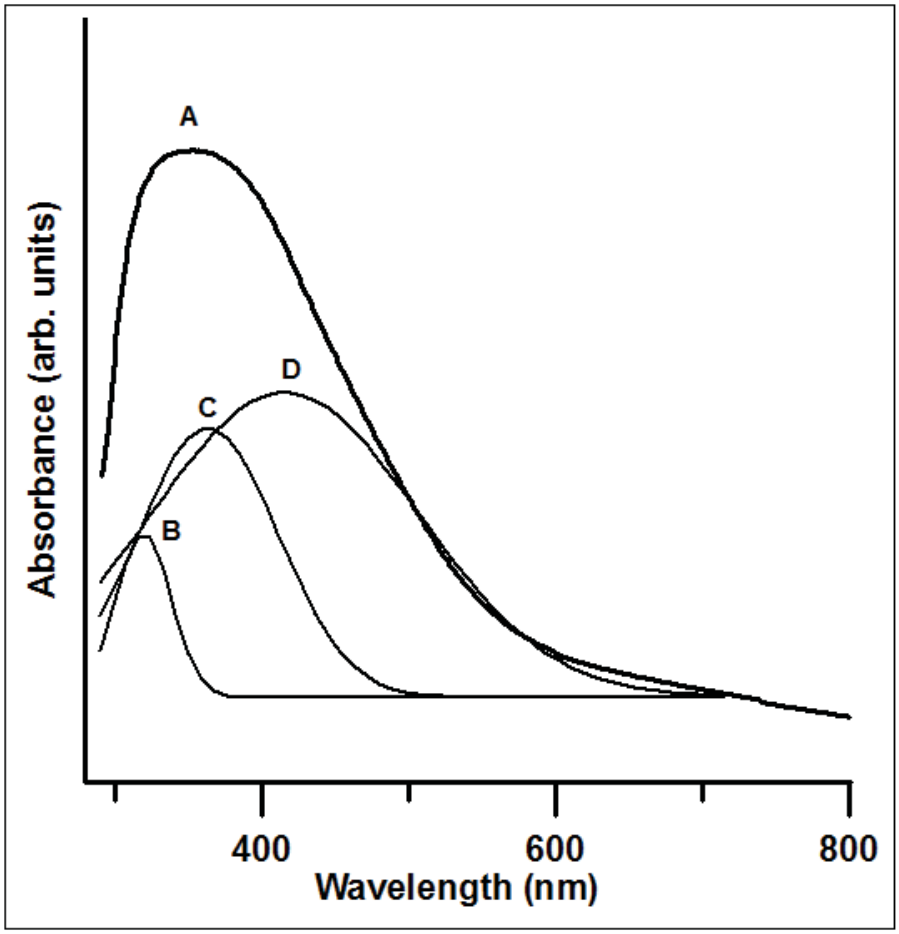

Figure 4-17 Absorption spectrum (A) of synthesized nanomaterial in 5 % of H_2O_2 in the DW. The Guassian Peak fit is shown in (B), (C) and (D).

In the absence of H_2O_2 in the liquid medium (Fig. 4-14), the product material show four peaks of which the most intense is at 217 nm is due to the inter-band transition of copper electrons close to Fermi levels, the broad peak at 641 nm is due to surface Plasmon resonance of Cu [55, 82-83] and the absorption peaks at 334 nm 277 nm are due to the Brillouin transitions of cuprous oxide [55, 82-83]. With the addition of H_2O_2 in DW, the absorption spectra (A) of the product material as indicated in Fig. 4-15, 4-16and 4-17 are broadened indicating the presence of multiple peaks. So we carried out Guassian curve fitting on these broad peaks and found three component peaks (peak B, peak C and peak D) in the absorption spectra. Further increase of concentration of H_2O_2 in DW does not make any substantial change in the characteristics of the component peaks except a minor change in their relative intensities. As the structure and the shape of the synthesized nanomaterial change with the addition of H_2O_2, the plasmonic resonance peak of Cu at 641 nm is absent, which supports our earlier results. Peak B and C are respectively at 313 nm and 359 nm. The peak at 313 is due to the shape induced charge transfer between 2p oxygen orbital and 4s bands of Cu^{2+} ions and the peak at 359 nm is due to $O^{2-} \rightarrow Cu^{2+}$ charge transfer [55, 84-85]. The origin of peak D needs to be investigated further.

The band gap energy of the semiconductor material can be estimated using Tauc equation [86]:

$$\alpha E = A(E - E_g)^n \qquad (1)$$

Where (α) is the absorption coefficient, (E) is the photon energy, (A) is a constant and n takes the value ½ and 2 respectively for allowed direct and allowed indirect transitions.

$$\alpha E = A(E - E_g)^{1/2} \quad (2)$$

From the absorption data, Tauc plots ($(\alpha E)^2$ versus E) are drawn to determine the band gap energies of the product materials synthesized with varying concentration of H_2O_2 in DW and are shown in Fig. 4-18 for 0% H_2O_2 in DW, Fig. 4-19 for 1% H_2O_2 in DW, Fig. 4-20 for 3% H_2O_2 in DW, Fig. 4-21 for 5% H_2O_2 in DW.

The Tauc plot shows a linear nature over a wide range of photon energy for n=1/2 (equation 2) for the ablated material, indicating that the synthesized material is of direct band gap semiconductor.

As it is obvious from the Tauc plots that the band gap energy drastically red shifted from 3.3 eV (376 nm) in the case of zero percent of H_2O_2 in DW (favoring Cu/Cu_2O) to approximately 2.5 eV (496 nm) with the addition of H_2O_2 in DW (favoring Cu/CuO). The minor variation in the band gap energies with increased concentrations of H_2O_2 in DW can be considered as an experimental variation. As transition metal oxides in general, and copper oxide in particular are good photocatalysts, the red shift brought about in copper oxide by the addition of H_2O_2 in the liquid medium is quite advantageous for any photocatalytic applications. H_2O_2 in the liquid medium shifted the band gap energy to 496 nm, which is active in the visible region of the solar spectrum and hence this material might be suitable as an effective photocatalyst for harnessing the solar radiation.

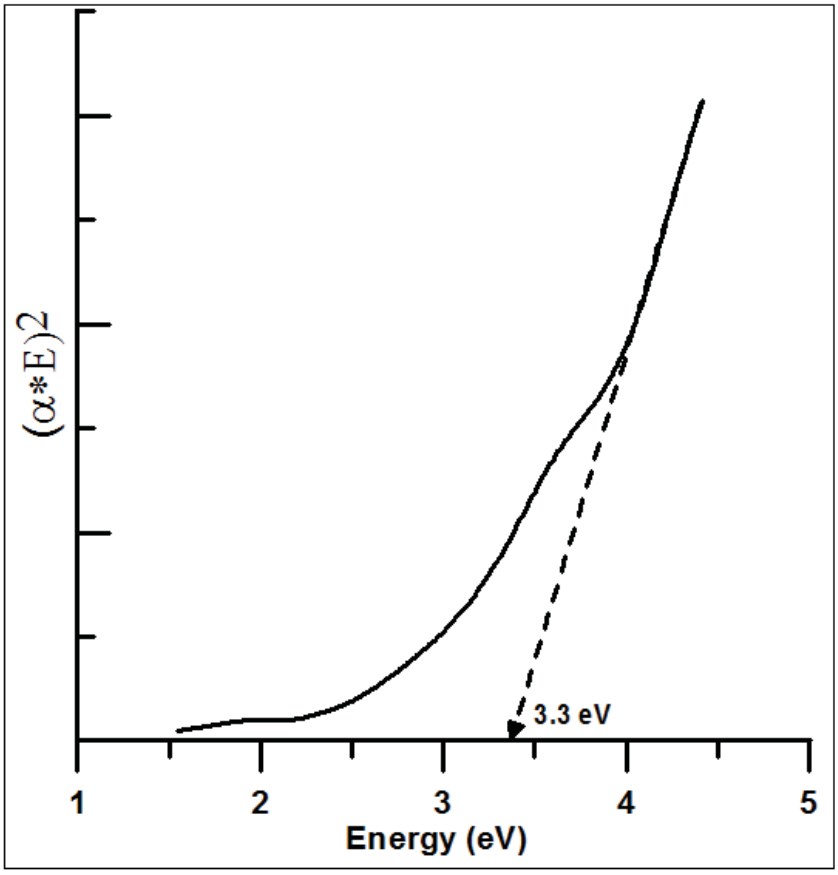

Figure 4-18 Tauc plot of the synthesized nanomaterial in 0 % of H_2O_2 in the DW.

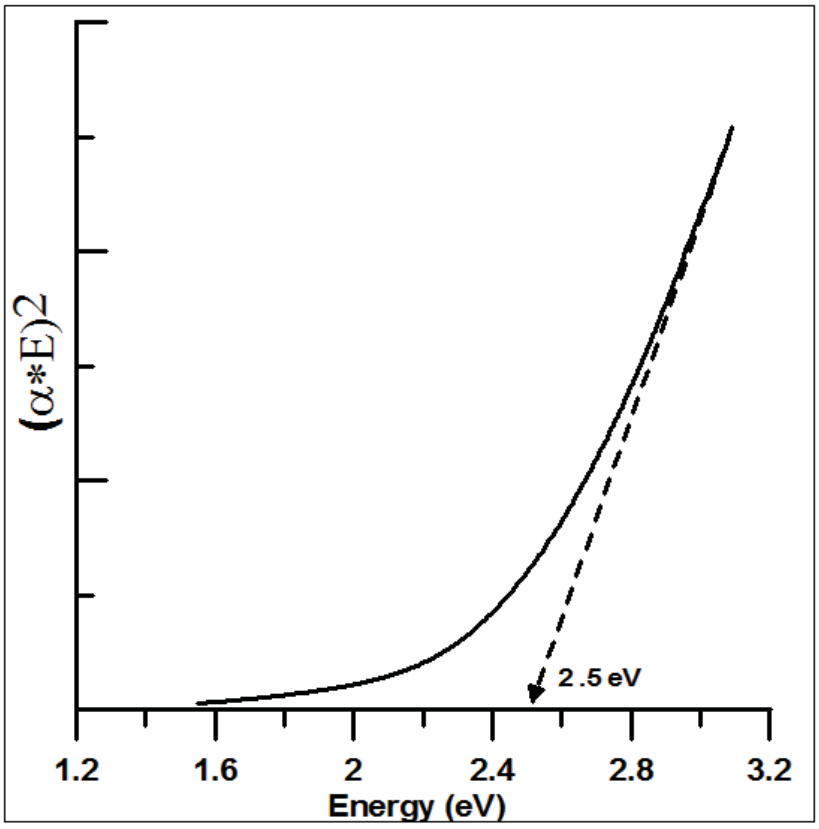

Figure 4-19 Tauc plot of the synthesized nanomaterial in 1 % of H_2O_2 in the DW.

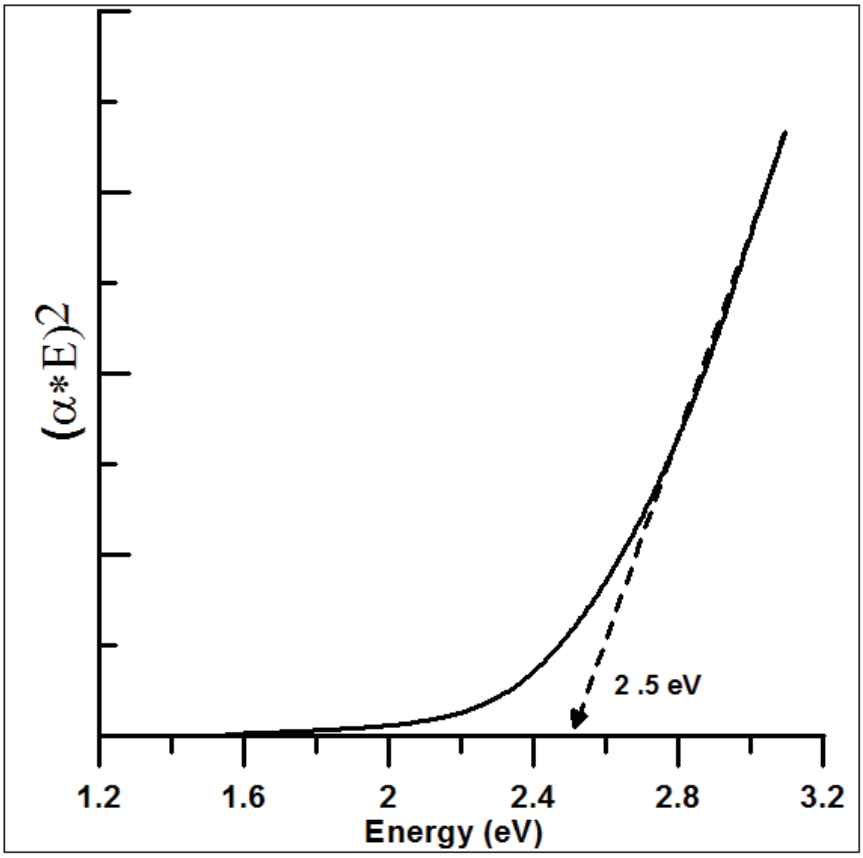

Figure 4-20 Tauc plot of the synthesized nanomaterial in 3 % of H_2O_2 in the DW.

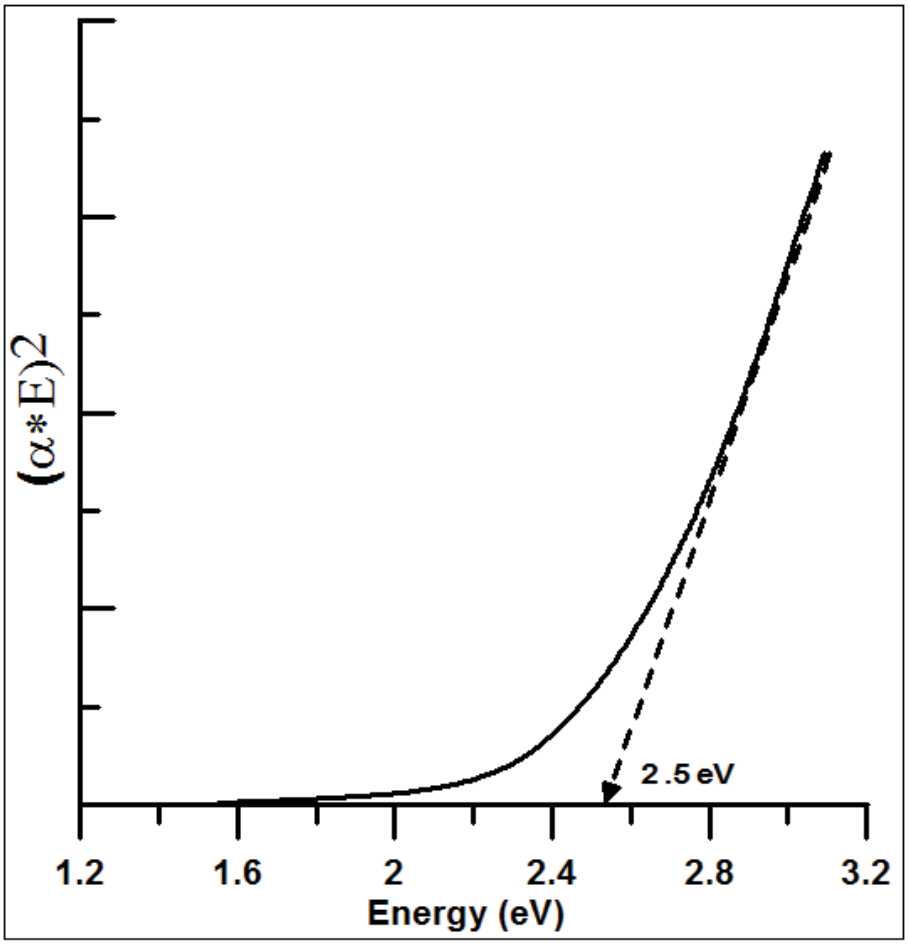

Figure 4-21 Tauc plot of the synthesized nanomaterial in 5 % of H_2O_2 in the DW.

The PL spectrum gives insight to study the efficiency of the charge carrier trapping and the electron-hole recombination in the semiconductor. Fig. 4-22, 4-23, 4-24, 4-25 depicts the photoluminescence (PL) spectra of the product material of PLAL synthesis process Fig. 4-22 for 0% H_2O_2 in DW, Fig. 4-23 for 1% H_2O_2 in DW, Fig. 4-24 for 3% H_2O_2 in DW, Fig. 4-25 for 5% H_2O_2 in DW. The excitation wavelengths are 283 nm and 330 nm for the synthesized samples in pure DW (0% H_2O_2) and different concentrations (1, 3 and 5 %) of H_2O_2 in DW respectively.

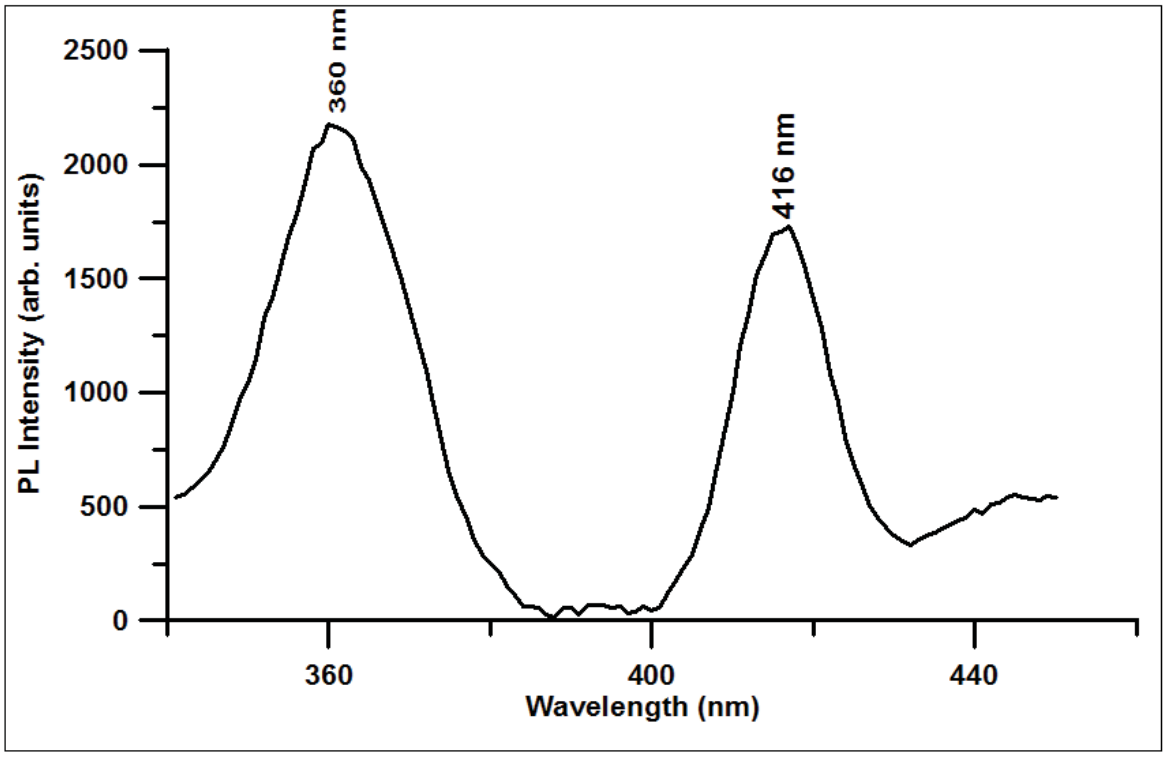

Figure 4-22 Photoluminescence emission spectrum of the synthesized nanomaterial in 0 % of H_2O_2 in the DW.

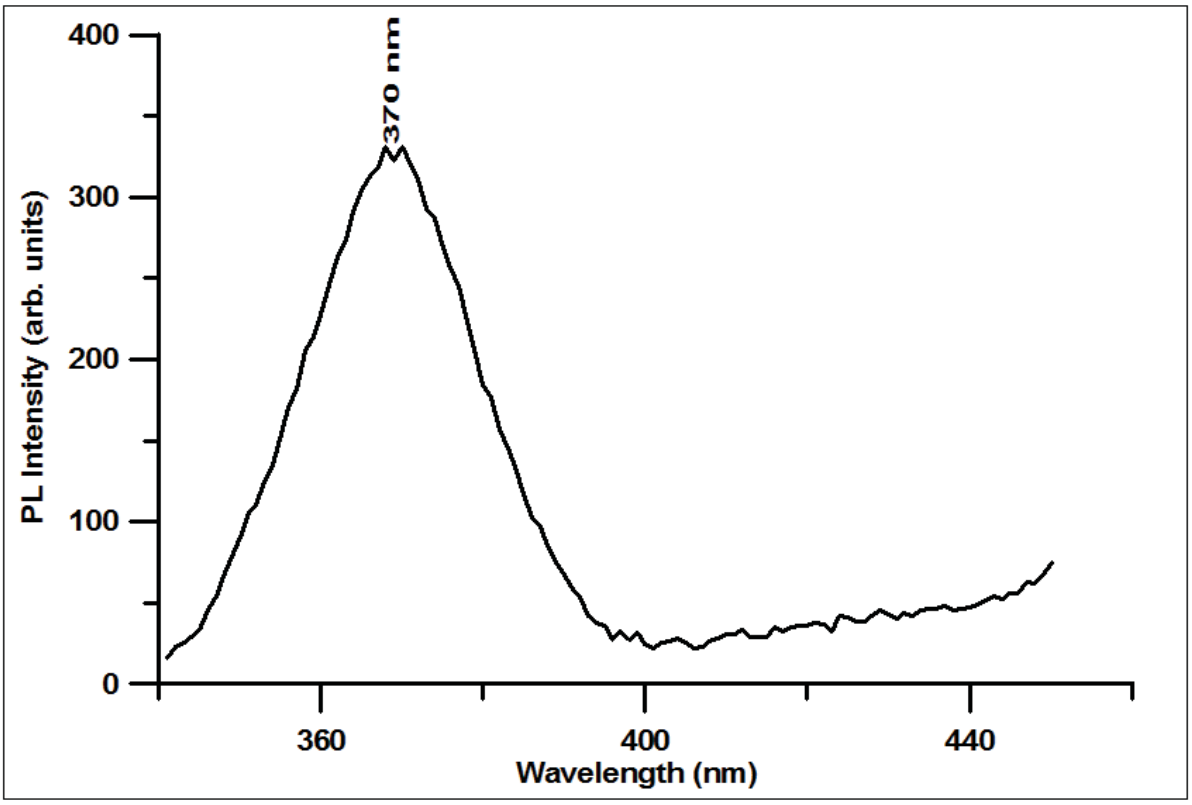

Figure 4-23 Photoluminescence emission spectrum of the synthesized nanomaterial in 1 % of H_2O_2 in the DW.

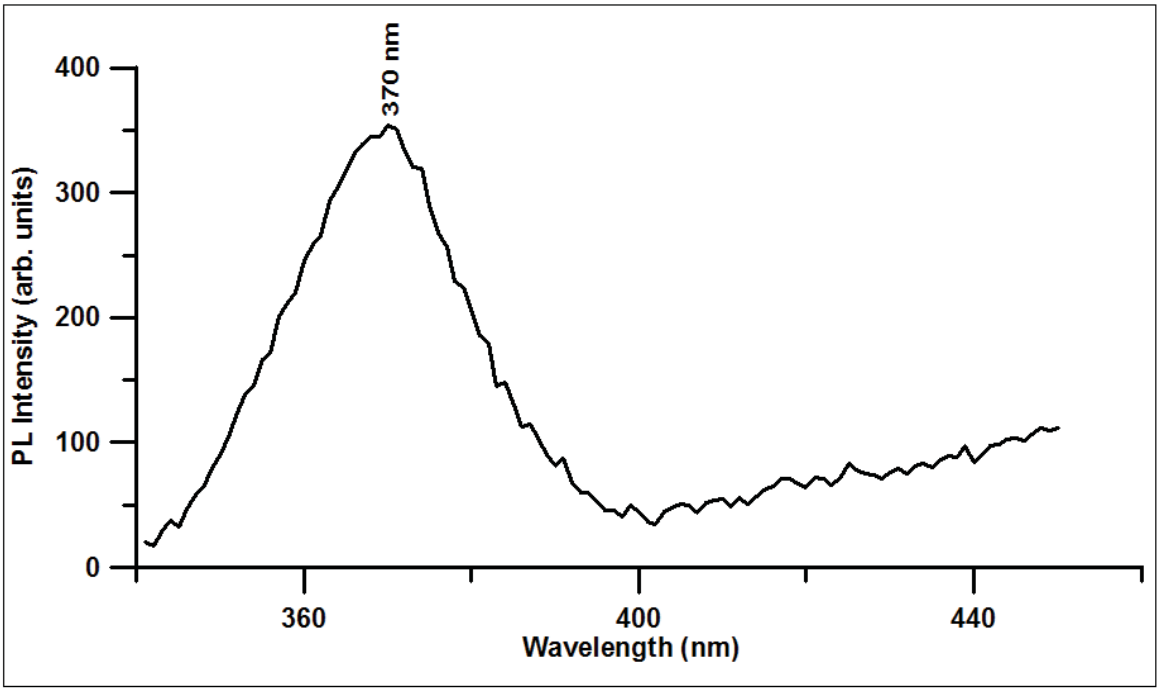

Figure 4-24 Photoluminescence emission spectrum of the synthesized nanomaterial in 3 % of H_2O_2 in the DW.

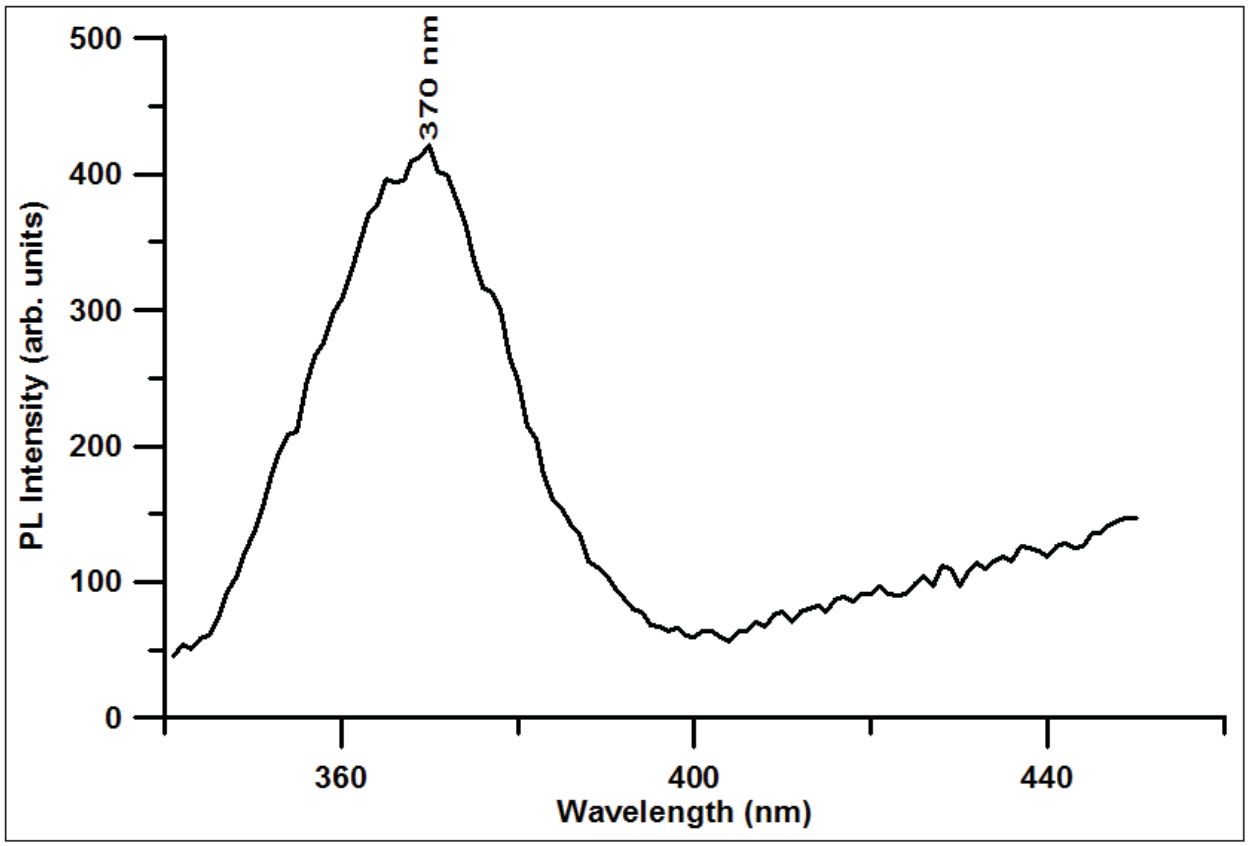

Figure 4-25 Photoluminescence emission spectrum of the synthesized nanomaterial in 5 % of H_2O_2 in the DW.

There are two striking difference between the PL spectra of the resultant materials: (1) with addition of H_2O_2, the resultant material was Cu/CuO and there is an 7 fold decrease in the overall PL intensity, which can be seen from the axes of the PL spectra (2) there are two PL peaks (360 nm and 416 nm) observed in the case of the resultant material (Cu/Cu_2O) with no H_2O_2 in the PLAL synthesis. While the peak at 300 nm is assigned to interband transition of the sample prepared in DW, the peak at 416 nm may be due to defects. From these observations it could be inferred that the resultant material synthesized in the presence of H_2O_2 in PLAL process have reduced amount of defects and reduced rate of electron hole pair recombination, which is another positive attribute desired in a good photocatalytic material.

Fig. 4-26 exhibits FTIR spectra of the PLAL product materials. As indicated in Fig. 4-26, the broad absorption bands at around 1600 and at around 3450 cm^{-1} are mainly assigned to the stretching and bending modes of the hydroxyls of adsorbed water due to the chemisorbed and/or physisorbed H_2O on the surface of nanostructured crystals [87]. Fig. 4-26-a depicts the FTIR spectrum of the sample prepared by PLAL in DW(with no H_2O_2). The wide absorption band around 620 cm^{-1} is assigned to the characteristic vibrational mode of Cu_2O [88-90]. No active modes from CuO detected by FTIR can be observed as shown in Fig. 4-26-a. In all other spectra, there are one IR absorption peak centered around 533 cm^{-1} revealing the vibrational properties of Cu-O [91-93]. The broad FTIR bands in the zones of 650–1500 cm^{-1} and1500–3000 cm^{-1} reflect the existence of surface adsorption states on the CuO nanoparticles [94]. These peaks appear at 1000-1200 and 1300-1500 cm^{-1},in the spectra b, c and d in Fig. 4-26 with increasing intensity from c to d.

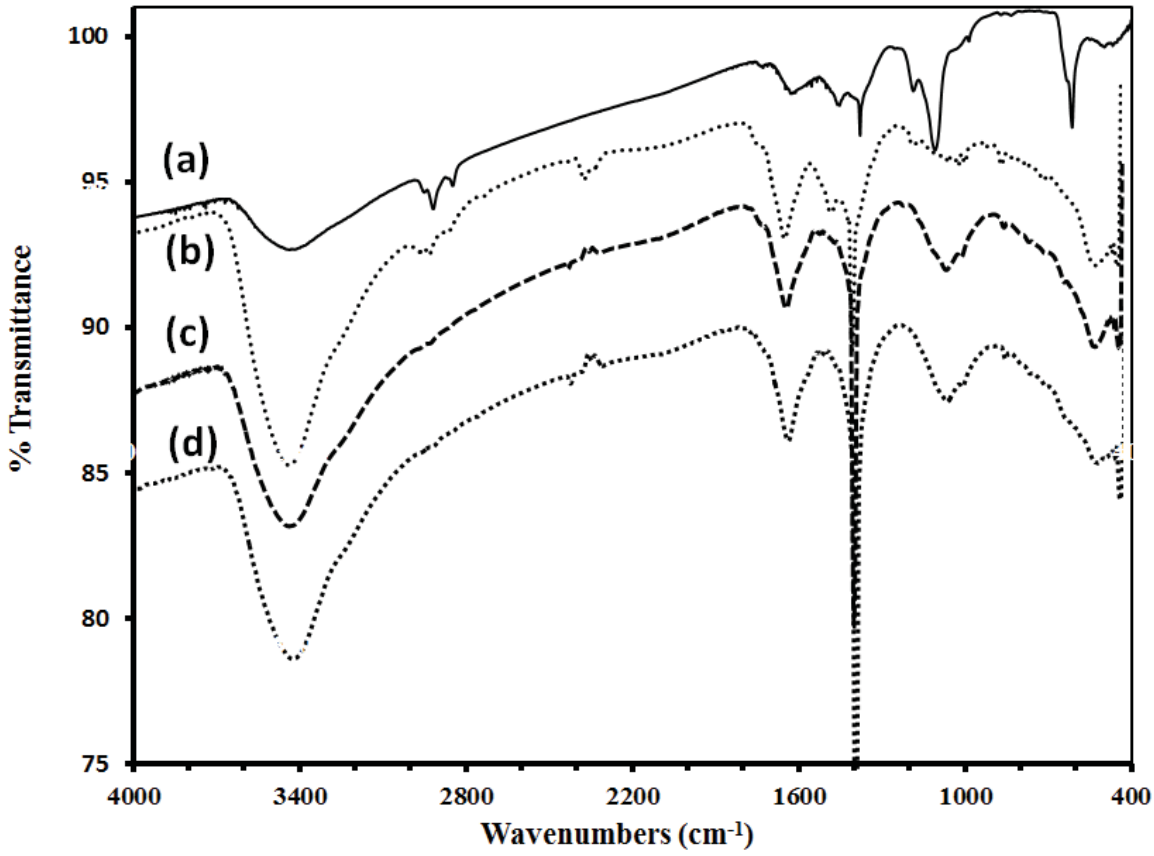

Figure 4-26 Typical FTIR spectra of the synthesized product material by varying concentrations of H_2O_2 in the DW. (a) for 0% H_2O_2 in DW, (b) for 1% H_2O_2 in DW, (c) for 3% H_2O_2 in DW, (d) for 5% H_2O_2 in DW.

The intensity of these peaks increase by increasing the concentration of H_2O_2 during the ablation process. This observation can be used as an indirect indication to the formation of CuO nanoparticles, with increasing amount from c to d. According to the reaction $2Cu_2O + H_2O_2 \rightarrow 4CuO + H_2$, there should be significant increase in the formation of CuO by increasing H_2O_2, as it is observed in the IR spectra. IR-spectroscopy analysis of the interaction products upon various H_2O_2 concentrations show that the appearance of the CuO becomes significant after addition of 1% H_2O_2 (Fig. 4-26-b). By increasing the concentration of H_2O_2, the formation of CuO increases.

4.1.2 Effects of Annealing Temperature

In this section, the effect of annealing temperature on nanostructured pure copper (Cu) and cuprous oxide (Cu_2O) synthesized using PLAL technique in DI water will be discussed. The same experimental setup and parameters mentioned in section 4.1. were used for this purpose. The ablated material in the DW was filtered out and annealed in air at three different temperatures (300 °C, 600 °C, and 900 °C). In the initial unannealed colloidal suspension, Cu and Cu_2O NPs were obtained and identified as discussed in section 4.1.1. Further we noticed the product (Cu/Cu_2O) was converted predominantly into CuO at annealing temperature of 300 ºC for 3 hours. As the annealing temperature was raised from 300 to 900 ºC, the grain size of CuO increased from 9 to 26 nm. The structure and the morphology of the prepared samples were investigated using X-ray diffraction and transmission electron microscopy. Photoluminescence and UV-Vis absorption spectrometry studies revealed that the band gap and other optical properties of nanostructured CuO were changed due to post annealing. Fourier transform spectrometry also confirmed the transformation of Cu/Cu_2O into CuO.

4.1.2.1 Structure and Morphology of unannealed/annealed Copper oxides NPs

XRD spectra depicted in Fig. 4-27, 4-28, 4-29 and 4-30 show the presence of copper (Cu), cuprous oxide (Cu_2O) and cupric Oxide (CuO) synthesized using pulsed laser ablation.

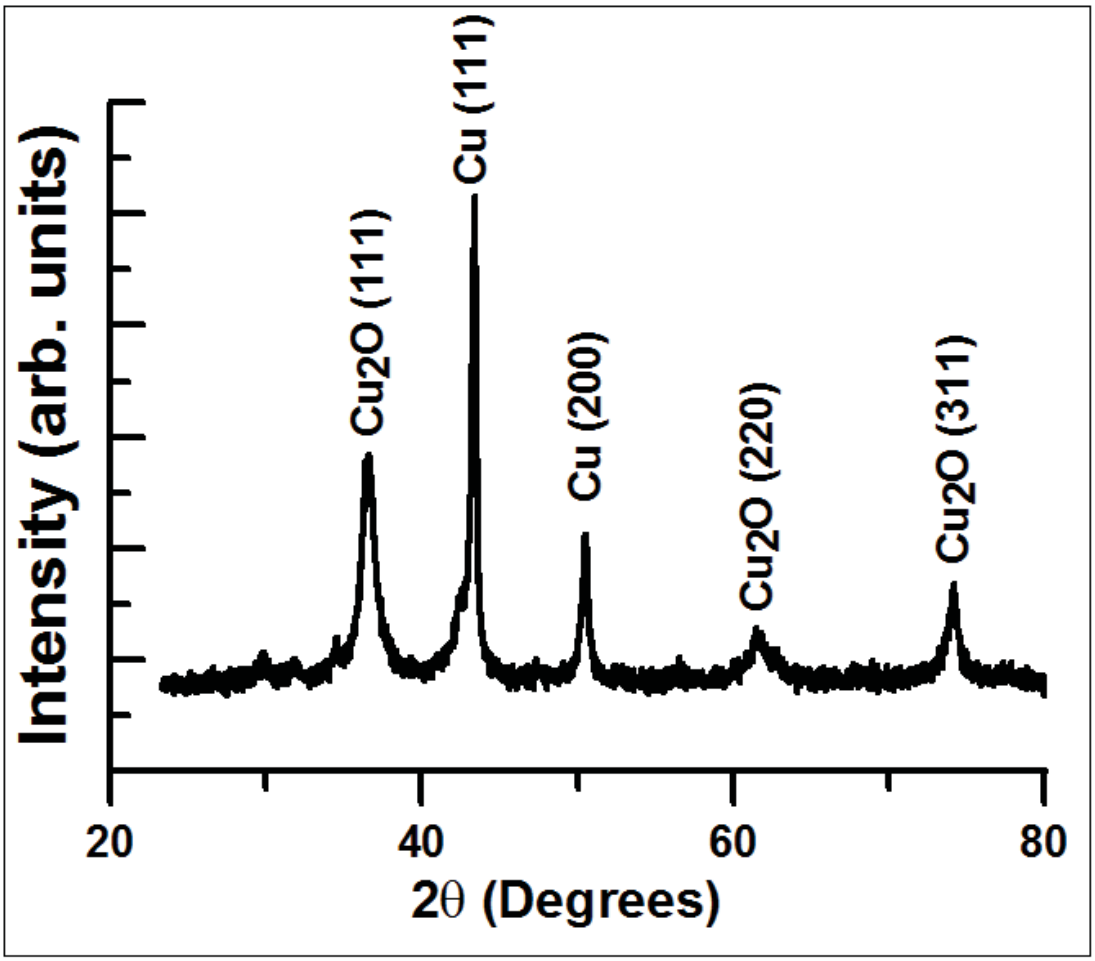

Figure 4-27 X-ray diffraction of Cu/Cu_2O prepared by pulsed laser ablation in DW.

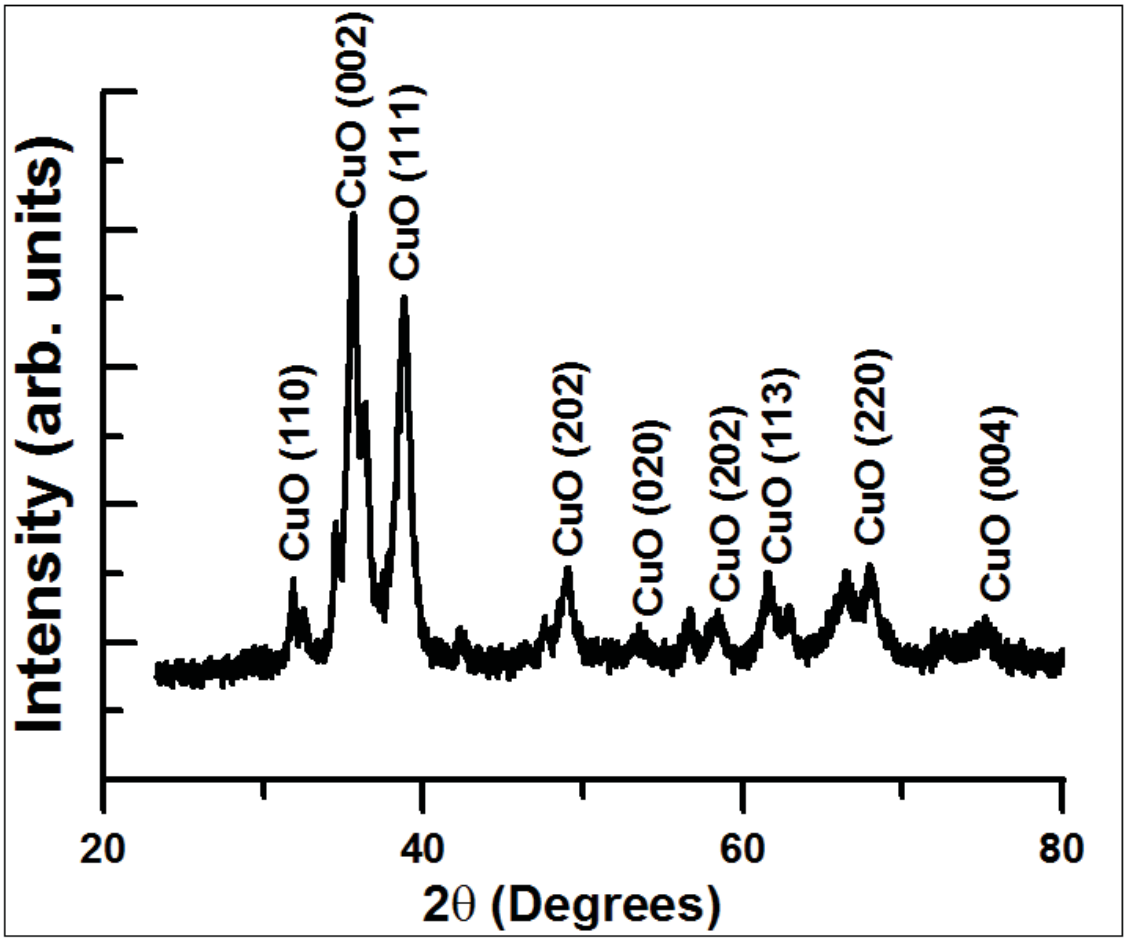

Figure 4-28 XRD patterns of CuO prepared by annealing Cu/Cu_2O at 300 ºC for three hours.

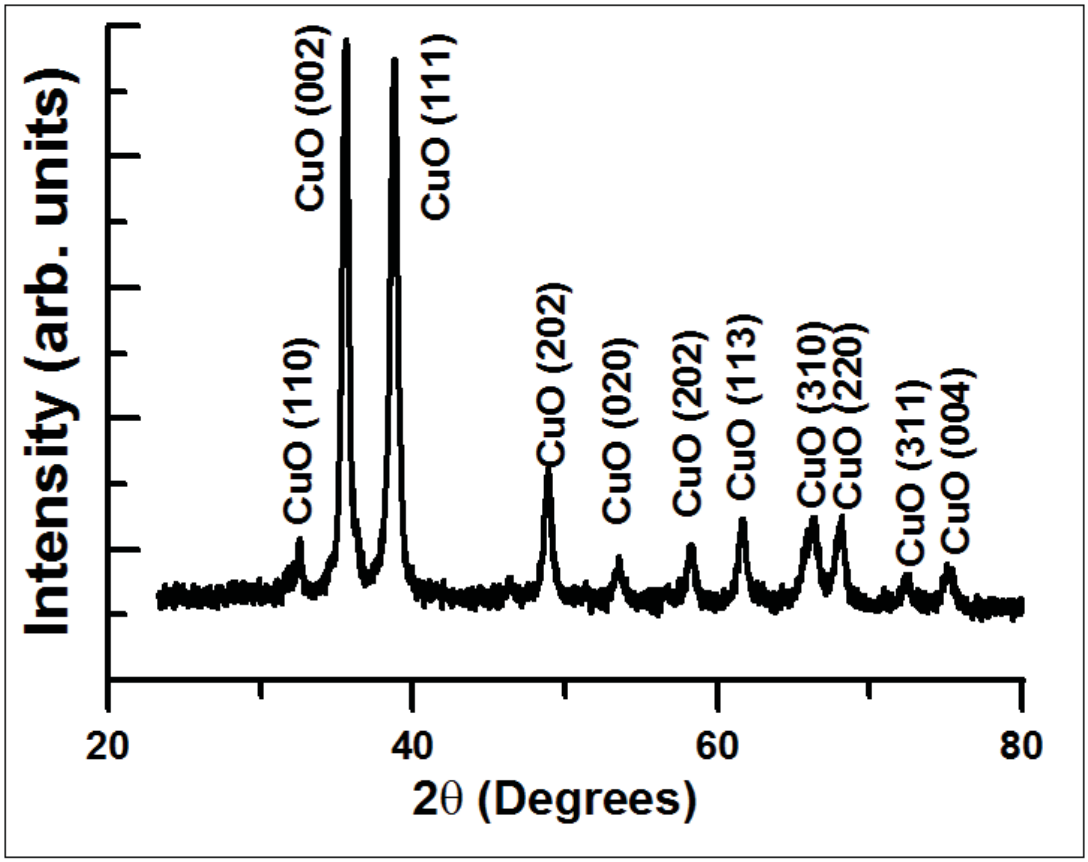

Figure 4-29 XRD patterns of CuO prepared by annealing Cu/Cu_2O at 600 ^oC for three hours.

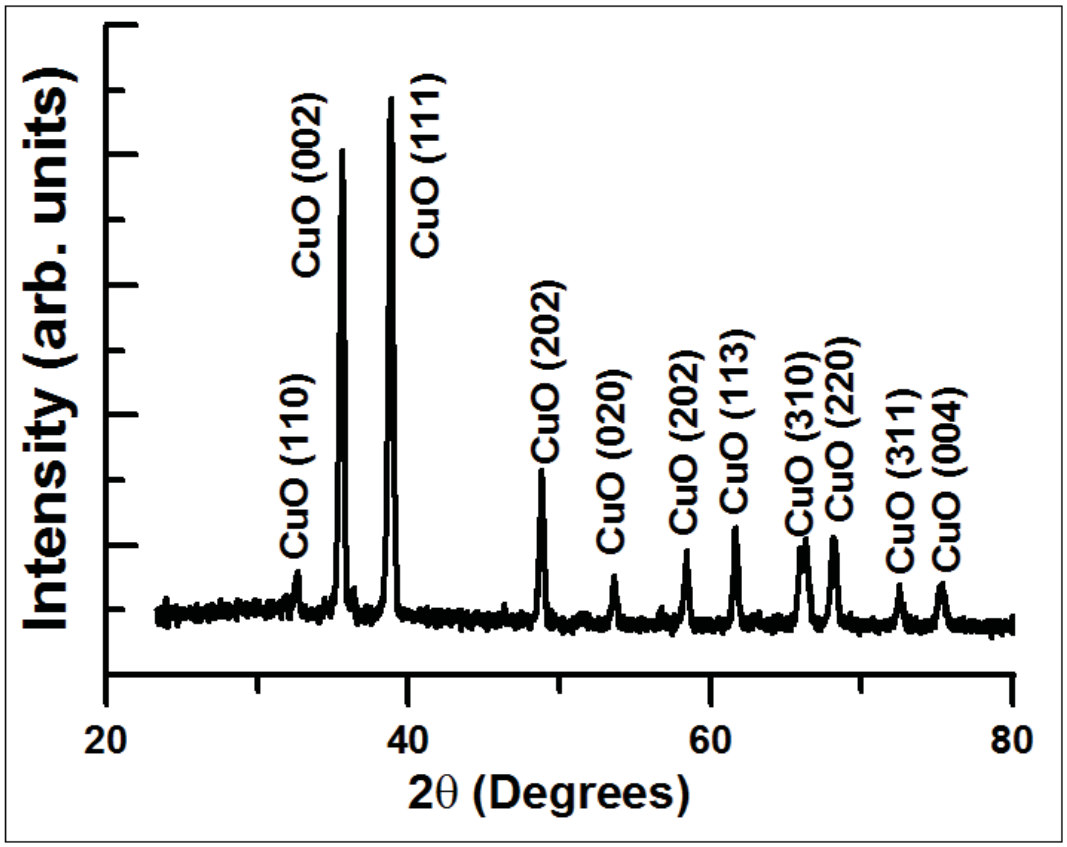

Figure 4-30 XRD patterns of CuO prepared by annealing Cu/Cu_2O at 900 ºC for three hours.

As it is clear from Fig. 4-27, the XRD pattern for the synthesized material without subjecting to any annealing, shows the presence of copper (Cu) and cuprous oxide (Cu_2O), and as we anneal the material, a further oxidation brings about cupric oxide (CuO) and gradually depriving the presence of copper (Cu) and cuprous oxide (Cu_2O) as the annealing temperature is raised from 300 ºC to 900 ºC. In addition to this, the produced CuO became more crystalline with increased annealing temperature. Before annealing, the XRD pattern in Fig. 4-27 shows dominant Cu_2O (111) and Cu_2O (220) peaks. When the material is subjected to annealing at 300 ºC, we can only see the traces of these Cu_2O peaks in Fig. 4-28 and upon subsequent increase of annealing temperature, these peaks fully disappear to give way to CuO peaks and becomes more crystalline. This result confirms the transformation of Cu/Cu_2O into CuO.

4.1.2.2 Effect of annealing temperature on grain size

In the case of laser ablation, the local temperature momentarily goes quite high and this favors the formation of Cu_2O from the ablated Cu and oxygen present in the water. The chemical reaction, $4Cu + O_2 \rightarrow 2Cu_2O$ requires only 1000 ºC, which is adequately given by the laser pulse. In addition, the non reacting ablated Cu remains as is, in the water sample along with Cu_2O and this explains the presence of Cu and Cu_2O in the material before annealing [95]. As this material is filtered from the water and annealed in the atmosphere, cuprous oxide (Cu_2O) turns into cupric oxide (CuO) by the chemical reaction $2Cu_2O + O_2 \rightarrow 4CuO$ at about 300 ºC and CuO becomes more crystalline with the increase of temperature.

As expected, the XRD peaks of CuO narrow down with increasing temperature, indicating the growth of grain size. The grain size (D) of CuO nanoparticles at different annealing conditions was estimated using the familiar Scherrer formula [96] $D = \frac{k\lambda}{\beta \cos\theta}$. Where (β) is the full width at half maximum of diffraction peak, (θ) is the diffraction angle, (λ) is the X-ray wavelength and (k) is the Scherrer constant and its value is between 0.9 and 1. The estimated grain size is 9 ± 1 nm, 16 ± 1 nm and 26 ± 1 nm at 300 ^{o}C, 600 ^{o}C and 900 ^{o}C respectively. It is well known that grain size increase due to the coalescence of small grains (agglomeration) or due to Ostwald ripening (thermal effect) [97] where the formation of larger particles is more energetically favored than smaller particles. This stems from the fact that molecules on the surface of a particle are energetically less stable than the ones already well ordered and packed in the interior. Large particles, with their lower surface to volume ratio, have a lower overall surface energy. Therefore, the number of smaller particles continue to shrink while larger particles continue to grow in size [98-99]. The size of the CuO nano particles and their increased grain size, observed through the XRD data, are substantiated by the TEM images shown in Fig. 4-31, 4-32 and 4-33.

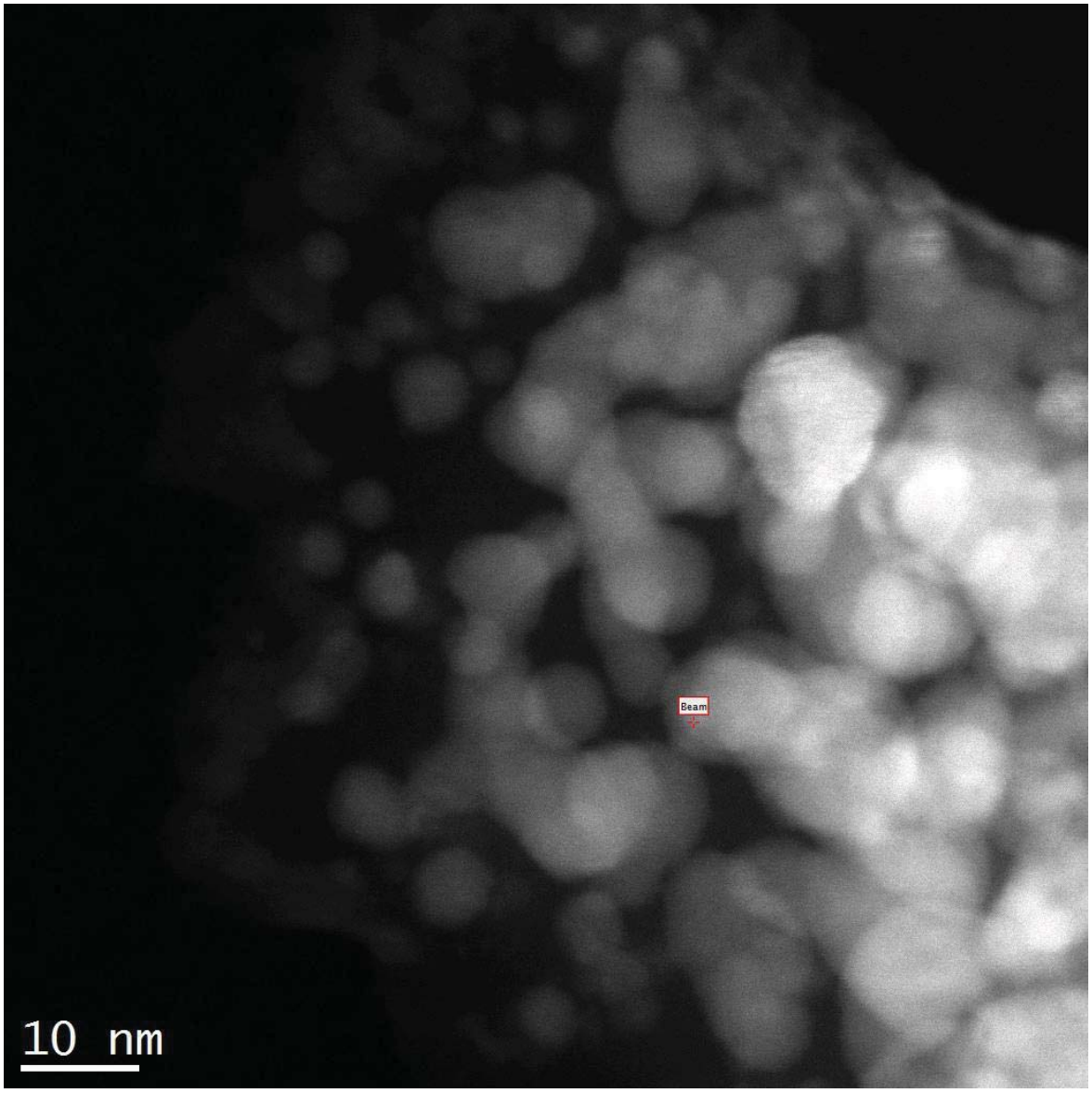

Figure 4-31TEM image of unannealed Cu/Cu_2O sample.

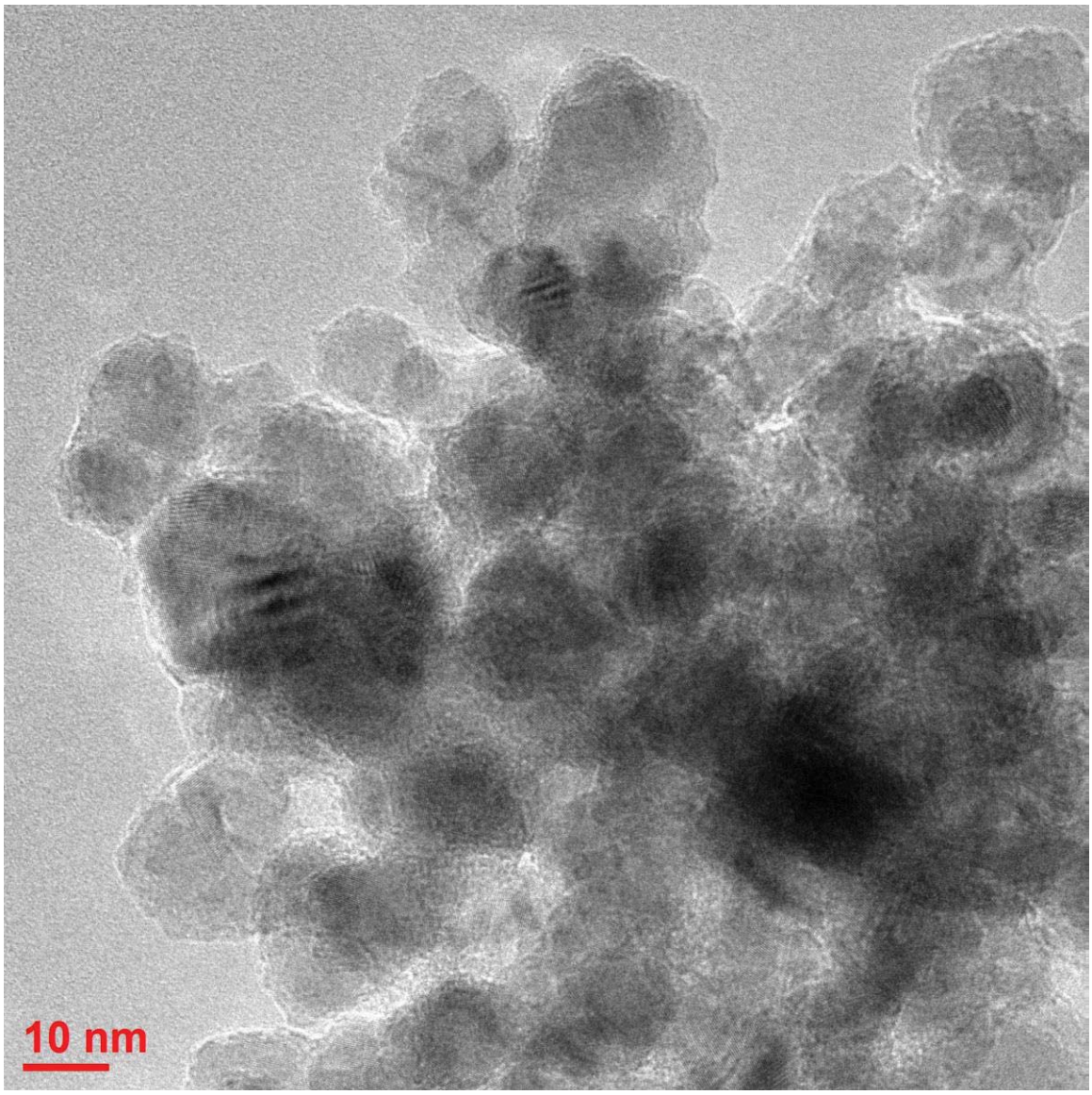

Figure 4-32 TEM image of annealed Cu/Cu_2O sample at 600°C.

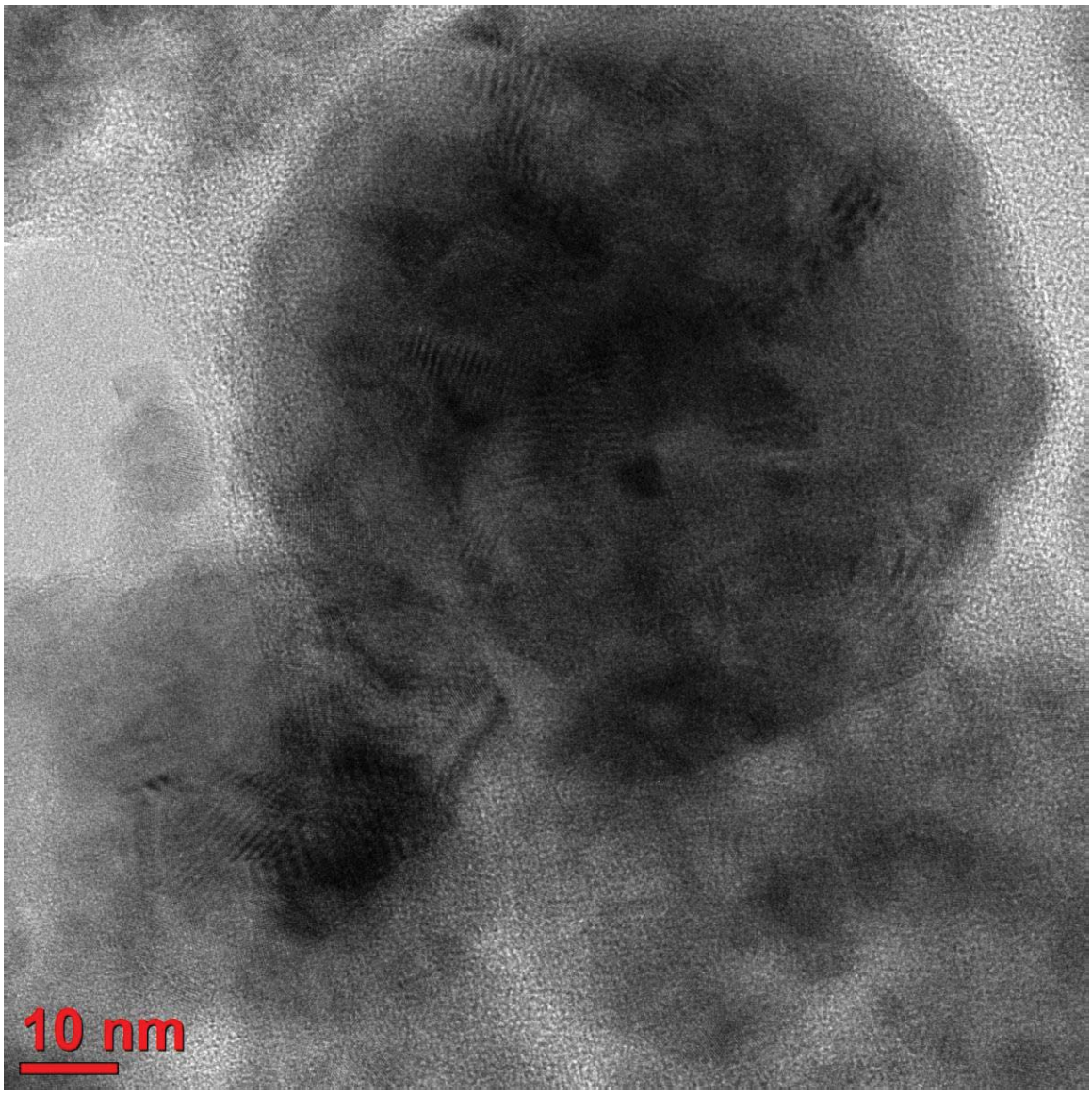

Figure 4-33 TEM image of annealed Cu/Cu_2O sample at 900°C.

4.1.2.3 Optical Characterization of unannealed/ annealed copper oxide NPs

In this section, we present the effect of annealing temperature on the optical characteristics of the synthesized material. The material as prepared, without any heat treatment (in the colloidal form) is used as a benchmark to study the variations in the optical characteristics with annealing temperature. The absorption spectrum of aqueous Cu/Cu_2O colloid as prepared is presented in Fig. 4-34 and the four peaks are marked at 641 nm, 335 nm, 274 nm and 217 nm [55, 82-83]. As mentioned in section 4.1.1.2, the broad peak (641 nm) is attributed to the surface plasmon resonance (SPR) of Cu [55] (present in the prepared colloid). The weak absorption shoulders centered around 335 nm, 274 nm are due to the Brillouin transitions of cuprous oxide, whereas the highest peak (217 nm) in the spectrum is due to the inter-band transition of copper electrons close to the Fermi level [55, 82-83].

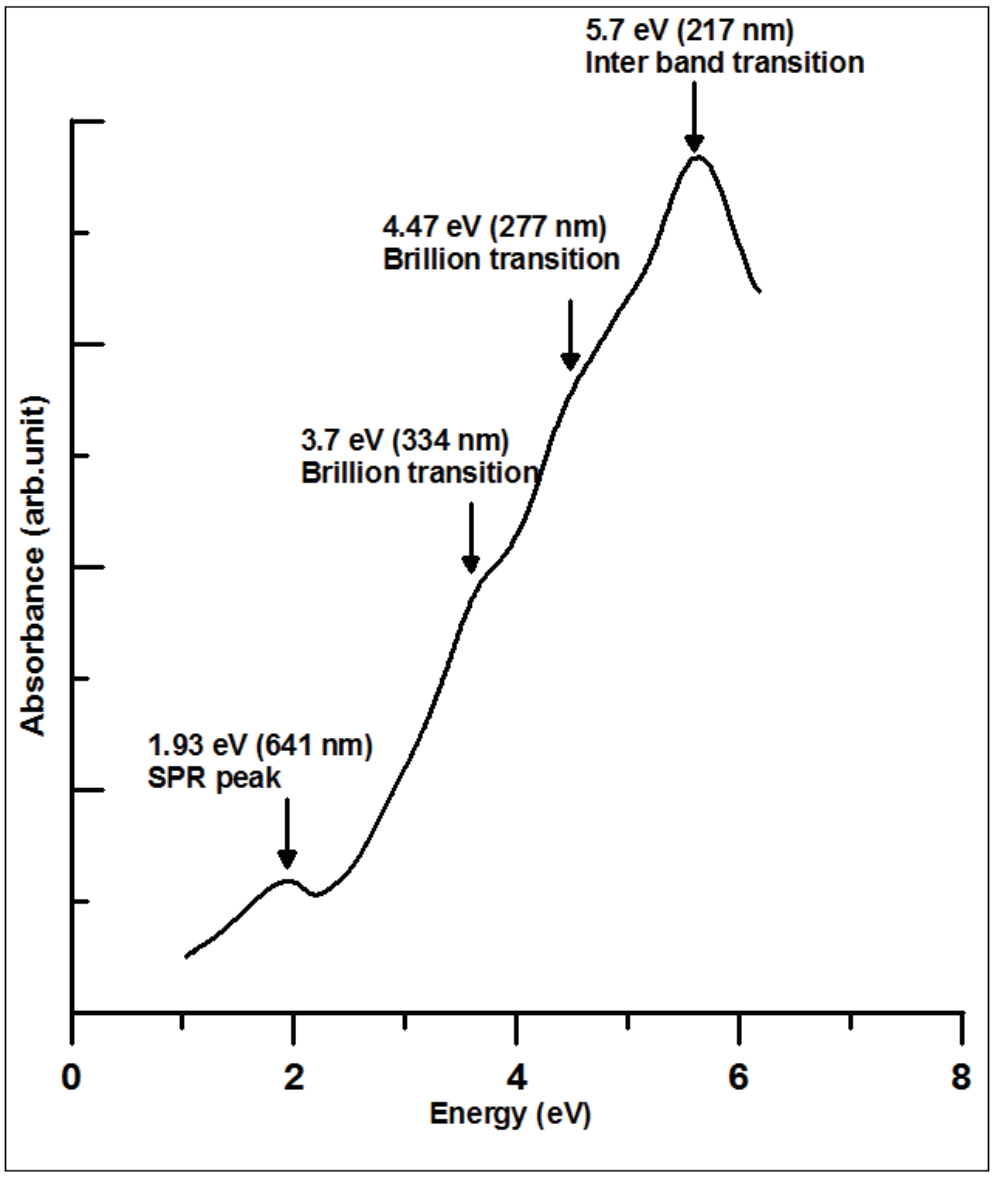

Figure 4-34 Absorption spectra of Cu/Cu_2O nanoparticles prepared by laser ablation of Copper in DW.

The band gap energy, the energy difference between the top of the valance band and the bottom of the conduction band, is an important characteristic of semiconducting material. For Direct Band gap material, plotting $(\alpha * E)^2$ *vs.* E linearises this relation. Hence, we can find the band gap energy of the material from the absorption coefficient (α) using Tauc plot. From the Tauc plot presented in Fig. 4-35, the band gap energy of Cu/Cu_2O is estimated to be 3.3 eV. The band gap energy of Cu/Cu_2O estimated from our work (3.3eV) is about 1 eV more than the bulk Cu_2O [46-48].

In addition to the absorption spectra, we recorded the room temperature photoluminescence spectra of unannealed Cu/Cu_2O. A study of the Photoluminous (PL) of semiconducting material gives the insight of various pathways of radiative transitions. Fig. 4-36 shows the PL spectrum of the unannealed colloidal suspension, where we can see two peaks centered around 360 nm and 416 nm. The emission signal was optimized for various excitation wavelengths and it was found that 283 nm excitation wavelength showed the PL signal maximum.

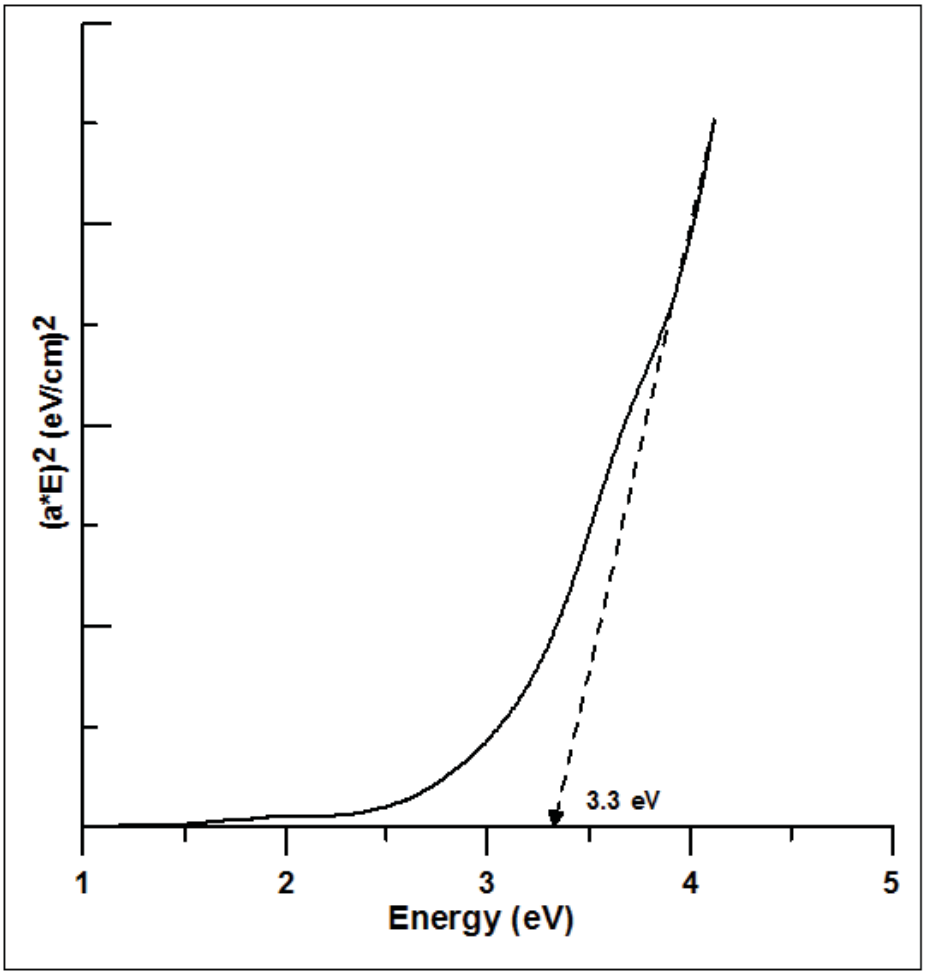

Figure 4-35 Tauc's plot of as-prepared material.

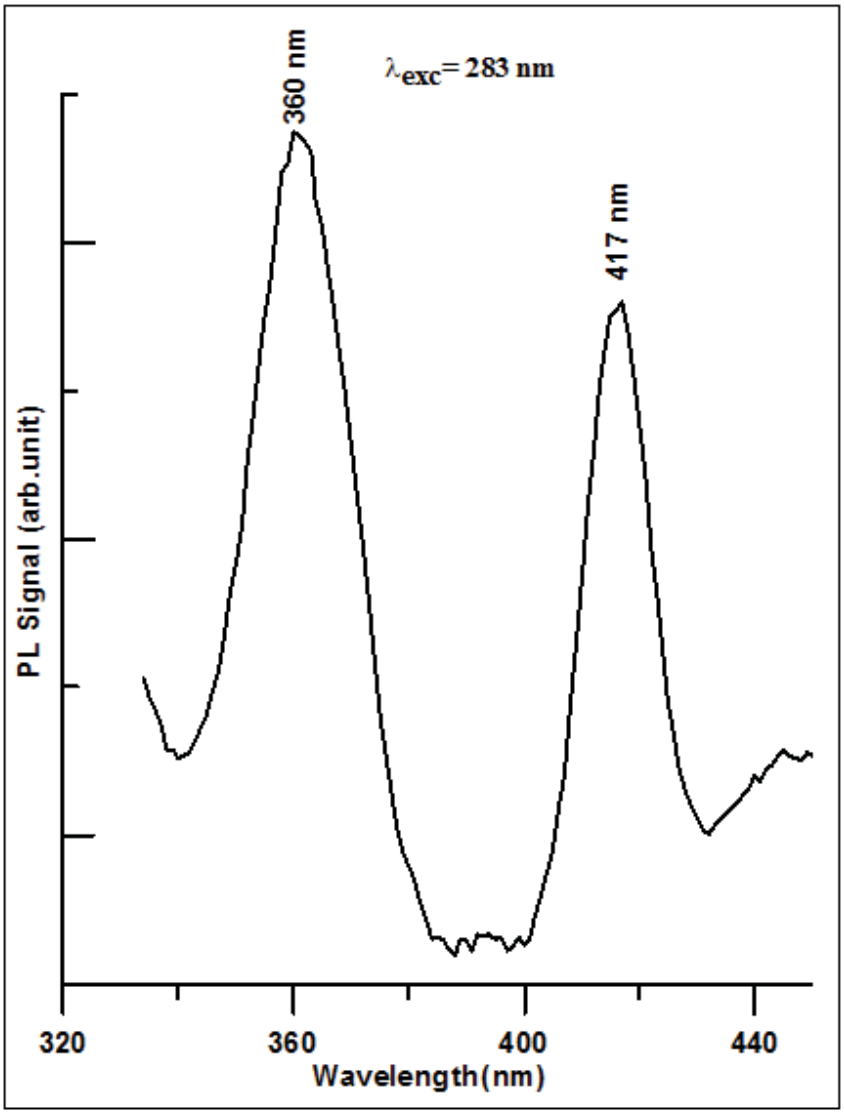

Figure 4-36 Photoluminescence emission spectra of as-prepared sample.

In the case of annealed samples, diffuse reflectance spectrum was carried out to find the band gap energy. Reflectance is converted into Kubelka –Munk function [100-101]. Kubelka- Munk function for reflectance is expressed as $F(R) = (1-R)^2/2R = K/S$, where R is the reflectance, K apparent absorption coefficient and S apparent scattering coefficient. The K and S are related to the true absorption coefficient α and scattering coefficient σ respectively as $\alpha(\nu) = \eta.K$ and $\sigma(\nu) = \chi.S$ [100-101], where η and χ are constants. The diffuse reflectance spectra are shown in Fig. 4-37 where we can see the absorption maxima (Kubelka Munk function) peaks at 435 and 459 nm for the annealing temperatures at 300 and 600 ^{o}C respectively. From the XRD data, it is clear that the Cu/Cu_2O initially produced by laser ablation is converted into CuO upon annealing. So, it is clear that the band gap energy estimated from the diffuse reflectance is for CuO (Fig. 4-38) for different annealing temperatures. Like in the case of Cu/Cu_2O, the band gap energies of CuO increase as the particle size gets into nano level. Fig. 4-38-a and b depicts comparison of the band gaps of annealed copper oxide at 300 and 600 ^{o}C respectively. The semiconductor CuO nanoparticles, with sizes comparable to or below their exciton Bohr radius, have distinctive electronic and optical behaviors due to exciton quantum confinement phenomena. The UV-Vis absorption result confirms the presence of Cu/Cu_2O in the solution of colloidal NPs (as-synthesized) and the annealing transforms Cu/Cu_2O into CuO NPs.

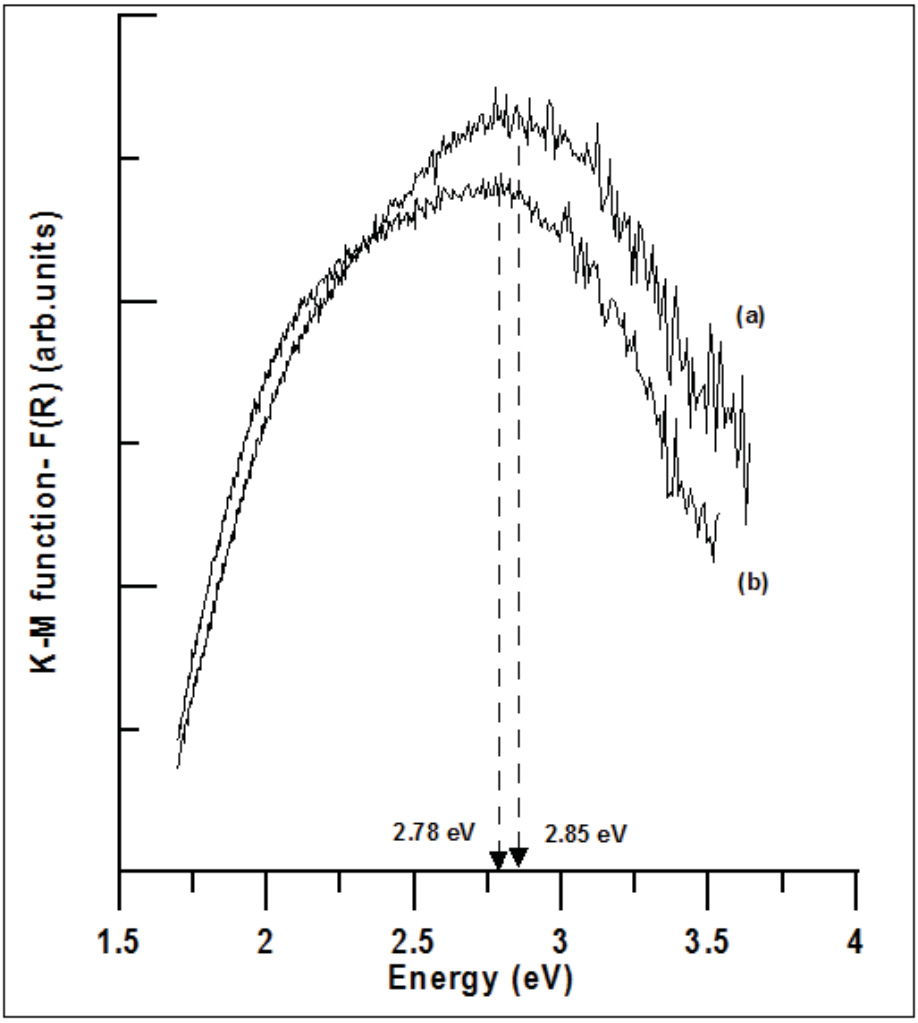

Figure 4-37 Kubelka Munk function of annealed samples at (a) 300 ºC , (b) 600 ºC for three hours.

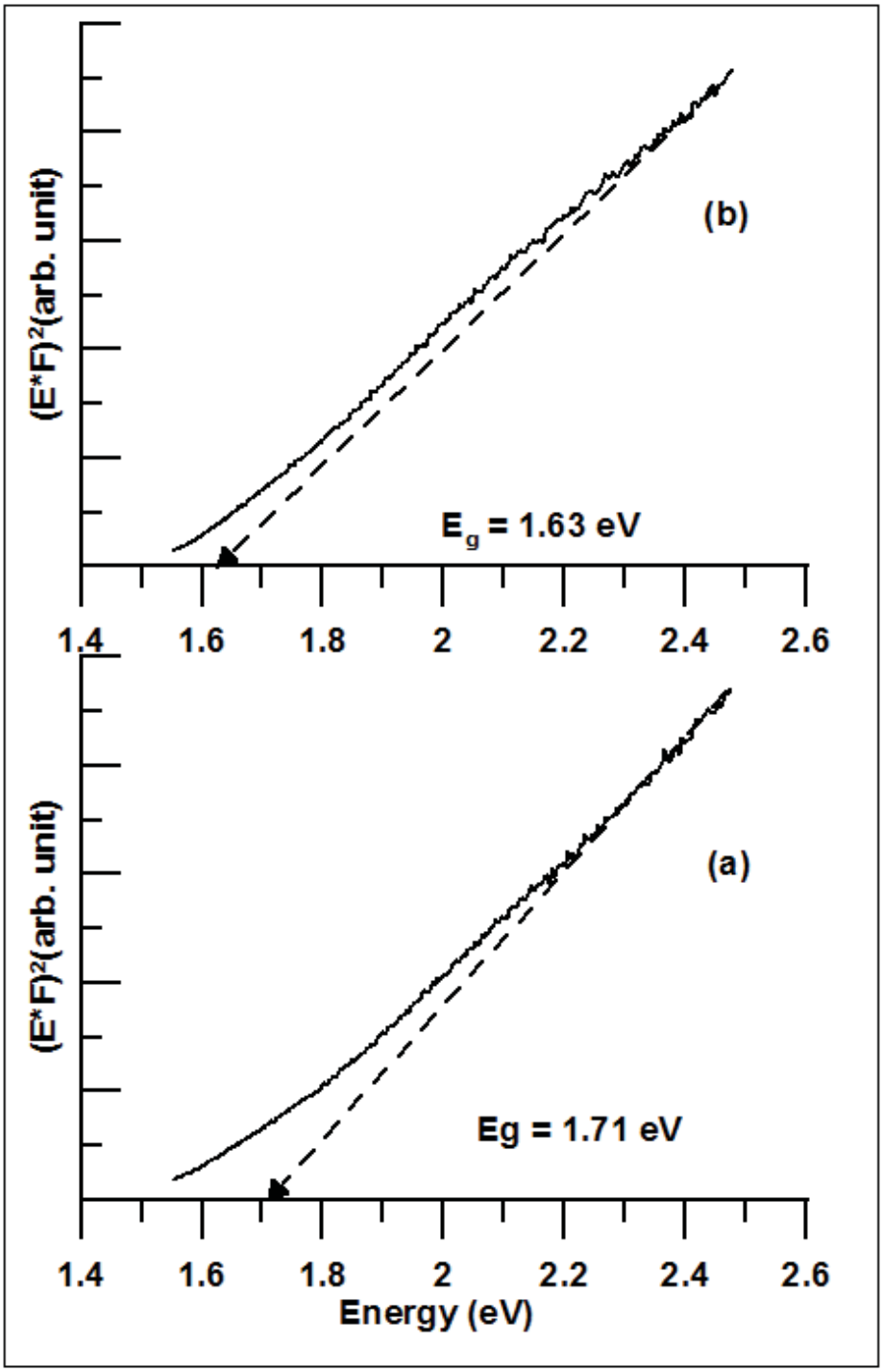

Figure 4-38 Energy band gap of annealed samples at (a) 300 ºC and (b) 600 ºC for three hours.

The room temperature photoluminescence (PL) spectra of annealed sample, supposedly CuO (according to our earlier results) were recorded in the 375-600 nm regions and are depicted in Fig. 4-39, 4-40 and 4-41.

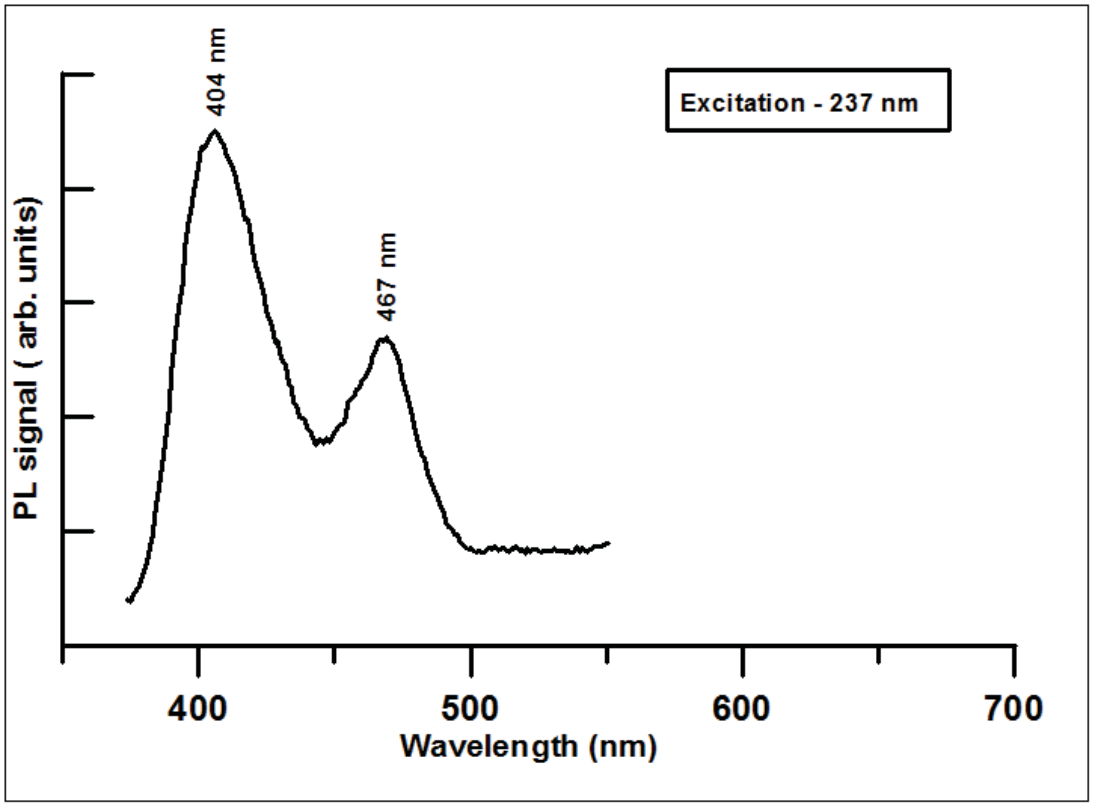

Figure 4-39 Photoluminescence emission spectra for CuO prepared by post annealing of Cu/Cu_2O at 300 ^oC for three hours.

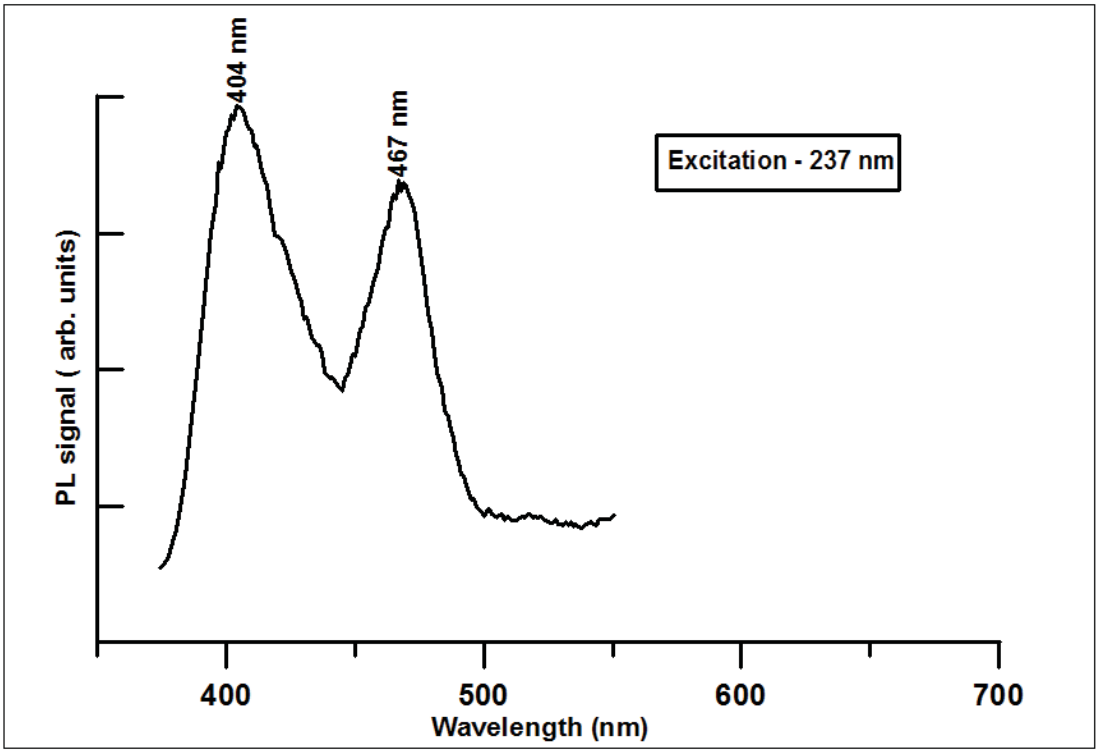

Figure 4-40 Photoluminescence emission spectra for CuO prepared by post annealing of Cu/Cu_2O at 600 ºC for three hours.

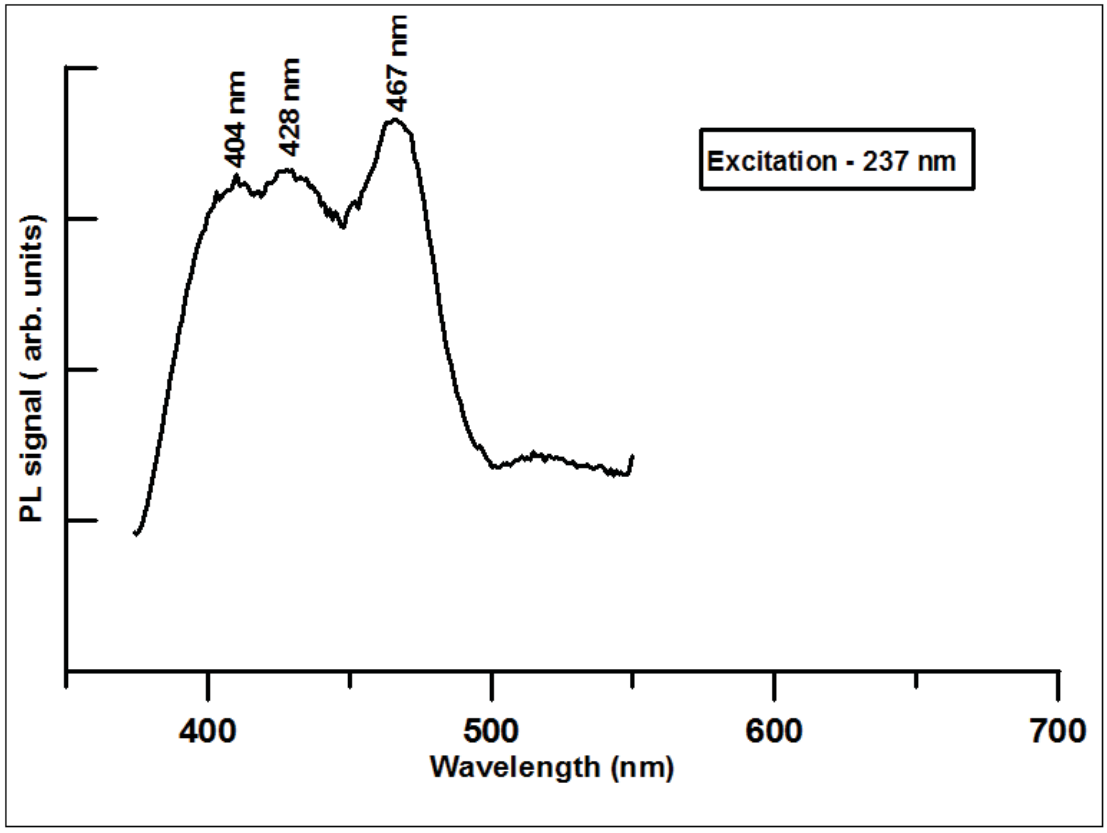

Figure 4-41 Photoluminescence emission spectra for CuO prepared by post annealing of Cu/Cu_2O at 900 ºC for three hours.

There are two changes noticed in the PL spectra of the annealed samples in comparison to the unannealed one: the excitation wavelength for these samples was found to be at 237 nm and the emission peak positions have gone through a red shift. There are two kinds of emissions bands in CuO particles. The intense emission in the spectrum exhibited at the shorter wavelength (404 nm) is due to the electron hole recombination in the valence band, whereas the long wavelength emission at 467 nm can be attributed to the oxygen vacancies and Cu interstitials [102-103]. One can notice a third peak (at 428 nm) develops as temperature increases. This may also be due to defects. The nature of this defect needs further investigation. Moreover the relative intensities of these two emission peaks (404 nm and 467 nm) vary with the increase in the annealing temperature. The PL result confirms the annealing transformation of Cu/Cu_2O into CuO.

FTIR analysis was performed to understand the effect of annealing on the structural change taking place in the nano- CuO during the transformation from Cu/Cu_2O to CuO. Six infrared vibrational modes are suggested for CuO which are at 147, 161, 321, 478, 530 and 590 cm^{-1} [104-109]. Two vibrational modes are reported for Cu_2O which are located at 610 and 147 cm^{-1} [110]. The minor differences between the reported values by different works are attributed to the type and the temperature of the sample [111]. Fig. 4-42-a is the FTIR spectrum of unannealed nano-structured Cu/Cu_2O. The peak located at 620 cm^{-1} belongs to the vibrational mode of Cu–O in Cu_2O phase. This result confirms the presence of cuprous oxide (Cu_2O) in the as-prepared sample.

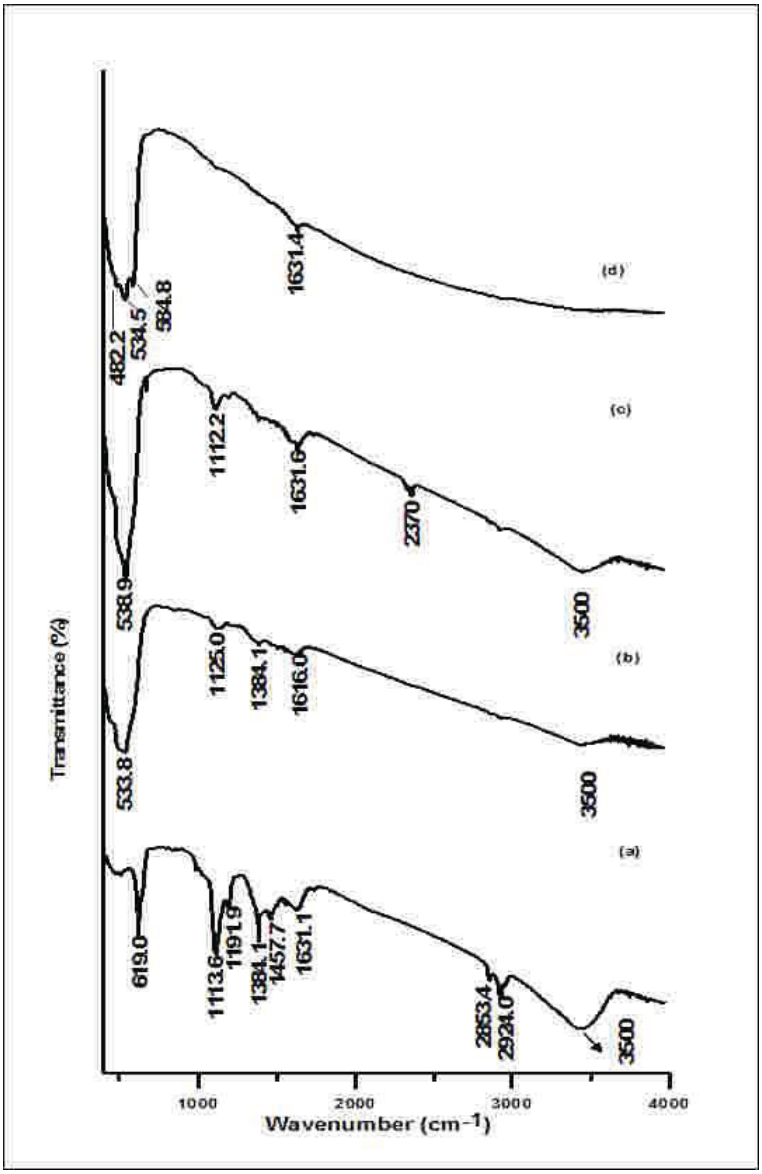

Figure 4-42 Typical FTIR spectra of the samples: a) as-prepared samples, b), c) and d) nanoparticles product annealed at 300°C, 600°C and 900°C respectively.

.

Fig 4-42-b, -c and -d are FTIR spectra of annealed CuO generated from the annealing of as-prepared samples at 300 ^{o}C, 600 ^{o}C and 900 ^{o}C which show strong vibrational modes at 534, 539 and (482, 534 and 585) cm^{-1} repectively which is in good agreement with the vibrational modes of CuO. Moreover, no mode due to Cu_2O is seen in these spectra. This result confirms the transformation of Cu/Cu_2O into CuO. The broad absorption peaks in the range of 3500 cm^{-1} correspond to infrared active –OH group, and indicates the existence of water absorbed on the surface of nanocrystals. The presence of this band can be clearly attributed to the adsorption of some atmospheric water during FT-IR measurements and one around 2370 cm^{-1} is the infrared active C = O asymmetric stretching mode arising from the absorption of atmospheric CO_2 on the surface of the nanoparticles [87, 94].

4.2 Synthesis and Characterization of CdSe Quantum Dots (QDs)

In this section the synthesis of CdSe QDs will be discussed. CdSe powder was used as a starting material with different confining media (acetone, ethanol, methanol, deionized (DW) water) to synthesize CdSe colloidal QDs. It was found that with all the confining media except acetone, the agglomeration of synthesized CdSe colloidal QDs were quite fast, and start to take place immediately after ablation and get worse with time. However in the case of acetone, the synthesized CdSe colloidal QDs was free from particle agglomeration even after 6 months. The synthesized CdSe QDs with acetone as the confining medium were characterized using various analytical methods such as, XRD, HRTEM and UV-Vis absorption.

4.2.1 Synthesis of CdSe QDs

The experimental setup depicted in Fig. 3-2 was employed for the synthesis of CdSe QDs. CdSe powder was used as the starting material and acetone as the confining medium. For this purpose, CdSe powder (micron size) was dispersed in 40 ml of acetone and color of this suspension was originally dark black. In order to make the suspension homogeneous, a high speed magnetic stirrer was used during the synthesis. The dark colored suspension was ablated using 250 mJ energy at 532 nm wavelength, and after 15 minutes of laser ablation, the color of the suspension transformed to yellow and this nanostructured yellow colloidal suspension was collected.

The colors of the suspension before and after laser ablation are presented in Fig. 4-43 and the change of color is the first indicator for the formation of CdSe QDs.

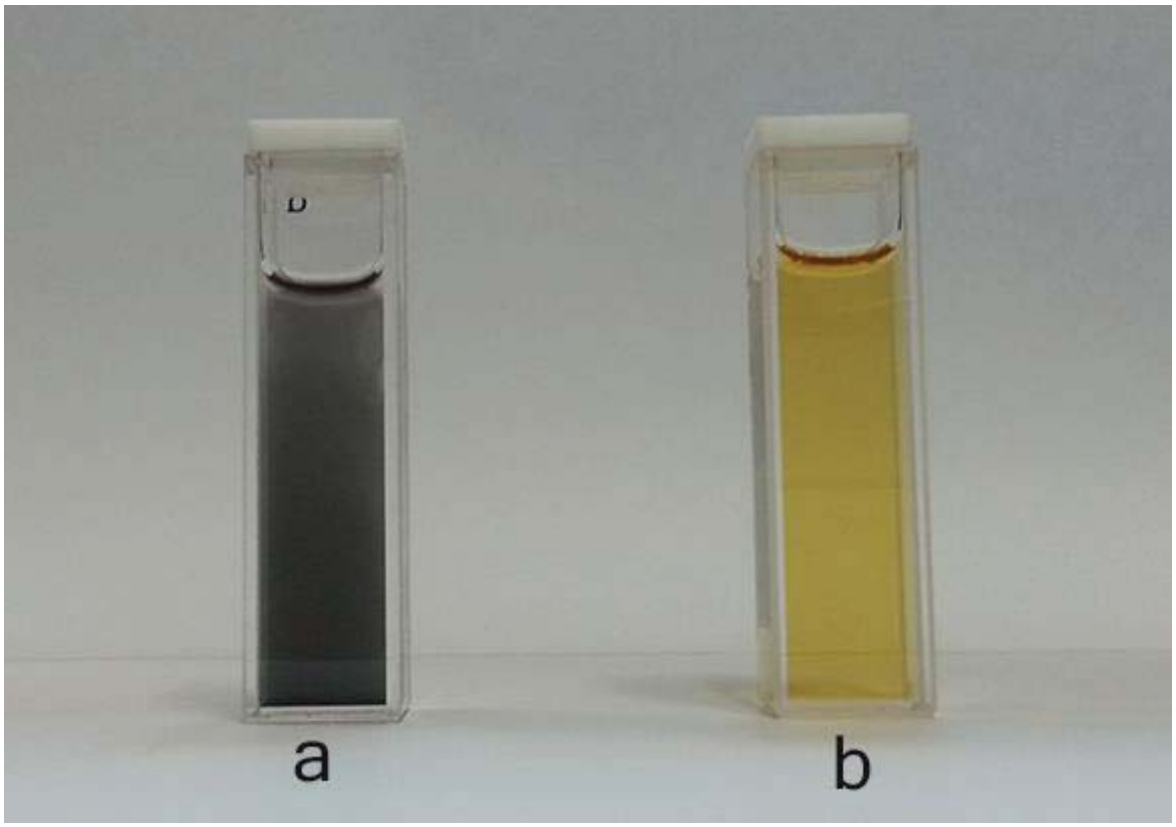

Figure 4-43 The appearance and color of the CdSe before (a) and after the ablation (b).

The laser ablation brings about the reduction in the size of the particle dispersed in the suspension, with or without retaining the shape, phase and composition depending on the interaction between the particles and surrounding medium. In this case, two mechanisms are suggested for the ablation of powder target: the first mechanism is a thermal process, in which a pulsed laser beam melts and evaporates the large particles into small species which in turn rearrange themselves into smaller nanostructured particles that have the same or different morphology and structure depending on the reactivity of surrounding medium and laser parameters [25]. The second mechanism is the Columbic explosion, in which the laser beam ejects electrons from the outer surface of the ablated particles by photoelectron or thermal effect. The electrostatic repulsion between the induced surface charges (positive charges) on the different parts of the particles, leads to the explosion of the primary particle into many smaller fragments, which leads to synthesis of nano ultrafine particles [25, 31-32]. The laser pulses of very short pulse width (femtosecond) can favor the Columbic explosion mechanism. In our case, we used laser with the pulse width of 5 nanosecond, we can rule out the second mechanism and the process involved in the synthesis of CdSe QDs is probably due to the first mechanism. By using femtosecond laser, one can easily generate the ultrafine nanoparticles compared to nanosecond pulses due to the two completely different mechanism (Columbic explosion and thermal process). In the case of femtosecond laser, thermal induced agglomeration cannot take place because the duration of the femtosecond is too short for the thermal induced agglomeration. On the other hand, in nanosecond laser, the duration of thermal effect is quite significant and there is ample time for the particles to agglomerate and this makes the nanosecond lasers quite incapable of producing QDs. In our study, we were

able for the first time to synthesize the CdSe QDs by the nanosecond laser without focusing the laser beam on the target material and the mechanism of the formation of CdSe QDs can be explained as follows: In the ablation process, the temperature on the target rises quite high for the duration equal to that of the laser pulse, and this rise of temperature initially helps to generate the nanosized particles and as the heat persists for a longer time, the agglomeration of the generated particle takes place due to thermal effect. It is well known that the temperature of the laser induced plasma is much higher in the focused laser beam than the unfocussed one and also the ejection of the particle begins in the picosecond time scale. In order to avoid the thermal induced agglomeration with the nanosecond laser, the laser beam was defocused and the local temperature was reduced and this condition favored the generation of CdSe QDs though the pulse duration was in nanoseconds.

4.2.2 Structure and morphology of CdSe QDs

Fig. 4-44 compares the XRD patterns of CdSe powder (Fig. 4-44-a) and the ablated CdSe particles (Fig. 4-44-b). It is quite evident from Fig. 4-44 that the full width at half maximum (FWHM) of CdSe diffraction peaks of the ablated CdSe particles are much greater (smaller crystal size) than that of the micron sized original CdSe, indicating the reduced grain size due to the ablation process. This result is substantiated by TEM images. Fig. 4-45 shows TEM image of the ablated CdSe and Fig. 4-46 depicts HRTEM images using Selected Area Electron Diffraction (SAED) patterns.

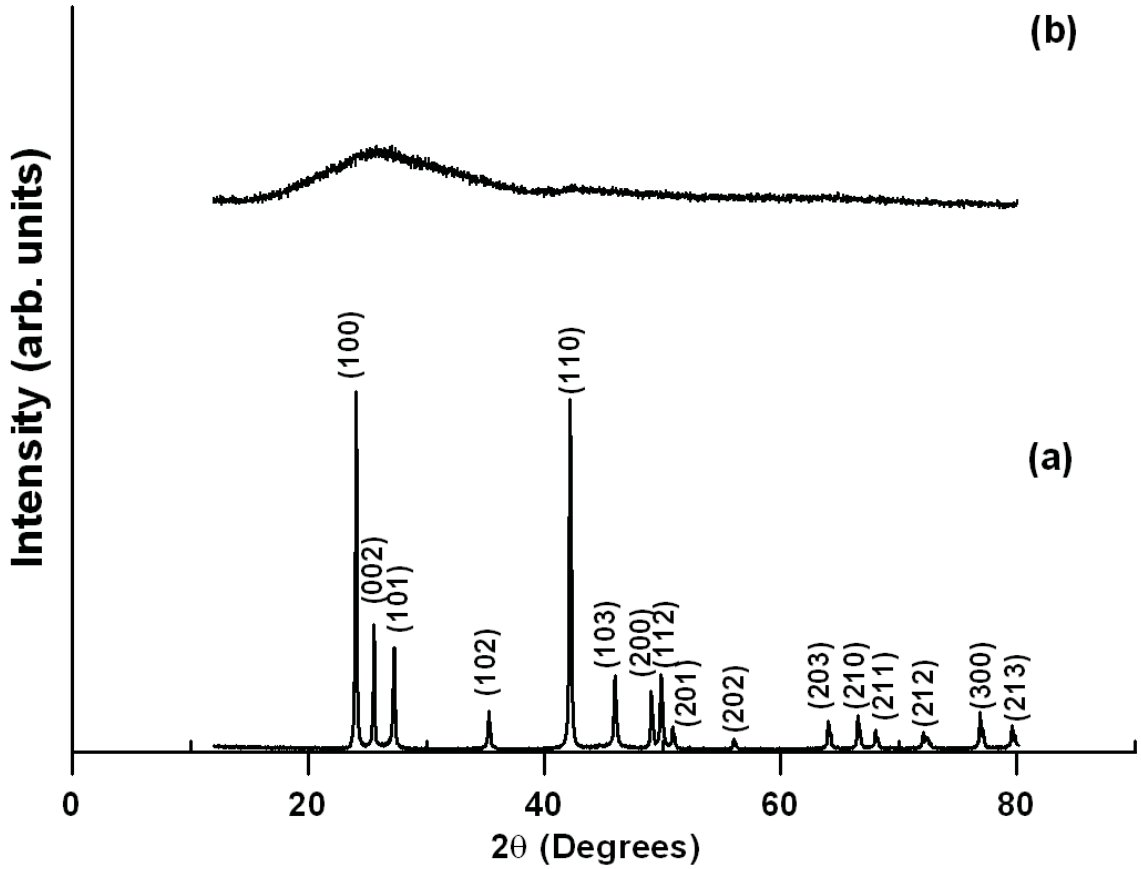

Figure 4-44 X-ray diffraction patterns: (a) micron sized CdSe powder, (b) CdSe QDs.

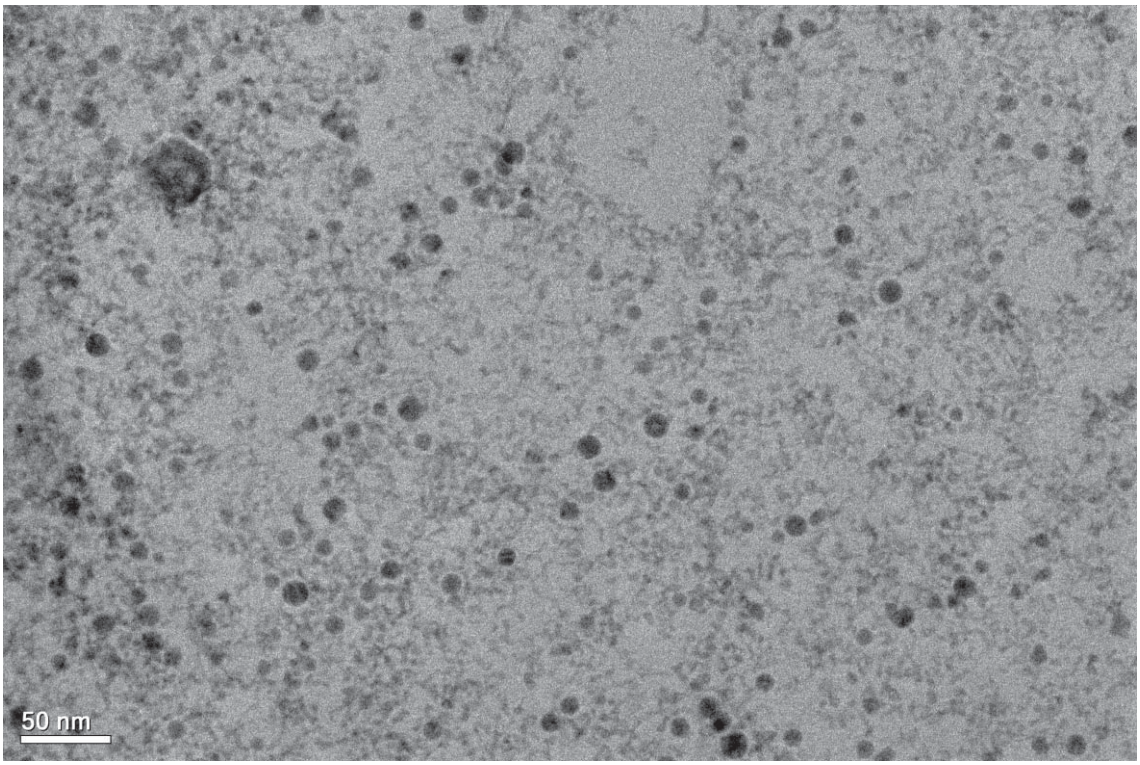

Figure 4-45 TEM image of CdSe QDs.

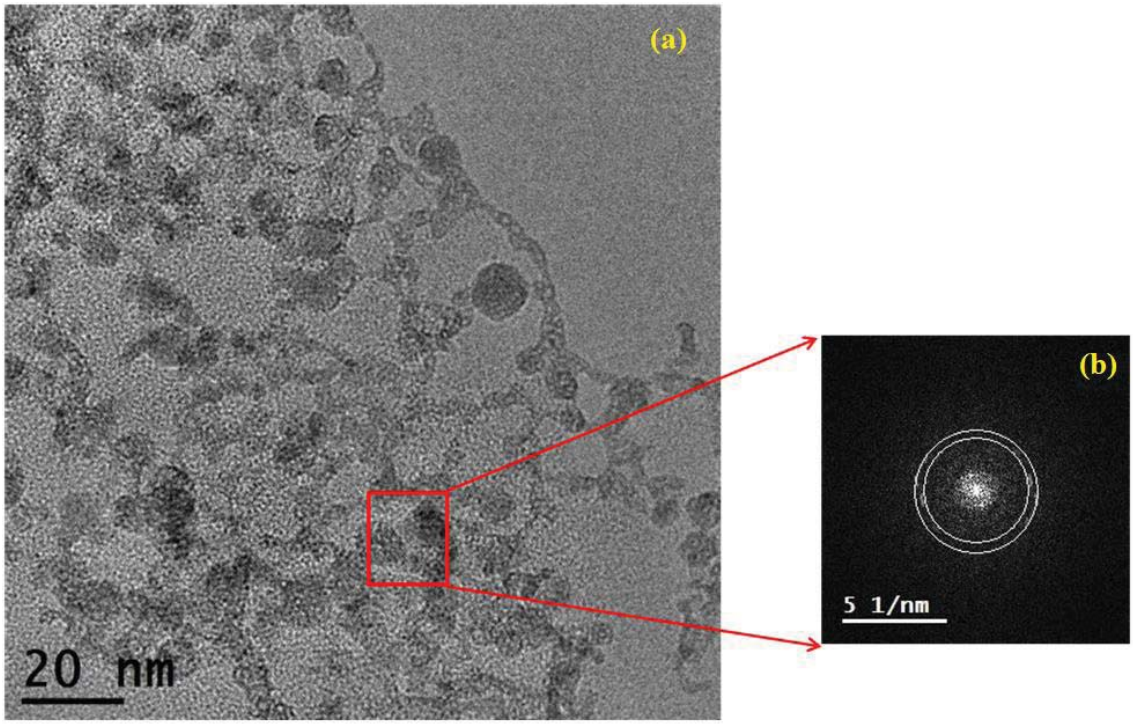

Figure 4-46 (a) HRTEM image of CdSe QDs (b) Selected area electron diffraction pattern of CdSe QDs.

In SAED pattern, the outer and inner rings correspond to the value of d spacing equal to 0.370 nm (for (100) planes) and 0.350 nm (for (002) planes) respectively. Particle size distribution, measured using image processing program of HRTEM is depicted in Fig. 4-47 and the average particle size was 3 nm.

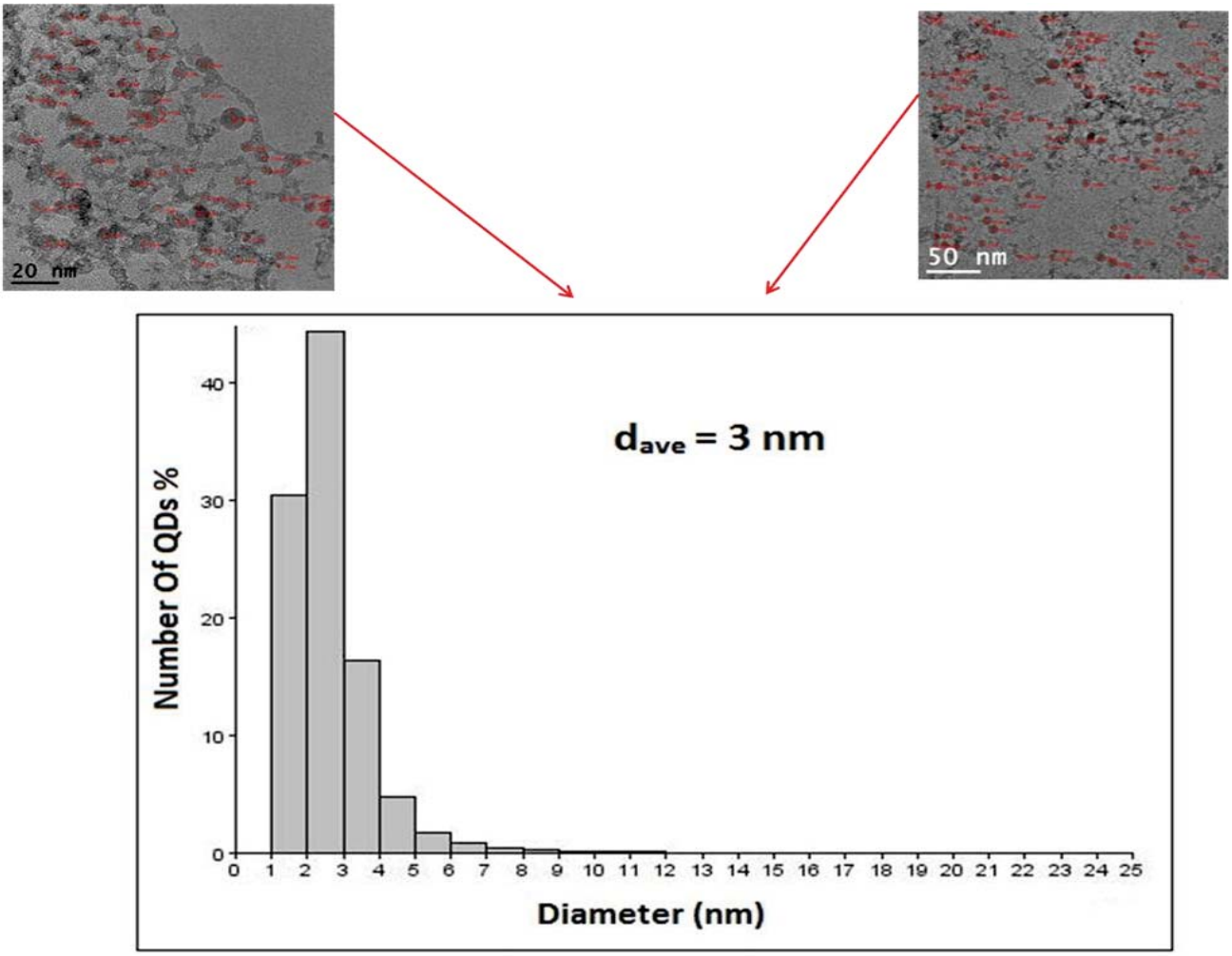

Figure 4-47 Particle size distribution of CdSe QDs.

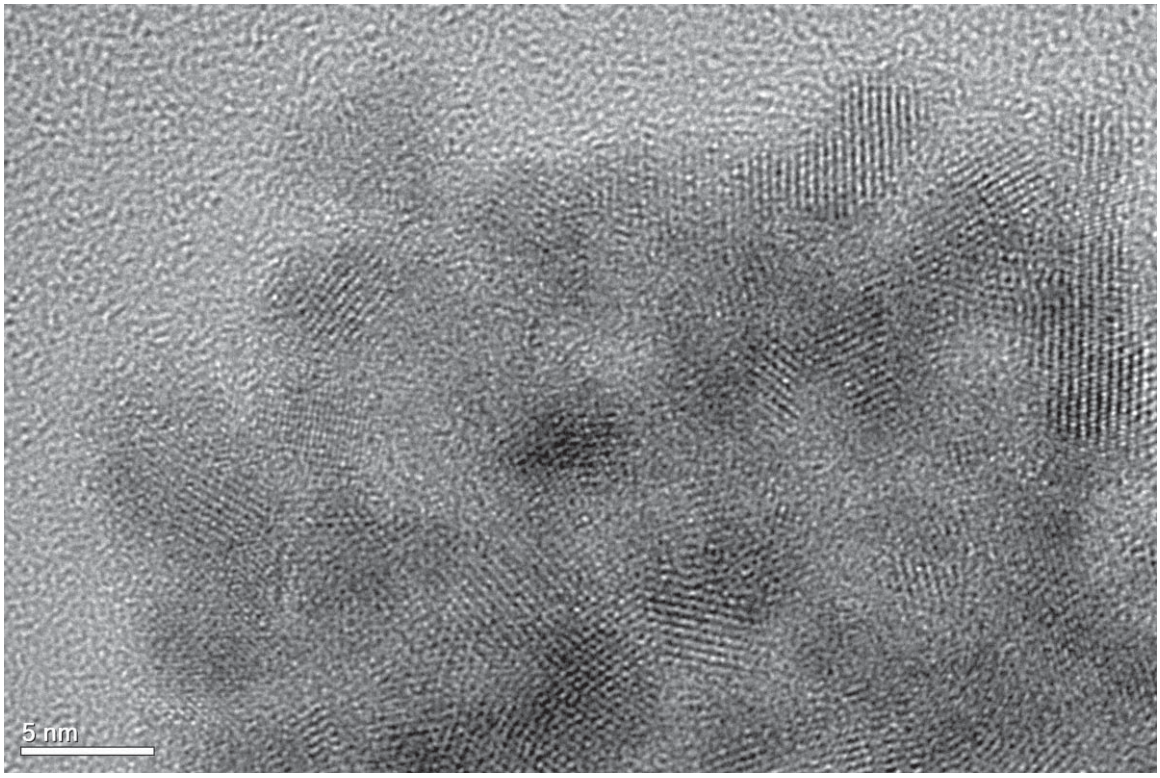

Figure 4-48 HRTEM image of CdSe QDs.

4.2.3 Optical Characterization of CdSe QDs

In semiconducting materials, the band gap energy is one of the key operational parameters and this can be modified by doping [112]. Small band gap in the semiconductors, promotes the electrons from valance band to conduction band, even at room temperature, forming a positive (holes) and negative (electron) charge carriers and these electron-hole pairs (excitons) have many properties similar to the hydrogen atom. When the size of semiconducting nano particles get to the size of the exciton-Bohr radius of the semiconductor, the electronic and the optical properties of the materials become size dependent. In order to compare the particle size of the synthesized CdSe, we estimated the exciton-Bohr radius of CdSe using the following equation [113-114].:

$$B = \frac{4\pi \in_0 \in_r \hbar^2}{e^2 \mu} \qquad (3)$$

Where e is the elementary charge; $\in_0$, permittivity of vacuum, $\in_r$, relative permittivity of the semiconductor and $\mu = (\frac{m_e m_h}{m_e + m_h})$ is the exciton's reduced mass, which depends on the effective masses of electron (m_e) and (m_h)of the hole. The exciton-Bohr radius of CdSe was estimated using equation 3 to be 5.3 nm where $\in_r$ = 10.2 m_e == 0.13 m_o and m_h = 0.45 m_o [113-114].

When the semiconductor material gets to the few nano meter scale, the band gap energy is blue shifted compared to its bulk counterpart due to quantum confinement. In quantum confined conditions, the energy structure of the semiconducting material becomes more

and more molecular like making it possible to tune absorption and emission spectra [115]. The band gap energy dependence on the size of the semiconducting material is evident from the following Brus equation [116]

$$E_{QDs} = E_{bulk} + \frac{h^2\pi^2}{2R^2}\left(\frac{1}{m_e} + \frac{1}{m_h}\right) - \left(\frac{1.789e^2}{4\pi \in_0 \in_r R}\right) \qquad (4)$$

Where, E_{QDs} is band gap energy of quantum dot, E_{bulk} is band gap energy of bulk semiconductor, R is the radius of quantum dot; m_e is the effective mass of excited electron, m_h is the effective mass of excited hole, h is Planck's constant, e is the elementary charge, ϵ_o is the permittivity of vacuum and $\in_r$ relative permittivity of the semiconductor. Based on this equation, the shift in the band gap energy of the QDs depends strongly on the material (E_{bulk} and $\in_r$) and the particle size (R).

Fig. 4-49 shows the optical absorption spectrum of ablated colloidal CdSe QDs in the 300 - 800 nm wavelength range and it is quite clear that the spectrum is deprived of a well defined absorption onset, expected in the case of CdSe QDs synthesized by chemical methods [76]. However, the absorption spectrum presented in Fig. 4-49 is qualitatively in good agreement with the absorption spectrum of the CdSe QDs synthesized by femtosecond laser ablation [78-79]. The inset of Fig. 4-49 shows the $(\alpha E)^2$ versus E plot (Tauc plot) for the ablated colloidal CdSe QDs, using the same absorption data. The optical band gap energy for the ablated colloidal CdSe QDs estimated from the Tauc plot is 2.4 eV. The band gap energy of the ablated colloidal CdSe QDs is much higher than that for the CdSe bulk material (E_g = 1. 74 eV) [116], indicating a prominent blue shift of the band gap energy from the near infra red region (713 nm) to the visible region (517

nm). This blue shift makes the ablated CdSe QDs, suitable for many photocatalytic and solar cell applications by harnessing the full spectrum of solar radiation.

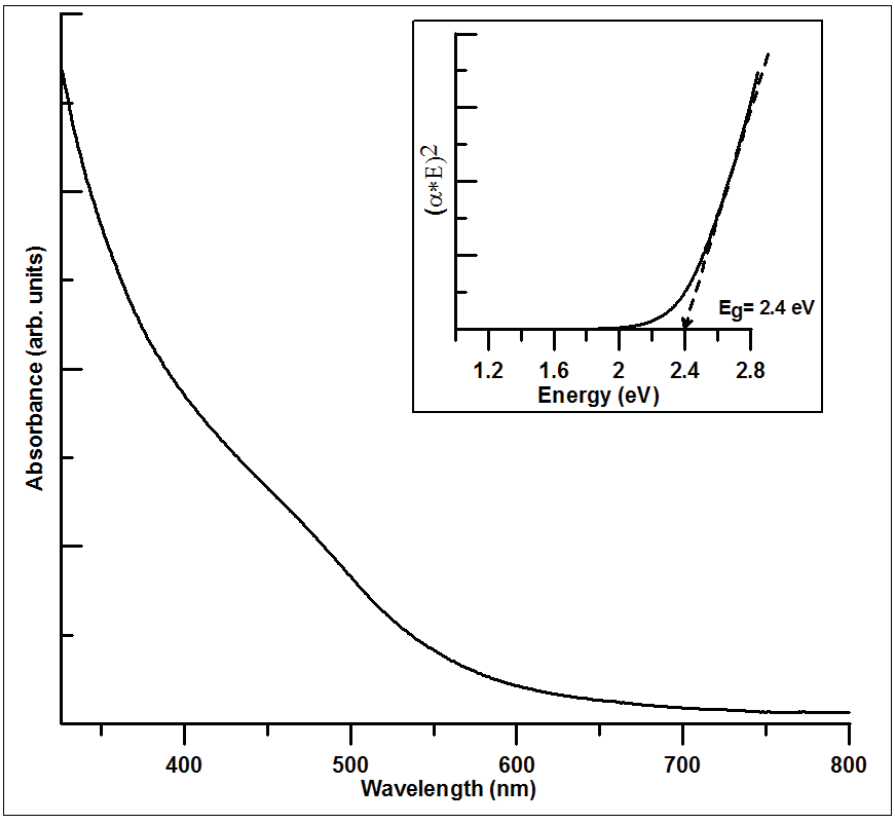

Figure 4-49 Absorption spectrum of CdSe QDs and the inset is the estimated band gap energy.

CHAPTER 5

CONCLUSION

Pulsed laser Ablation in liquid using 532 nm wavelength laser having 10 Hz, 5 ns pulse duration was used to produce nanostructured copper oxide from copper in the presence of hydrogen peroxide (oxidizing agent) in aqueous solution. This brought about some positive attributes in the product material. First of all, the presence of H_2O_2 in the PLAL process favored the production of (Cu/CuO) with nanorod-like structure, which is more versatile in terms of its applications. Also the presence of H_2O_2 in the PLAL process made a considerable red shift in the band gap energy of the synthesized material, and reduced electron hole recombination rate as revealed by the photoluminescence spectra. The red shift in the band gap energy and the reduced electron hole recombination rate make the product material an ideal photocatalyst to harvest solar radiation.

In addition, we synthesized nano structured CuO by annealing Cu/Cu_2O at different temperatures via an indirect scheme. Cu/Cu_2O was synthesized by pulsed laser ablation of Cu in deionised water. Different techniques (XRD, TEM, UV spectro-photometery PL, and FTIR) were applied for the characterization of synthesized nano CuO. The optical properties, grain size, band gap and IR absorption band of CuO vary with annealing temperature. The synthesized material using this indirect method could be applied in developing materials for sensors for various applications in industry, medicine and environment.

Furthermore, the pulsed laser with nanosecond pulse duration was used to synthesize CdSe quantum dots of 3 nm grain size, by employing the PLAL technique. The synthesized material showed characteristics similar to the ones which is synthesized using a laser of femtosecond pulse duration. The prolonged pulse duration in the case of nanosecond laser pulse compared to the femtosecond one brings about the thermally induced particle agglomeration after the formation of the nanostructured particles. This thermally induced agglomeration was successfully eliminated by using the unfocussed laser pulse irradiating the commercially available micron sized CdSe in the acetone medium. The band gap energy of the synthesized CdSe QDs measured using optical absorption spectrum was 2.4 eV, and this value is in good agreement with the value reported for the CdSe QDs synthesized by chemical methods. Relative to the micron sized material, the band gap energy of the synthesized CdSe QD showed a blue shift from near infrared spectral region to the visible region, making this material capable of harnessing the visible spectral region of the solar spectra in applications like photocatlysis and solar cells. It is worth to mention that this work has resulted in numerous publications [117-123] in ISI journals which is a good testimony of the originality of this work.

References

[1] R. Feynman, There's plenty of room at the bottom, Miniaturization, edited by H.D.Gilbert, Reinhold, New York, 1961.

[2] N. Taniguchi (On the Basic Concept of Nano-Technology in International Conference of Product Engineers), Japan Society of Precision Engineering , 1974.

[3] J. Ba (Nonaqueous Syntheses of Metal Oxide Nanoparticles and Their Assembly into Mesoporous Materials) PhD thesis, University of Potsdam, 2006.

[4] C.P. Poole, F.J. Owens, Introduction to Nanotechnology, Wiley and Sons, 2003.

[5] M. Di Ventra, Introduction to Nanoscale Science and Technology, Springer, 2004.

[6] R.W. Kelsall, I.W. Hamley, M. Geoghegan, Nanoscale Science and Technology, John Wiley and Sons, 2005.

[7] M. J. Pitkethly, Nanoparticles as building blocks?, Materials Today 6 (2003) 36-42.

[8] F. E. Kruis, H. Fissan, A. Peled, Synthesis of nanoparticles in the gas phase for electronic, optical and magnetic applications-a review, Journal of Aerosol Science, 29 (1998) 511-535.

[9] C.-H. Yu, Kin Tam, Edman S.C. Tsang, Chemical Methods for Preparation of Nanoparticles in Solution, Elsevier 5, (2008) 113-141.

[10] Helmut Schmidt, Nanoparticles by chemical synthesis, processing to materials and innovative applications, Appl. Organometal. Chem. 15 (2001) 331–343.

[11] G.W. Yang, Laser ablation in liquids: Applications in the synthesis of nanocrystals, Progress in Materials Science 52 (2007) 648-698.

[12] G. W. Yang, Laser Ablation in Liquids: Principles and Applications in the Preparation of Nanomaterials, Pan Stanford Publishing, Singapore (2012).

[13] Zijie Yan and Douglas B. Chrisey, Pulsed laser ablation in liquid for micro-/nanostructure generation , Journal of Photochemistry and Photobiology 13 (2012) 204-223.

[14] Haibo Zeng, Xi-Wen Du , Subhash C. Singh , Sergei A. Kulinich , Shikuan Yang , Jianping He and Weiping Cai, Nanomaterials via Laser Ablation/Irradiation in Liquid: A Review , Adv. Funct. Mater. 22 (2012) 1333-1353.

[15] P. Liu, H. Cui, C. X. Wang and G. W. Yang, From nanocrystal synthesis to functional nanostructure fabrication: laser ablation in liquid, Phys. Chem. Chem. Phys. 12 (2010) 3942-3952.

[16] H. B. Zeng , W. Cai , Y. Li , J. Hu and P. Liu , Composition/Structural Evolution and Optical Properties of ZnO/Zn Nanoparticles by Laser Ablation in Liquid Media, J. Phys. Chem. B 109 (2005) 18260–18266.

[17] P. S. Liu , W. P. Cai and H. B. Zeng , Fabrication and Size-Dependent Optical Properties of FeO Nanoparticles Induced by Laser Ablation in a Liquid Medium, J. Phys. Chem. C 112 (2008) 3261–3266.

[18] H. B. Zeng , Z. Li , W. Cai , B. Cao , P. Liu and S. Yang , Microstructure Control of Zn/ZnO Core/Shell Nanoparticles and Their Temperature-Dependent Blue Emissions, J. Phys. Chem. B 111 (2007) 14311–14317.

[19] H. B. Zeng , X. Xu , Y. Bando , U. K. Gautam , T. Zhai , X. Fang , B. Liu and D. Golberg , Template Deformation-Tailored ZnO Nanorod/Nanowire Arrays: Full Growth Control and Optimization of Field-Emission, *Adv. Funct. Mater.* 19 (2009) 3165–3172.

[20] K. Y. Niu , J. Yang , S. A. Kulinich , J. Sun , H. Li and X. W. Du , Morphology Control of Nanostructures via Surface Reaction of Metal Nanodroplets, J. Am. Chem. Soc. 132 (2010) 9814–981.

[21] K. Y. Niu , J. Yang , J. Sun and X. W. Du , One-step synthesis of MgO hollow nanospheres with blue emission, Nanotechnology 21 (2010) 295604.

[22] F. Lin , J. Yang , S. H. Lu , K. Y. Niu , Y. Liu , J. Sun and X. W. Du , Laser synthesis of gold/oxide nanocomposites, *J. Mater. Chem.* 20 (2010) 1103-1106.

[23] K. Y. Niu , J. Yang , S. A. Kulinich , J. Sun and X. W. Du , Hollow Nanoparticles of Metal Oxides and Sulfides: Fast Preparation via Laser Ablation in Liquid, Langmuir 26 (2010) 16652–1665.

[24] N. Takada, T. Nakano and K. Sasaki, Formation of cavitation-induced pits on target surface in liquid-phase laser ablation, Appl. Phys. A 101 (2010) 255-258.

[25] J.H. Bang and K.S. Suslick, Applications of Ultrasound to the Synthesis of Nanostructured Materials , Adv. Mater. 22 (2010) 1039–1059.

[26] A. Schwenke, P. Wagener, S. Nolte and S. Barcikowski, Influence of processing time on nanoparticle generation during picosecond-pulsed fundamental and

second harmonic laser ablation of metals in tetrahydrofuran, Appl. Phys. A 104 (2011) 77-82.

[27] Y.H. Yeh, M.S. Yeh, Y.P. Lee and C.S. Yeh, Formation of Cu Nanoparticles from CuO Powder by Laser Ablation in 2-Propanol , Chem. Lett. 27 (1998) 1183-1184.

[28] M.S. Yeh, Y.S. Yang, Y.P. Lee, H.F. Lee, Y.H. Yeh and C.S. Yeh, Formation and Characteristics of Cu Colloids from CuO Powder by Laser Irradiation in 2-Propanol, J. Phys. Chem. B 103 (1999) 6851–6857.

[29] P. V. Kamat , M. Flumiani and G. V. Hartland , Picosecond Dynamics of Silver Nanoclusters. Photoejection of Electrons and Fragmentation, J. Phys. Chem. B 102 (1998) 3123–3128.

[30] A. Giusti , E. Giorgetti , S. Laza , P. Marsili and F. Giammanco , Multiphoton Fragmentation of PAMAM G5-Capped Gold Nanoparticles Induced by Picosecond Laser Irradiation at 532 nm, J. Phys. Chem. C 111 (2007) 14984–14991.

[31] K. Yamada , Y. Tokumoto , T. Nagata and F. Mafune , Mechanism of Laser-induced Size-reduction of Gold Nanoparticles as Studied by Nanosecond Transient Absorption Spectroscopy , J. Phys. Chem. B 110 (2006) 11751–11756.

[32] H. Muto , K. Miyajima and F. Mafune , Mechanism of Laser-Induced Size Reduction of Gold Nanoparticles As Studied by Single and Double Laser Pulse Excitation, J. Phys. Chem. C 112 (2008) 5810–5815.

[33] R. S. Devan , R. A. Patil , J. -H. Lin , Y. –R. Ma, One-Dimensional Metal-Oxide Nanostructures: Recent Developments in Synthesis, Characterization, and Applications, Adv. Funct. Mater. 22 (2012) 3326–3370.

[34] S. Link, M. A. El-Sayed, Size and Temperature Dependence of the Plasmon Absorption of Colloidal Gold Nanoparticles, J. Phys. Chem. B 103 (1999) 4212-4217.

[35] A. Takami, H. Kurita, S. Koda, Laser-induced size reduction of noble metal particles, J. Phys. Chem. B 103 (1999) 1226-1232.

[36] A. C. Curtis, D. G. Duff, P. P. Edwards, D. A. Jefferson, B. F. G. Johnson, A. I. Kirkland, A. S. Wallace, Preparation and structural characterization of an unprotected copper sol, The Journal of Physical Chemistry 92 (1998) 2270-2275.

[37] M.S. Yeh, Y.S. Yang, Y.P. Lee, H.F. Lee, Y.H. Yeh, C.S. Yeh, Formation and characteristics of cu colloids from CuO powder by laser irradiation in 2-propanol, J. Phys. Chem. B 103 (1999) 6851-6857.

[38] S.C. Singh, R.K. Swarnkar, R. Gopal, Zn/ZnO core/shell nanoparticles synthesized by laser ablation in aqueous environment: Optical and structural characterizations. Bull. Mater. Sci. 33 (2010) 21-26.

[39] K.S. Lee, M. A. El-Sayed, Gold and silver nanoparticles in sensing and imaging: sensitivity of plasmon response to size, shape, and metal composition, J. Phys. Chem. B 110 (2006) 19220-19225.

[40] J. Lee, D. K. Kim, W. Kang, Preparation of Cu nanoparticles from Cu powder dispersed in 2-propanol by laser ablation, Bulletin of the Korean Chemical Society 27 (2006) 1869–1872.

[41] C. Arijit, G. Vinay, K. Sreenivas, Thickness Dependence Effects of CuO Islands on SnO2 in the Nano-scale Range for H2S gas Sensing Applications, Rev. Adv. Mater. Sci. 4 (2003) 75-785.

[42] M.Yang, J. He, X. Hu, C. Yan, Z. Cheng, Y. Zhao, G. Zuo, Copper oxide nanoparticle sensors for hydrogen cyanide detection: Unprecedented selectivity and sensitivity, Sensors and Actuators B 155 (2011) 692–698.

[43] M. -H. Chang, H –S. Liu, C. Y. Tai, Preparation of copper oxide nanoparticles and its application in nanofluid, Powder Technology 207 (2011) 378–386.

[44] K. Gopalakrishnan, C. Ramesh, V. Ragunathan and M. Thamilselvan, Antibaterial Activit of C_2O Nanaoparticles on E.Coli Synthesized from Tridax Procumbens Leaf Extract and Surface Coating wih Polyaniline, Digest Journal of Nanomaterials and Biostructures 7 (2012) 833 – 839.

[45] B.P.Rai, Cu_2O solar cells: a review, Solar Cells 25 (1988) 265–272.

[46] K.H. Yoon, W.J. Choi, D.H. Kang, Photoelectrochemical properties of copper oxide thin films coated on an n-Si substrate, Thin Solid Films 372 (2000) 250-256.

[47] A.Y. Oral, E. Mensur, M.H. Aslan, E.B. Basaran, The preparation of copper(II) oxide thin films and the study of their microstructures and optical propeties, Materials Chemistry and Physics 83 (2004) 140-144.

[48] S.C. Ray, Preparation of copper oxide thin film by the sol–gel-like dip technique and study of their structural and optical properties, Sol. Energy Mater. Sol. Cells. 68 (2001) 307-312.

[49] Ming-Shin Yeh,Yuh-Sheng Yang,Yi-Pei Lee,Hsiu-Fang Lee,Ya-Huey Yeh, Chen-Sheng Yeh, Formation and Characteristics of Cu Colloids from CuO Powder by Laser Irradiation in 2-Propanol, The Journal of Physical Chemistry B 103 (1999) 6851-6857.

[50] Kazuyuki Amikura, Takeshi Kimura, Mika Hamada, Noriko Yokoyama, Jun Miyazaki, Yasuhiro Yamada, Copper oxide particles produced by laser ablation in water, Applied Surface Science, Volume 254 (2008) 6976-6982.

[51] X. Z. Lin , P. Liu , J. M. Yu and G. W. Yang, Synthesis of CuO Nanocrystals and Sequential Assembly of Nanostructures with Shape-Dependent Optical Absorption upon Laser Ablation in Liquid, J. Phys. Chem. C 113 (2009) 17543–17547.

[52] Ming-Tsang Lee, David J. Hwang, Ralph Greif, Costas P. Grigoropoulos, Nanocatalyst fabrication and the production of hydrogen by using photon energy, International Journal of Hydrogen Energy 34 (2009) 1835-1843.

[53] K.Y. Niu, J. Yang, S. A. Kulinich, J. Sun , H. Li, X. W. Du, Morphology Control of Nanostructures via Surface Reaction of Metal Nanodroplets, J. Am. Chem. Soc. 132 (2010) 9814–9819.

[54] K. Y. Niu, J. Yang, S. A. Kulinich, J. Sun, and X. W. Du, Hollow Nanoparticles of Metal Oxides and Sulfides: Fast Preparation via Laser Ablation in Liquid, Langmuir 26 (2010) 16652-16657.

[55] A. Nath, A. Khare, Size induced structural modifications in copper oxide nanoparticles synthesized via laser ablation in liquids, J. Appl. Phys. 110 (2011) 043111.

[56] M. Kawasaki , Laser-Induced Fragmentative Decomposition of Fine CuO Powder in Acetone as Highly Productive Pathway to Cu and Cu_2O Nanoparticles, J. Phys. Chem. C 115 (2011) 5165-5173.

[57] M. Muniz-Miranda, C. Gellini, E. Giorgetti, Surface-Enhanced Raman Scattering from Copper Nanoparticles Obtained by Laser Ablation, J. Phys. Chem. C 115 (2011) 5021-5027.

[58] A.D.Dinsmore, D.S.Hsu, H.F.Gray, S.B.Quadri, Y.Tian,B.R.Ratna, Mn-doped ZnS nanoparticles as efficient low-voltage cathodoluminescent phosphors, Applied Physics Letters75(1999)802-804.

[59] R.Maity,K.K.Chattopadhyay, synthesis and optical characterization of ZnS and ZnS:Mn nanocrystalline thin films by chemical route, Nanotechnology15(2004) 812-816.

[60] S.Mahamuni,K.Borgohain,B.S.Bendre,V.J.Leppert,S.H.Risbud, Spectroscopic and structural characterization of electrochemically grown ZnO quantum dots, Journal of Applied Physics85(1999)2861-2865.

[61] J.Tittel,W.Gohde,F.Koberling,Th.Basche,A.Kornowski,H.Weller, A. Eychmuller, Fluorescence Spectroscopy on Single CdS Nanocrystals, Journal of Physical ChemistryB101(1997)3013-3016.

[62] J.H.Lai,C.L.Ren,X.Y.Liu,Z.D.Hu,D.S.Xue, “Green” synthesis of starch capped CdSe nanoparticles at room temperature, Materials Science and Engineering A 458 (2007)319-322.

[63] P.D. Persans, A. Tu, Y.J. Wu, M. Lewis , Size-distribution-dependent optical properties of semiconductor microparticle composites, J. Opt. Soc. Am. 6 (1989) 818-823.

[64] V. Jungnickel, F. Henneberger, Luminescence related processes in semiconductor nanocrystals —The strong confinement regime, 70 (1996) 238-252.

[65] T. Arai, K. Matsuishi, Electronic states of Cd-chalcogenide microcrystals embedded in GeO2 glasses studied by means of spectroscopy, J. Lumin. 70 (1996) 281-293.

[66] C.B. Murray, D.J. Norris, M.G. Bawendi, Synthesis and characterization of nearly monodisperse CdE (E = sulfur, selenium, tellurium) semiconductor nanocrystallites, J. Am. Chem. Soc. 115 (1993) 8706-8715.

[67] K. Yu, S. Singh, N. Patrito, V. Chu, Effect of Reaction Media on the Growth and Photoluminescence of Colloidal CdSe Nanocrystals, Langmuir 20 (2004) 11161-11168.

[68] C.R. Bullen, P. Mulvaney, Nucleation and Growth Kinetics of CdSe Nanocrystals in OctadeceneNano Lett. 4 (2004) 2303-2307.

[69] B. R. Sankapal, S. D. Sartale, C. D. Lokhande, and A. Ennaoui, Chemical synthesis of Cd-free wide band gap materials for solar cells, Sol. Energy Mater. Sol. Cells 83 (2004) 447-458 .

[70] Q. Shen, J. Kobayashi, L. J. Diguna, and T. Toyoda, Effect of ZnS coating on the photovoltaic properties of CdSe quantum dot-sensitized solar cells, J. Appl. Phys. 103 (2008) 084304.

[71] I. Mora-Sero and J. J. Bisquert, Breakthroughs in the Development of Semiconductor-Sensitized Solar Cells, Phys. Chem. Lett. 1 (2010) 3046-3052.

[72] Y. Tak, S. J. Hong, J. S. Lee, and K. Yong, Solution-Based Synthesis of a CdS Nanoparticle/ZnO Nanowire Heterostructure Array ,Cryst. Growth Des. 9 (2009) 2627-2632.

[73] D. R. Baker and P. V. Kamat, Photosensitization of TiO2 Nanostructures with CdS Quantum Dots, Adv. Funct. Mater. 19(2009) 805-811.

[74] N. P. Dasgupta, H. J. Jung, O. Trejo, M. T. McDowell, A. Hryciw, M. Brongersma, R. Sinclair, and F. B. Prinz, Atomic Layer Deposition of Lead Sulfide Quantum Dots on Nanowire Surfaces, Nano Lett. 11 (2011) 934-940.

[75] Q. Dai, J. Chen, L. Lu, J. Tang, and W. Wang, Pulsed Laser Deposition of CdSe Quantum Dots on Zn2SnO4 Nanowires and Their Photovoltaic Applications, Nano Lett. 12 (2012) 4187-4193.

[76] Waleed E. Mahmoud, Amal M. Al-Amri, S.J. Yaghmour, Low temperature synthesis of CdSe capped 2-mercaptoethanol quantum dots, Optical Materials 34 (2012) 1082–1086

[77] Albert A. Ruth and John A. Young, Generation of CdSe and CdTe nanoparticles by laser ablation in liquids, Colloids and Surfaces A: Physicochem. Eng. Aspects 279 (2006) 121–127.

[78] N. G. Semaltianos, S. Logothetidis, W. Perrie, S. Romani, R. J. Potter, M. Sharp, P. French, G. Dearden and K. G. Watkins, CdSe nanoparticles synthesized by laser ablation, A letter journal exploring the frontiers of physics, 84 (2008) 47001.

[79] N.G. Semaltianos, S. Logothetidis, W. Perrie, S. Romani · R.J. Potter · M. Sharp, P. French, G. Dearden · K.G.Watkins, II–VI semiconductor nanoparticles synthesized by laser ablation, Appl Phys A (2009) 94: 641–647.

[80] S.V.Gaponenko, Optical properties of semiconductor nanocrystals, Cambridge: Cambridge University Press, 1998.

[81] L.E. Brus, Electron–electron and electron-hole interactions in small semiconductor crystallites: The size dependence of the lowest excited electronic state , J. Chem. Phys. 80 (1984) 4403-4409.

[82] W. Y. Ching, Y-N. Xu, and K. W. Wong, Ground-state and optical properties of Cu_2O and CuO crystals, Phys. Rev. B. 40 (1989) 7684-7695.

[83] T. Ito, T. Kawashima, H. Yamaguchi, T. Masumi, and S. Adachi, Optical Properties of Cu $_2$O Studied by Spectroscopic Ellipsometry, J. Phys. Soc. Jpn. 67 (1998) 2125-2131.

[84] K. V. R. Chary, G. V. Sagar, C. S. Srikanth, and V. V. Rao, Characterization and Catalytic Functionalities of Copper Oxide Catalysts Supported on Zirconia, J. Phys. Chem. B. 111 (2007) 543-550.

[85] D. B. Pedersen, S. Wang, and S. H. Liang, Charge-Transfer-Driven Diffusion Processes in Cu@Cu-Oxide Core−Shell Nanoparticles: Oxidation of 3.0 ± 0.3 nm Diameter Copper Nanoparticles, J. Phys. Chem C. 112 (2008) 8819-8826.

[86] J. Tauc, R. Grigorovici and A. Vancu, Optical properties and electronic structure of amorphous germanium. Phys. Status Solidi 15 (1966) 627-637.

[87] F. L. Weichman, Photoconductivity of cuprous oxide in relation to its other semiconducting properties, Phys Rev 117 (1960) 998 -1002.

[88] Y. Xu, X. Jiao, D. Chen, PEG-Assisted Preparation of Single-Crystalline Cu_2O Hollow Nanocubes, J. Phys. Chem. C 112 (2008) 16769–16773.

[89] E. C. Heletmes, Far-Infra red Properties of Cuprous Oxide, Phys Rev 27 (1965) 803 -806.

[90] K. Borgohain, N. Murase, S. Mahamuni, Synthesis and properties of Cu_2O quantum particles, J. Appl. Phys. 92 (2002) 1292 -1297.

[91] F. Svegl, B. Orel, The application of FT-IR reflection-absorption spectroscopy for determining the textural properties of copper oxide thin films, MTAEC9 37 (2003) 29-32.

[92] G. Busca, FT-IR study of the surface of copper oxide, Journal of Molecular Catalysis, 43 (1987) 225–236.

[93] H. Fan, L. Yang, W. Hua, X. Wu, Z. Wu, S. Xie, B. Zou, Controlled synthesis of monodispersed CuO nanocrystals, Nanotechnology 15 (2004) 37–42.

[94] K. Zhong , J. Xue , Y. Mao , C. Wang , T. Zhai , P. Liu, X. Xia , H. Li, Y. Tong, Facile synthesis of CuO nanorods with abundant adsorbed oxygen concomitant with high surface oxidation states for CO oxidation, RSC Adv. 2 (2012) 11520-11528

[95] Rutian Jin, Juan Gao, Xiaoyu Liu, Wei Yang, Xiaoxia Peng, Tao Zhang, and Yifa Zhou, Ginsenoside Rg3: Spectral Analysis and Sensitive Detection with Silver Nanoparticles Decorated Graphene, Sci. Adv. Mater. 4 (2012) 1160-1165.

[96] C. C. Hsu, N.L. Wu, Synthesis and photocatalytic activity of ZnO/ZnO2 composite Original Research Article, J. Photochemistry and Photobiology A: Chemistry, 172 (2005) 269-274.

[97] Z. Ji, S. Zhao, C. Wang, K. Liu, ZnO nanoparticle films prepared by oxidation of metallic zinc in H2O2 solution and subsequent process, Materials Science and Engineering B 117 (2005) 63-66.

[98] A . Imre, D.L. Beke, E. Gontier-Moya, I.A. Szab´o, E. Gillet, Surface Ostwald ripening of Pd nanoparticles on the MgO (100) surface , Appl. Phys. A 71 (2000) 19-22.

[99] F. Fillot, Z. TÖkei, G.P. Beyer, Surface diffusion of copper on tantalum substrates by Ostwald ripening, Surface Science, 601 (2007) 986-993.

[100] P. Kubelka and F. Munk, An Article on Optics of Paint Layers, Zeit. Für Tekn. Physik 12 (1931) 593-601.

[101] P. Kubelka, New contribution to the optics of intensely light scattering materials. part I. J. Opt. Soc. Am., 38 (1948) 448-448.

[102] J. Hu, Y. Bando, Growth and optical properties of single-crystal tubular ZnO whiskers, Appl. Phys. Lett. 82 (2003) 1401-1403.

[103] A. El-Trass, H. ElShamy, I. El-Mehasseb, M. El-Kemary, CuO nanoparticles: Synthesis, characterization, optical properties and interaction with amino acids , Applied Surface Science, 258, (2012) 2997– 3001.

[104] S. Guha, D. Peebles, and T. J. Wieting, Phys. Rev. B, Zone-center (q=0) optical phonons in CuO studied by Raman and infrared spectroscopy 43 (1991)13092-13101.

[105] G. Kliche, and Z. V. Popovic, Far-infrared spectroscopic investigations on CuO, Phys. Rev. B 42 (1990) 10060–10066.

[106] H. Hagemann, H. Bill, W. Sadowski, E. Walker, and M. rancois, Raman spectra of single crystal CuO, Solid State Commun 73 (1990) 447-451.

[107] Z. V. Popovic, C. Thomsen, M. Cardona, R. Liu, G. Stanisic, R.Kremer and W. Konig, Phonon characterization of Bi2 (Sr1-xCax)2 CuO6+δ by infrared and Raman spectroscopy, Solid State Commun. 66 (1988) 965-969.

[108] L. Degiorgi, E. Kaldis, and P. Wachter, Electronic- and phononic structure of La1−xSrxCuO4, Physica C 153 (1988) 657-658.

[109] S. N. Narang, V. B. Kartha, and N. D. Patel, Fourier transform infrared spectra and normal vibrations of CuO, Physica C 204 (1992) 8-14.

[110] E. C. Heltemes, Far-Infrared Properties of Cuprous Oxide, Phys. Rev. 14 (1966) 803-805.

[111] M. Abdul Momin, Roksana Pervin, M. Jalal Uddin, G.M. Arifuzzaman Khan, Momtazul Islam, One Step Synthesis and Optical Evaluation of Copper Oxide (CuO) Nanoparticles, J. Bangladesh Electron. 10 (2010) 57-63.

[112] P. Michler, Single Quantum Dots: Fundamentals, Applications and New Concept, Physics and Astronomy Classification Scheme (PACS), Springer-Verlag, Berlin, 2003.

[113] R. Cohen, M.D. Sturge, Fluorescence line narrowing, localized exciton states, and spectral diffusion in the mixed semiconductor CdS_xSe_{1-x}, Phys. Rev. B 25 (1982) 3828-3840.

[114] C.T. Giner, A. Debernardi, M. Cardona, E.M. Proupin, A.I. Ekimov, Optical vibrons in CdSe dots and dispersion relation of the bulk material, Phys. Rev. B 57 (1998) 4664-4669.

[115] C. Wang, M. Shim and P. Guyot-Sionnest, “Electrochro-mic Nanocrystal Quantum Dots,” Science 291(2001) 2390-2392.

[116] S.V.Gaponenko, Optical properties of semiconductor nanocrystals, Cambridge: Cambridge University Press, 1998.

[117] M.A. Gondal, Talal F. Qahtan and M. A. Dastageer, Synthesis of Cu/Cu2o Nanoparticles by Laser Ablation in Deionized Water and Their Annealing Transformation into CuO Nanoparticles, Journal of Nanoscience and Nanotechnology, Vol. 13, 1–8, 2013.

[118] M.A.Gondal, Talal F. Qahtan, M.A. Dastageer and T.A. Saleh, Effects of Oxidizing Medium on the Composition, Morphology and Optical Properties of Copper Oxide Nanoparticles produced by Pulsed Laser Ablatio, Appl. Surface

Science, Vol. 286, 149–155, 2013.

[119] Talal F. Qahtan, M.A.Gondal, Z. H. Yamani and M.A. Dastageer, Syntheisis of CdSe quantum dots by pulsed laser ablation in acetone. (submitted)

[120] M.A.Gondal, Talal F. Qahtan , Z. H. Yamani and M.A. Dastageer, Syntheisis of CdS quantum dots by pulsed laser ablation in liquids. (in progress).

[121] M.A. Gondal, T.F. Qahtan M.A. Dastageer, T.A. Saleh ,Synthesis and Characterization of Copper Oxides Nanoparticles Using Pulsed LaserAblation in Water, 10th International Conference on High Capacity Optical Networks and Emerging Technolgy (HONET), IEEE sponsored (Magosa,11-13 Dec, 2013 Cyprus).

[122] M.A. Gondal, T.F. Qahtan M.A. Dastageer, T.A. Saleh ,Generation of Copper Oxides Nanoparticles in Using Pulsed LaserAblation in H2O2, IEEE Proceeding, The 9th International Conference and Exhibition on Chemistry in Industry, Manama (Nov2 - 6, 2013) Bahrain.

[123] M.A. Gondal, T.F. Qahtan M.A. Dastageer, Synthesis and Characterization Of Metal Oxides (Al2O3, Cuo) Nanoparticles Using Pulsed Laser Ablation Technique, The Saudi International Nanotechnologies Conference, 1—13 November, 2012, Riyadh

Vitae

Name : TALAL FARHAN AHMED QAHTAN

Nationality : YEMENI

Date of Birth : 12-12-1981

Email : talalphysics@yahoo.com

Address : Taiz University, Taiz City, Yemen

Academic Background : B.Sc. in Physics from Taiz University in 2007

PUBLICATIONS AND CONFRENCES

1. M.A. Gondal, **Talal F. Qahtan** and M. A. Dastageer, Synthesis of Cu/Cu_2o Nanoparticles by Laser Ablation in Deionized Water and Their Annealing Transformation into CuO Nanoparticles, *Journal of Nanoscience and Nanotechnology, Vol. 13, 1–8, 2013.*

2. M.A.Gondal, **Talal F. Qahtan**, M.A. Dastageer and T.A. Saleh, Effects of Oxidizing Medium on the Composition, Morphology and Optical Properties of Copper Oxide Nanoparticles produced by Pulsed Laser Ablatio, *Appl. Surface Science, Vol. 286, 149–155, 2013.*

3. **Talal F. Qahtan**, M.A.Gondal, Z. H. Yamani and M.A. Dastageer, Syntheisis of CdSe quantum dots by pulsed laser ablation in acetone. (submitted)

4. M.A.Gondal, **Talal F. Qahtan** , Z. H. Yamani and M.A. Dastageer, Syntheisis of CdS quantum dots by pulsed laser ablation in liquids. (in progress).

5. M.A. Gondal, **T.F. Qahtan** M.A. Dastageer, T.A. Saleh ,Synthesis and Characterization of Copper Oxides Nanoparticles Using Pulsed LaserAblation in Water, 10th International Conference on High Capacity Optical Networks and Emerging Technolgy (HONET), IEEE sponsored (Magosa,11-13 Dec, 2013 Cyprus).

6. M.A. Gondal, **T.F. Qahtan** M.A. Dastageer, T.A. Saleh ,Generation of Copper Oxides Nanoparticles in Using Pulsed LaserAblation in H_2O_2, IEEE Proceeding, The 9th International Conference and Exhibition on Chemistry in Industry, Manama (Nov2 - 6, 2013) Bahrain.

7. M.A. Gondal, **T.F. Qahtan** M.A. Dastageer, Synthesis and Characterization Of Metal Oxides (Al_2O_3, Cuo) Nanoparticles Using Pulsed Laser Ablation Technique, The Saudi International Nanotechnologies Conference, 1—13 November, 2012, Riyadh